

**BIOREMEDIATION OF SEDIMENTS  
CONTAMINATED BY PERSISTENT ORGANIC  
POLLUTANTS: AN IN-SILICO APPROACH**

**A Thesis Submitted to  
the Graduate School of Engineering and Sciences of  
İzmir Institute of Technology  
in Partial Fulfillment of the Requirements for the Degree of**

**MASTER OF SCIENCE**

**in Environmental Engineering**

**by  
Batuhan YILDIRIM**

**December 2024  
İZMİR**

We approve the thesis of **Batuhan YILDIRIM**

**Examining Committee Members:**

---

**Prof. Dr. Orhan GÜNDÜZ**

Department of Environmental Engineering, Izmir Institute of Technology

---

**Assist. Prof. Hale DEMİRTEPE**

Department of Environmental Engineering, Izmir Institute of Technology

---

**Assoc. Prof. Dr. Yetkin DUMANOĞLU**

Department of Environmental Engineering, Dokuz Eylül University

**13 December 2024**

---

**Assist. Prof. Hale DEMİRTEPE**

Supervisor, Department of  
Environmental Engineering  
Izmir Institute of Technology

---

**Assoc. Prof. Dr. Hatice Eser ÖKTEN**

Co-Supervisor, Department of  
Environmental Engineering  
Izmir Institute of Technology

---

**Prof. Dr. Sait Cemil SOFUOĞLU**

Head of the Department  
of Environmental Engineering

---

**Prof. Dr. Mehtap EANES**

Dean of the Graduate School  
of Engineering and Sciences

## **ACKNOWLEDGEMENTS**

I would like to thank my advisor Assist. Prof. Hale Demirtepe for guidance, suggestions, and her believing in me for this research. I sincerely thank all the faculty members in my department for their support. I am especially grateful to Professor İpek İmamoglu for sharing her model and data, which helped me advance this study, and to my advisor for providing their model and the previously collected Camkoru Ankara PBDEs microcosm data. I would also like to express my appreciation to Prof. Dr. Orhan Gündüz, and Assoc. Prof. Dr. Yetkin Dumanoglu for being on the examination committee.

I would also like to thank my department professors, IZTECH, and my family for their contributions in helping me reach this stage of my thesis.

## ABSTRACT

### BIOREMEDIATION OF SEDIMENTS CONTAMINATED BY PERSISTENT ORGANIC POLLUTANTS: AN IN-SILICO APPROACH

Polybrominated diphenyl ethers (PBDEs), one of the most commonly used flame retardants, are classified as persistent organic pollutants that pose significant risks to the environment and human health. Therefore, they should be removed from the environment using degradation processes. However, in complex environmental matrices the progress of degradation is challenging to follow. Hence, modelling studies are necessary to understand the fate of PBDEs and develop effective remediation strategies. This study aims to model the anaerobic dehalogenation of PBDEs in sediments and analyze the degradation pathways and rates under various bioremediation scenarios. For this purpose, experimental data from a microcosm study simulating natural attenuation, biostimulation, and bioaugmentation scenarios were utilized. A previously developed anaerobic dehalogenation model (ADM) was enhanced and integrated to create a new model called “ADM-IE.” ADM-IE has the capability to list all possible dehalogenation pathways for PBDEs, calculate the degradation rate constants for the measured compounds, and estimate the rate constants for those not measured, using machine learning algorithms.

As a result, the model performed better in predicting higher-concentration compounds, whereas its accuracy decreased for lower-concentration compounds. It was determined that the position of bromine atoms (ortho, meta, para) played a critical role in dehalogenation pathways. Among the bioremediation scenarios, bioaugmentation generally achieved the highest degradation rates, while biostimulation showed higher rates in some cases. However, certain pathways supported the formation of toxic products, emphasizing the need for caution when applying biostimulation. The model provided an analysis framework for optimizing bioremediation strategies by achieving less harmful degradation products.

## ÖZET

### KALICI ORGANİK KİRLETİCİLERLE KİRLENMİŞ SEDİMANLARIN BİYOİYİLEŞTİRİLMESİ: BİR İN-SİLİKO YAKLAŞIM

Bromlu alev geciktiriciler arasında en yaygın kullanılanlardan biri olan polibromlu difenil eterler (PBDE), çevre ve insan sağlığı üzerinde ciddi riskler oluşturan kalıcı organik kirleticiler olarak bilinmektedir. Bu nedenle, bozunma süreçleri ile çevresel ortamlardan giderilmeleri gerekmektedir. Fakat, karmaşık çevresel ortamlarda bozunmanın ilerleyişini takip etmek zordur. Bu sebeple, PBDE'lerin bozunma süreçlerini anlamak ve etkili iyileştirme yöntemleri geliştirmek için modelleme çalışmaları gereklidir. Bu çalışma, PBDE'lerin sedimanlardaki anaerobik dehalojenasyonunu modellemek ve iyileştirme senaryoları altında bozunma yollarını ve bozunma hızlarını analiz etmeyi amaçlamaktadır. Bu amaçla, doğal giderim, biyostimulasyon ve biyoogmentasyon senaryolarını taklit eden bir mikrokozmu çalışmasının deneysel verileri kullanılmıştır. Daha önce geliştirilmiş olan anaerobik dehalojenasyon modeli (ADM), geliştirilip entegre edilerek "ADM-IE" adı verilen yeni bir model oluşturulmuştur. ADM-IE, PBDE bozunması için tüm olası dehalojenasyon yollarını listeleme, bu yolların reaksiyon miktarlarını belirleme, ölçülen bileşikler için bozunma hız sabitlerini hesaplama ve ölçülmeyen bileşikler için makine öğrenimi algoritmalarıyla hız sabitlerini tahmin etme yeteneklerine sahiptir.

Sonuç olarak, modelin yüksek konsantrasyonlu bileşikler için daha başarılı tahminler yaptığını, ancak düşük konsantrasyonlu bileşikler için tahmin doğruluğunun daha düşük olduğunu gösterilmiştir. Brom atomlarının pozisyonlarının dehalojenasyon yollarında kritik bir rol oynadığı belirlenmiştir. İyileştirme senaryoları arasında, biyoogmentasyon genellikle en yüksek bozunma hızlarını sağlarken, bazı durumlarda biyostimulasyon daha yüksek hızlar göstermiştir. Bununla birlikte, belirli reaksiyonlar toksik ürünlerin oluşumunu desteklemiştir, bu da biyostimulasyon uygulamasında dikkatli olunması gerektiğini vurgulamıştır. Model, iyileştirme stratejilerinin optimize edilmesi ve daha az zararlı ürünlerin elde edilmesi için bir analiz çerçevesi sunmaktadır.

# TABLE OF CONTENTS

LIST OF FIGURES .....	viii
LIST OF TABLES .....	x
ABBREVIATIONS.....	xii
CHAPTER 1. INTRODUCTION .....	1
CHAPTER 2. LITERATURE REVIEW .....	4
2.1. Persistent Organic Pollutants (POPs).....	4
2.2. Polybrominated Diphenyl Ether (PBDE).....	5
2.3. Physical and Chemical Properties of PBDEs.....	7
2.4. Occurrence of PBDEs in the environment .....	8
2.5. Degradation of PBDEs in the environment.....	9
2.6. Remediation .....	13
2.7. Bioremediation .....	14
2.8. Modelling efforts on dehalogenation of halogenated POPs.....	15
2.9. Description of Terminology .....	16
2.9.1. Coeluting congener.....	16
2.9.2. Dehalogenation pathway .....	16
2.9.3. Marker and non-marker congeners.....	17
2.9.4. Mother/daughter .....	17
2.9.5. Linear Regression.....	18
2.9.6. Model Training.....	18
2.9.7. Reaction Amount.....	19
2.10. Anaerobic Dehalogenation Model .....	19
2.10.1. Description of Model.....	19
2.10.2. Model Development and History .....	20
2.11. Support Vector Machine Model.....	21
2.12. Neural Network Model .....	24
CHAPTER 3. METHOD .....	30
3.1. PBDE data set.....	30
3.2. Development and Evolution of the ADM .....	40

3.2.1. Anaerobic dehalogenation model .....	40
3.2.2. Integrated model .....	43
3.2.3. Integrated and Enhanced Model (ADM-IE) .....	45
3.3. Linear Regression Principles .....	48
3.4. Support Vector Machines Principles .....	49
3.5. Neural network model .....	50
CHAPTER 4. RESULT AND DISCUSSION .....	57
4.1. Validation of ADM-IE using artificial data set .....	57
4.2. ADM-IE application to PBDE bioremediation scenarios .....	61
4.2.1. Evaluation of PBDE dehalogenation after 180 days .....	61
4.2.2. Sequential degradation analysis in defined time intervals .....	74
4.3. Analysis of machine learning results .....	75
4.3.1. Pathways and degradation rates estimated by machine learning ...	76
4.3.2. Natural attenuation neural network results .....	79
4.3.3. Biostimulation 0-180 day neural network results .....	84
4.3.4. Bioaugmentation 0-180 day neural network results .....	89
4.4. Discussion on the findings of ADM-IE .....	93
4.4.1. Evaluation of model results and the experimental results .....	93
4.4.2. Previous usage of machine learning in degradation of persistent organic pollutants .....	95
4.4.3. Comparison of the degradation rate constants with previous model applications .....	97
CHAPTER 5. CONCLUSION .....	99
REFERENCES .....	102
APPENDICES	
APPENDIX A. BDE PATHWAYS REVIEW .....	110
APPENDIX B. NORMALIZED PROFILE DATA SETS .....	113
APPENDIX C. ANALYSIS OF ML PERFORMANCE .....	118
APPENDIX D. MODEL MANUAL .....	119

# LIST OF FIGURES

<b><u>Figure</u></b>	<b><u>Page</u></b>
Figure 2.1. General structure of PBDEs.....	6
Figure 2.2. The pathway of BDE-47 degradation under anaerobic conditions.....	9
Figure 2.3. The chronology of ADM development and modification. ....	20
Figure 2.4. The structure of SVM (Source: Raghavendra N. and Deka 2014).....	22
Figure 2.5. Typical neural network architecture (Source: The MathWorks 2024). ....	24
Figure 2.6. Structure of neural network (Source: Hafeez et al. 2024).....	27
Figure 2.7. Structure of neural network (Source: Isah et al. 2024).....	28
Figure 3.1. PBDE congener concentrations at sampling times in natural attenuation....	31
Figure 3.2. PBDE congener concentrations at sampling times in biostimulation.....	32
Figure 3.3. PBDE congener concentrations at sampling times in bioaugmentation.....	32
Figure 3.4. General algorithm in the first step of ADM (Source: Demirtepe 2012).....	34
Figure 3.5. General algorithm in the second step of ADM (Source: Demirtepe 2012)...	41
Figure 3.6. General algorithm in the last step of ADM (Source: Demirtepe 2012).....	42
Figure 3.7. General algorithm of integrated anaerobic dehalogenation model. ....	44
Figure 3.8. Integrated and Enhanced Anaerobic Dehalogenation Model Algorithm.....	47
Figure 3.9. Feed-Forward neural network diagram. ....	51
Figure 3.10. An example of the FNN command window. ....	52
Figure 3.11. Error histogram training plots graph. ....	53
Figure 3.12. Training state graph. ....	54
Figure 3.13. Regression Graph for Training, validation, and test.....	55
Figure 3.14. MSE Performance graph. ....	56
Figure 4.1. Manual/ADM-IE k values and measured/predicted profile plots. ....	56
Figure 4.2. Manual/ADM-IE k values and measured/predicted profile plots. ....	58
Figure 4.3. Measured vs predicted concentrations of all marker PBDE congeners for A) NA, B) BS, C) BA, except octa, nona, and deca-BDEs for D) NA, E) BS, F) BA. ....	61
Figure 4.4. Marker pathways k-values for all microcosm data sets 0-180day. ....	70
Figure 4.5. Degradation rate constant under BA 0-180 days. ....	71
Figure 4.6. Degradation rate constant under BS 0-180 days. ....	72

<b><u>Figure</u></b>	<b><u>Page</u></b>
Figure 4.7. Degradation rate constant under NA 0-180 days. ....	72
Figure 4.8. BS, NA and BA neural network model results. ....	76
Figure 4.9. ADM-IE NA 0-180day ML and calculated degradation rate.....	76
Figure 4.10. NA 0-180day MSE performance graph. ....	79
Figure 4.11. NA 0-180day training state graph. ....	80
Figure 4.12. NA 0-180day error histogram training plots.....	81
Figure 4.13. Regression graph for training, validation, and test. ....	82
Figure 4.14. ADM-IE BS 0-180day ML and calculated degradation rate. ....	83
Figure 4.15. BS 0-180day MSE performance graph. ....	85
Figure 4.16. BS 0-180day MSE performance graph.....	85
Figure 4.17. BS 0-180day error histogram training plots. ....	86
Figure 4.18. BS 0-180day regression graph for training, validation, and test. ....	86
Figure 4.19. ADM-IE BA 0-180day ML and calculated degradation rate. ....	87
Figure 4.20. BA 0-180day MSE performance graph. ....	87
Figure 4.21. BA 0-180day training state graph. ....	88
Figure 4.22. BA 0-180day error histogram training plots. ....	88
Figure 4.23. BA 0-180day regression graph for training, validation, and test. ....	89

## LIST OF TABLES

<b><u>Table</u></b>	<b><u>Page</u></b>
Table 2.1. Stockholm Convention categorization on POPs. ....	4
Table 2.2. Properties of PBDEs (Source: EPAWEB 1.0, 2023; USEPA, 2022). ....	7
Table 2.3. The concentration of PBDEs. ....	9
Table 2.4. PBDE degradation rate constants (k) following the first-order kinetics (Source: C. Zhao et al. 2018). ....	11
Table 2.5. Anaerobic degradation pathways of PBDEs. ....	12
Table 2.6. Examination of models. ....	21
Table 2.7. The application of SVM for the prediction of pollutants removal. ....	23
Table 2.8. Previous studies on contaminant degradation using with neural network ....	29
Table 3.1. First artificial data set input. ....	31
Table 3.2. First artificial data set input calculations. ....	31
Table 3.3. Second artificial data set calculations. ....	31
Table 3.4. Details of PBDE sediment microcosm sets (Source: Demirtepe 2017, 81)...	34
Table 3.5. Natural attenuation microcosm PBDE concentrations with time (ng/g).....	35
Table 3.6. Biostimulation microcosm PBDE concentrations with time (ng/g).....	36
Table 3.7. Bioaugmentation microcosm PBDE concentrations with time (ng/g).....	36
Table 3.8. Negative control microcosm PBDE concentrations with time (ng/g).....	37
Table 3.9. Sterile control microcosm PBDE concentrations with time (ng/g).....	38
Table 4.1. ADM-IE first artificial data set input. ....	55
Table 4.2. First validation comparison of manually calculated and ADM-IE k-values..	56
Table 4.3. ADM-IE second artificial data set input. ....	57
Table 4.4. Second validation comparison of manual and ADM-IE k-values. ....	58
Table 4.5. ADM-IE performance for 0-180 day microcosm data set.....	59
Table 4.6. Results of ADM-IE predicted and measured mole% profiles. ....	63
Table 4.7. All possible pathways for 23 marker congeners. ....	65
Table 4.8. NA, BS, BA, NC, and SC k-value results.....	68
Table 4.9. Novel pathways degradation rate constants under test microcosms.....	73
Table 4.10. Degradation rate constants for dehalogenation pathways in different time intervals.....	74

<b><u>Table</u></b>	<b><u>Page</u></b>
Table 4.11. Neural network model performance results under 3 test microcosms. ....	77
Table 4.12. k-values of non-marker pathways for bioremediation microcosms between 0 and 180 days, predicted by neural network model. ....	77
Table 4.13. k-values of non-marker significant pathways for natural attenuation. ....	81
Table 4.14. k-values of non-marker significant pathways for biostimulation .....	85
Table 4.15. k-values of non-marker significant pathways for bioaugmentation.....	89
Table 4.16. Selected studies on machine learning applications .....	89
Table 4.17. Degradation rate constants of eight pathways different studies.....	89

## ABBREVIATIONS

PBDE	Polybrominated diphenyl ether
POPs	Persistent organic pollutants
PCBs	Polychlorinated biphenyls
ADM	Anaerobic Dehalogenation Model
ADM-IE	Anaerobic Dehalogenation Model – Integrated and Enhanced
SC	Stockholm Convention
EU	European Union
DW	Dry Weight
GC/MS	Gas chromatography/mass spectrometry
BFR	Brominated flame retardant
c-PentaBDE	Commercial pentabromodiphenylether
c-OctaBDE	Commercial octabromodiphenyl ether
DecaBDE	Decabromodiphenyl ether
BA	Bioaugmentation
RSD	Relative Standard Deviation
SVM	Support Vector Model
FNN	Feed Forward Neural Network
MSE	Mass Square Error
MEX	MATLAB Executable
SVR	Support Vector Regression
PAH	Polycyclic Aromatic Hydrocarbons
BS	Biostimulation
NA	Natural Attenuation
DDT	Dichlorodiphenyltrichloroethane
Koc	Organic carbon-water partitioning coefficient
Kow	Octanol-water partitioning coefficient
US EPA	United States Environmental Protection Agency
SP	Significant Pathway
NC	Negative Control
SC	Sterile Control

# CHAPTER 1

## INTRODUCTION

Polybrominated Diphenyl Ethers (PBDEs) have gained attention due to their widespread use as flame retardants and their classification as Persistent Organic Pollutants (POPs) under the Stockholm Convention (Stockholm Convention, 2024). These compounds, which have been added to plastics, textiles, and electronics, are of concern due to their persistence, and toxicity (Hu and Hornbuckle 2010). Once released into the environment, PBDEs undergo slow degradation processes. The degradation of PBDEs, primarily through microbial dehalogenation, results in the formation of lower-brominated congeners (C. Zhao et al. 2018). While this process can reduce the overall bromine content, some daughter products may still be persistent and toxic (Linares, Bellés, and Domingo 2015). Hence, the persistence or toxicity of both the parent and daughter compounds in soils, sediments, and biota continues to be a significant challenge for environmental management (J. Li et al. 2014).

Given the persistence of POPs like PBDEs, efforts to remediate contaminated sites often focus on bioremediation techniques that stimulate microbial degradation. These methods, including biostimulation and bioaugmentation, aim to enhance the activity of naturally occurring or introduced microorganisms capable of dehalogenation (Demirtepe and Imamoglu 2019a). While such approaches show promise, ongoing research is needed to better understand the long-term effects of microbial degradation, the environmental fate of degradation products, and the effectiveness of different remediation strategies (Karakas, Aksoy, and Imamoglu 2020).

To facilitate the understanding of the fate of PBDEs in complex environments like sediments, modeling approaches have proven useful. Previous studies developed and improved mathematical models to identify possible dehalogenation pathways for halogenated organic compounds (Demirtepe 2012, 31; Karakas 2016, 52-5). Specific pathways were determined by the model as the dominant pathways in the environment (Demirtepe et al. 2015), and degradation rate constants were estimated for dehalogenation pathways resulting in the production of less toxic compounds (Karakas 2016, 55).

However, the models had some limitations, which need to be improved to obtain more comprehensive predictions on the fate of persistent compounds.

The aim of the present study was to improve the computational model for dehalogenation of POPs in contaminated sediments. The model improved in this study was a modified version of the “anaerobic dechlorination model” previously developed by Demirtepe (2012). The specific objectives of the study were:

1. To modify the previously developed anaerobic dehalogenation model, combining the prior model runs into a single MATLAB-based model allowing for a user-friendly version, and predicting the degradation rate constants of dehalogenation pathways in which the congeners measured in the experimental setup appeared
2. To incorporate machine learning algorithms to predict the degradation rate constant of dehalogenation pathways in which the congeners not measured in the experimental setup appeared
3. To apply the model on three test microcosms mimicking bioremediation of PBDEs in sediments and two control microcosms; by this way, a comparison of the dehalogenation of PBDEs under different environmental conditions was achieved.
4. To provide information on the fate of toxic or bioaccumulative PBDE congeners, and present recommendations for the PBDE congeners to be monitored in the sediments.

The microcosm dataset utilized in this study has not been previously used in any degradation rate prediction model. The application was deemed a novel aspect of this study in that a comprehensive list of PBDE dehalogenation pathways could be achieved. Furthermore, a comparative evaluation of different bioremediation methods enabled the observation of pathways, specific to the method applied. Some pathways identified by the model have not been previously reported in the literature, and consequently, the degradation rates of these pathways have not been investigated before. Moreover, this study addressed a gap in the literature by employing machine learning to define degradation rate constants for PBDEs using bioremediation methods such as natural attenuation, biostimulation, and bioaugmentation. In this context, modeling studies facilitate the understanding of the dehalogenation of POPs since only experimental observations may not be enough to calculate the rate constants in the environment where not all congeners can be measured, and dehalogenation pathways occur simultaneously. Previous studies have not applied machine learning to predict PBDE degradation rates, nor has machine learning been integrated into the previously developed ADM model.

In chapter 2, the general characteristics of PBDEs, and their environmental degradation were explained. Especially, biodegradation methods and degradation mechanism on the PBDEs were presented in detail. Moreover, anaerobic dehalogenation model history was summarized.

In chapter 3, the microcosm data was presented with PBDEs initial and final concentrations. Additionally, the artificial data sets prepared for validation of the developed model were presented. The “anaerobic dehalogenation model-integrated and enhanced” and machine learning methods were detailed in this chapter.

In chapter 4, the results of model validation with artificial data sets, and microcosm data set results were presented, evaluated, and discussed. Lastly, the degradation rates derived from this study were compared to the available literature values.

In chapter 5, the conclusions derived from the execution of the anaerobic dehalogenation model-integrated and enhanced to the microcosm data sets were given.

## CHAPTER 2

### LITERATURE REVIEW

#### 2.1. Persistent Organic Pollutants (POPs)

POPs are a class of highly toxic chemicals that resist environmental degradation through chemical and biological processes (Jones and de Voogt 1999). Their persistence in the environment allows them to bioaccumulate in the fatty tissues of organisms, biomagnify through food chains, and ultimately pose significant risks to human health and ecosystems (Wu et al. 2024). POPs include a wide range of substances, such as polychlorinated biphenyls (PCBs), dioxins, furans, and PBDEs, which have been used, and produced in various industrial and commercial applications (Ochs et al. 2024). Due to their persistency, POPs can remain in the environment for extended periods and are subject to long-range transport, resulting in their global distribution (Hale et al. 2006).

The Stockholm Convention has identified and regulated several classes of POPs due to their persistence, bioaccumulation, and potential for long-range environmental transport (Stockholm Convention 2024). All POPs listed under the Stockholm Convention are presented in Table 2.1.

Table 2.1. Stockholm convention categorization on POPs.

<b>Pesticide</b>	<b>Industrial Chemicals</b>	<b>Unintentional Production</b>
Aldrin	Decabromodiphenyl ether	Hexachlorobenzene
Chlordane	Dechlorane Plus	Hexachlorobutadiene
	Hexabromobiphenyl	Pentachlorobenzene
Dieldrin	Hexabromocyclododecane	Polychlorinated-biphenyls
Endrin		
Dicofol		

(cont. on next page)

**Table 2.1 (cont.)**

Alpha-Hexachlorocyclohexane	Perfluorooctanoic acid
Beta-Hexachlorocyclohexane	Perfluorohexane sulfonic acid
Dicofol	Short-chain chlorinated paraffins
Methoxychlor	Tetrabromodiphenyl ether
Mirex	Pentabromodiphenyl ether
Pentachlorobenzene	UV-328
Pentachlorophenol	Perfluorooctane sulfonyl-fluoride
Perfluorooctane-sulfonic acid	
DDT	

The global threat posed by POPs, highlights the need for stringent environmental management and regulatory measures (O’Sullivan and Sandau, 2014). International agreements such as the Stockholm Convention aim to eliminate or restrict the production and use of POPs to minimize their adverse impact on human health and the environment. As research on the degradation mechanisms and remediation of POPs continues to evolve, understanding the behavior of POPs in the environment remains a critical component of efforts to mitigate the risks associated with these persistent pollutants (Eddy Y. Zeng 2015).

## 2.2. Polybrominated Diphenyl Ethers (PBDE)

PBDEs are a group of POPs. They are synthetic chemicals and do not occur naturally in the environment. Structurally, PBDEs consist of two linked phenyl rings, each with attached bromine atoms as presented in

Figure 2.1, and are represented by the general formula  $C_{12}H_{(10-x)}Br_xO$ , where 'x' indicates the number of bromine atoms substituted, which can vary up to 10. This

variation allows for the existence of 209 possible congeners. The congeners are numbered according to the International Union of Pure and Applied Chemistry (IUPAC), regarding the presence and position of bromines in the diphenyl ether structure. Based on the number of bromines in the structure, PBDEs constitute ten homolog groups: mono-, di-, tri-, tetra-, penta-, hexa-, hepta-, octa-, nona-, and deca-BDE.

The first commercial productions of PBDEs began in the 1970s in Germany (Fromme et al. 2009). They were produced as mixtures of various congeners, and according to the presence of homolog groups, they were named as penta-BDE mixture, octa-BDE mixture, and deca-BDE mixture. The production of PBDE congeners has been restricted by the Stockholm Convention. The specific PBDE congeners that are regulated under the Stockholm Convention include penta-BDEs used mostly in furniture and mattresses, octa-BDE used widely in plastics and electronics, and deca-BDE used in textiles and electronics (Law et al. 2014). Until their ban, they have been produced as 67,125 metric tons (13% penta-, 5.7% octa- and 82% deca-BDEs) (Siddiqi, Laessig, and Reed 2003). They were used as an additive flame retardant and had a variety of applications including in plastics/polymers/composites, textiles, adhesives, sealants, coatings and inks. PBDEs containing plastics are used in paints, plastics, foam furniture padding, textiles, rugs, curtains, televisions, building materials, airplanes and automobiles (Siddiqi, Laessig, and Reed 2003). PBDEs are released into the environment during their manufacturing and processing, throughout the service life of products that contain PBDEs and when these products are disposed of.

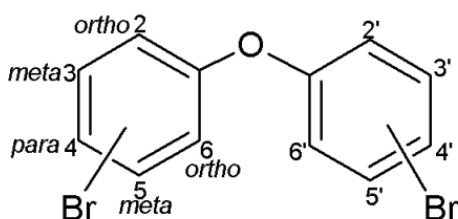


Figure 2.1. General structure of PBDEs.

### 2.3. Physical and Chemical Properties of PBDEs

The terms ortho, meta, and para are prefixes used in organic chemistry to indicate the position of non-hydrogen substituents on a hydrocarbon ring as displayed (Figure 2.1.). The stereochemistry of PBDEs is significant in determining their behavior and interaction with biological systems (Schwarzenbach 2003). For example, PBDEs with ortho-substituted bromines create steric hindrance, preventing the phenyl rings from rotating freely and resulting in a nonplanar configuration. This structural characteristic can affect their binding affinity to biological receptors, influencing their toxicological profile (Ji et al. 2011).

Table 2.2. Properties of PBDEs (Source: EPAWEB 1.0 2023; USEPA 2022).

25 °C	BDE-209	BDE-100	BDE-99	BDE-47
<b>Formula</b>	C <sub>12</sub> Br <sub>10</sub> O	C <sub>12</sub> H <sub>5</sub> Br <sub>5</sub> O	C <sub>12</sub> H <sub>5</sub> Br <sub>5</sub> O	C <sub>12</sub> H <sub>6</sub> Br <sub>4</sub> O
<b>Molar mass</b>	959.17g/mol	564.69g/mol	564.69g/mol	485.80g/mol
<b>Density</b>	3.0 g/cm <sup>3</sup>	2.3 g/cm <sup>3</sup>	2.3 g/cm <sup>3</sup>	2.3 g/cm <sup>3</sup>
<b>Solubility</b>	2.84x10 <sup>-11</sup> mg/L	7.86x10 <sup>-5</sup> mg/L	0.0004 mg/L	0.0015 mg/L
<b>Vapor PA</b>	6.23x10 <sup>-6</sup> Pa	3.25x10 <sup>-6</sup> Pa	1.44x10 <sup>-4</sup> Pa	3.21x10 <sup>-5</sup> Pa
<b>Henry's law</b>	1.1x10 <sup>-3</sup> atm.m <sup>3</sup> /mol	3.54x10 <sup>-6</sup> atm.m <sup>3</sup> /mol	3.54x10 <sup>-6</sup> atm.m <sup>3</sup> /mol	8.48 x 10 <sup>-6</sup> atm.m <sup>3</sup> /mol
<b>Log Kow</b>	12.11	7.66	7.66	6.7
<b>Boiling P.</b>	589.7 °C	436.21 °C	436.21 °C	405.51 °C
<b>Melting P.</b>	254.37 °C	182.80 °C	182.80 °C	161.73 °C
<b>Main property</b>				
Organic Particle Matter	Hydrophobic		Insoluble	

The Table 2.2 presents the molecular and physical properties of four PBDE congeners, including BDE-209, BDE-100, BDE-99, and BDE-47. These PBDE congeners vary in their degree of bromination and other characteristics, influencing their environmental behavior, persistence, and toxicity.

As the degree of bromination increases, solubility in water and vapor pressure decreases, while the partition coefficient ( $K_{ow}$ ) increases. For instance, BDE-209, with its high bromination, has extremely low water solubility and the lowest vapor pressure, making it highly hydrophobic and less volatile as indicated in Table 2.2. In contrast, lower-brominated congeners, such as BDE-47, show higher solubility and greater vapor pressure. The increasing log  $K_{ow}$  values with higher bromination, from 6.77 for BDE-47 to 12.11 for BDE-209, indicate a greater potential for accumulation of heavily brominated compounds in organic-rich systems.

Chemically, PBDEs are stable compounds, resistant to thermal degradation and chemical reactions under normal environmental conditions (Karakas and Imamoglu 2016). This stability, while beneficial for their role as flame retardants, also makes them POPs. Over time, PBDEs can bioaccumulate in the food chain, posing risks to human health and the environment (Hale et al. 2006). Based on the bioaccumulation factor (BAF) values presented in (B. Zhu et al. 2014), BDE-47 and 99 demonstrate the highest potential for bioaccumulation. The calculated BAF for BDE-47 is approximately  $1.3 \times 10^6$  mL/g dry weight, and for BDE-99, it is around  $1.4 \times 10^6$  mL/g dry weight. These high values indicate a significant ability to accumulate in organisms, particularly in aquatic environments, with BDE-47 showing the strongest bioaccumulation potential among the studied congeners (Gustafsson et al. 1999).

## **2.4. Occurrence of PBDEs in the environment**

PBDEs have become ubiquitous in various environmental matrices including air, water, soil, and biota. They have been detected worldwide, with higher concentrations often found in areas near industrial activities (Sun et al. 2020). The concentrations of PBDEs in sediments, soils, and sludge samples from around the world are presented in Table 2.3.

Table 2.3. The concentration of PBDEs in solid matrices.

<b>Medium</b>	<b>Concentration</b>	<b>PBDE</b>	<b>Reference</b>
Digested sludge	537.2 ng/mL	Deca- BDE	(Gerecke et al. 2005)
Soil in waste dumpsites	9.47 ng/g dw 23.4 ng/g dw 17.8 ng/g dw	BDE-28 BDE-153 BDE-183	(Oloruntoba et al. 2021)
Soil	138 ng/g dw 55 ng/g dw	BDE-209 BDE-47	(Song et al. 2015)
Soil	40 ng/g dw 70 ng/g dw	BDE-28 BDE-209	(Nyholm, Lundberg, and Andersson 2010)
Sediment	32.5 ng/g dw	BDE-209	(Toms et al. 2006)
Soil	770 ng/g dw	BDE-209	(McGrath et al. 2016)

The environmental PBDE concentrations are critical for understanding their environmental distribution and identifying their potential sources. Specifically, the levels of PBDEs detected in digested sludge samples from wastewater treatment plants provide valuable insights into the behavior of these compounds during treatment processes and highlight possible points of release.

## 2.5. Degradation of PBDEs in the environment

PBDEs are persistent in the environment, but their degradation primarily occurs through reductive dehalogenation, especially under anaerobic conditions. Anaerobic dehalogenation, particularly for POPs, offers a promising solution by using specific microorganisms capable of attacking carbon-halogen bonds of these pollutants (J. Li et al. 2014). This mechanism is also valid for other halogenated organic pollutants, such as PCBs, trichloroethylene, etc. (Bedard 2003). The reductive dehalogenation reaction involves the removal of the one bromine atom from the PBDE structure and its replacement with hydrogen atom. This process is catalyzed by anaerobic bacteria, such

as *Dehalococcoides* spp., in the presence of specific enzymes under physiological conditions. Like similar halogenated organic compounds, PBDEs serve as the terminal electron acceptor in anaerobic dehalogenation process, and hence get reduced during this reaction. The electron donors of dehalogenation reactions may be simple organic acids or complex substrates, including hydrogen, methane, acetate and compost leachate (Fennell and Gossett 2003). These can be inherently found in the environment or added when applying bioremediation.

The degradation of halogenated organic compounds was found to be influenced by various environmental factors, including the initial contaminant concentration, the presence of electron donors and the microbial community. In previous studies, initial contaminant and microbial concentrations were observed to affect the degradation, and first order kinetics have been commonly used (Cho et al. 2003; Siebielska and Sidełko 2015; Lombard et al. 2014). Table 2.4 presents the biodegradation of PBDE under anaerobic conditions.

During anaerobic dehalogenation of PBDEs, highly brominated congeners like BDE-209 are transformed into less brominated congeners, such as BDE-99 and BDE-47 via sequential dehalogenation reactions (L. K. Lee and He 2010). In anaerobic sediments, this process was observed to be slow extending over several years (Tokarz et al. 2008). The reactions can be categorized depending on the position of the removed bromine atoms (meta, ortho, or para). For instance, when a bromine atom is removed from the para position, the resulting compound is BDE-17, and when the bromine is removed from the ortho position, it forms BDE-28 (Figure 2.2).

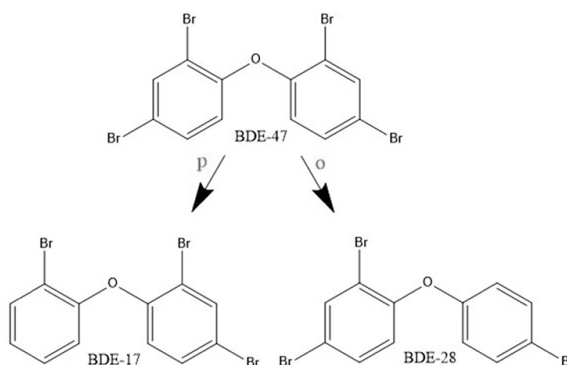


Figure 2.2. The pathway of BDE-47 degradation under anaerobic conditions.

Table 2.4. PBDE degradation rate constants ( $k$ ) following the first-order kinetics (Source: C. Zhao et al. 2018).

<b>Media</b>	<b><math>k(d^{-1})</math></b>	<b>Microcosm</b>	<b>References</b>
Lake sediment	0.0025	without substrates	
	0.0049	with Na, formate, ethanol	(Demirtepe 2017, 153)
	0.0028	with bacteria	
River sediment	0.0220	without substrates	(C. Huang et al. 2014)
Sewage sludge	0.0011	incubated with-culture medium	(Shih, Chou, and Peng 2012)
Li-Ming sludge	0.0012		
Sewage sludge	0.0011	with primers	(Gerecke et al. 2005)
Lake Sediment	0.00013	with phosphate buffer, methanol, dextrose	(Tokarz et al. 2008)

The anaerobic dehalogenation reaction can be referred to a pathway. The anaerobic dehalogenation pathways depend on factors such as the structure and halogenation pattern of the pollutants, the availability of electron donors, and the environmental conditions that support microbial activity (Demirtepe 2017, 153-59). The anaerobic dehalogenation pathways are expected to produce less toxic forms (S. Zhao et al. 2022). By this way, microbial processes can lead to a reduction in their overall toxicity.

Table 2.5, presents the anaerobic dehalogenation pathways of PBDEs, taken from several studies in literature (Tokarz et al. 2008; X. Zhu et al. 2019; Liu et al. 2022). The 'Pathway' columns represent the PBDE dehalogenation pathways. The 'Structure' columns show the structure of PBDEs appear in the pathways, involving the position of the bromine atoms on the PBDE congeners.

Table 2.5. Anaerobic degradation pathways of PBDEs.

Reference		(Tokarz et al. 2008)		(X. Zhu et al. 2019)				(Liu et al. 2022)			
Pathway		Structure		Pathway		Structure		Pathway		Structure	
209	208	23456-23456	23456-2356	208	202	23456-2356	2356-2356	209	208	23456-23456	23456-2356
209	207	23456-23456	23456-2346	208	199	23456-2356	2356-2345	209	207	23456-23456	23456-2346
209	206	23456-23456	23456-2345	206	199	23456-2345	2356-2345	208	202	23456-2356	2356-2356
207	197	23456-2346	2346-2346	206	194	23456-2345	2345-2345	208	201	23456-2356	2345-2356
207	196	23456-2346	2345-2346	202	178	2356-2356	2356-235	207	201	23456-2346	2345-2356
206	196	23456-2345	2345-2346	201	188	2345-2356	2356-246	207	197	23456-2346	2346-2346
197	184	2346-2346	2346-246	201	175	2345-2356	2346-235	207	196	23456-2346	2345-2346
197	184	2346-2346	2346-246	201	177	2345-2356	2356-234	206	196	23456-2345	2345-2346
196	184	2345-2346	2346-246	199	193	2356-2345	2356-345	206	203	23456-2345	23456-245
196	183	2345-2346	2346-245	199	177	2356-2345	2356-234	203	183	23456-245	2346-245
184	154	2346-246	246-245	199	172	2356-2345	2345-235	203	181	23456-245	23456-24
184	153	2346-246	245-245	197	171	2346-2346	2346-234	196	182	2345-2346	2345-246
183	154	2346-246	246-245	196	182	2345-2346	2345-246	196	183	2345-2346	2346-245
154	99	246-245	245-24	196	171	2345-2346	2346-234	183	139	2346-245	2346-24
154	118	245-246	246-34	194	180	2345-2345	2345-245	181	166	23456-24	23456-4
154	100	246-245	246-24	194	172	2345-2345	2345-235	157	108	234-345	234-45
153	99	245-245	245-24	191	161	2346-345	2346-35	157	105	234-345	234-34
100	47	246-24	24-24	188	150	2356-246	236-246	156	105	2346-345	234-34
99	66	245-24	24-34	184	150	2346-246	236-246	153	99	245-245	245-24
99	47	245-24	24-24	183	144	2346-245	2346-25	139	85	2346-24	234-24
99	49	245-24	24-25	182	154	2345-246	246-245	138	85	234-245	234-24
49	17	24-25	24-2	180	146	2345-245	235-245	119	71	246-34	26-46
47	17	24-24	24-2	180	153	2345-245	245-245	118	66	2346-245	24-34
47	28	24-24	24-4	178	133	2356-235	235-235	99	66	245-24	24-36
28	15	24-4	4-4	175	161	2346-235	2346-35	85	47	234-24	24-24
17	4	24-2	2-2	175	144	2346-235	2346-25	71	33	26-46	2-34
15	3	4-4	4	172	146	2345-235	235-245	66	33	24-34	2-34
4	1	2-2	2	172	133	2345-235	235-235	49	25	24-25	24-3
3	-	4	-	171	128	2346-234	234-234	47	28	24-24	24-4
1	-	2	-	154	102	246-245	245-26	33	8	2-34	2-4
				154	103	246-245	246-25	33	12	2-34	34
				153	101	245-245	245-25	30	8	246	2-4
				146	92	235-245	235-25	30	7	246	24
				144	103	2346-25	246-25	25	7	2-4	24
				133	92	235-235	235-25	17	4	24-2	2-2
				101	52	245-25	25-25	8	3	2-4	4
				92	52	235-25	25-25	8	3	2-4	4
								8	1	2-4	2

## 2.6. Remediation

Remediation refers to the broad range of methods employed to reduce, remove, or neutralize contaminants from environmental media, such as soil, water, and air. The primary objective of remediation is to restore ecosystems to safe and healthy conditions by mitigating the adverse effects of pollutants. Remediation techniques can be classified into physical, chemical, and biological approaches, depending on the nature of the contamination and the environmental context.

- **Physical Remediation:** This involves physically remove or isolate contaminants including methods such as soil excavation, sediment dredging, and thermal desorption. These techniques are often employed in sites where contamination is concentrated and pose immediate risks to human health and the environment (Suthersan et al. 2016, 32).
- **Chemical Remediation:** Chemical processes, such as oxidation, reduction, or neutralization, are used to transform hazardous contaminants into less toxic or inert forms. For example, chemical oxidants like hydrogen peroxide or potassium permanganate may be applied to degrade organic pollutants, including polycyclic aromatic hydrocarbons (PAHs) and chlorinated solvents, through chemical reactions (Suthersan et al. 2016, 33).
- **Biological Remediation (Bioremediation):** This approach utilizes the metabolic processes of microorganisms, plants, or enzymes to degrade or transform environmental contaminants into less harmful substances. Bioremediation offers a more sustainable and environmentally friendly option compared to physical and chemical methods, often enabling in situ treatment of pollutants (Suthersan et al. 2016, 34).

In many cases, a combination of these approaches, referred to as integrated remediation, may be necessary to achieve effective clean-up, especially when dealing with complex mixtures of contaminants (Suthersan et al. 2016, 34-5). The selection of the most appropriate remediation strategy is contingent on several factors, including the type and concentration of contaminants, site characteristics, and the time frame available for remediation.

## 2.7. Bioremediation

Bioremediation is the use of microorganisms for the removal of contaminants by degradation or transformation of pollutants. It offers a more sustainable and environmentally friendly approach to dealing with POPs (Omokhagbor et al. 2020). Microorganisms or plants are employed to break down these persistent compounds into less harmful substances through biological processes. While bioremediation may take longer than traditional methods, it is often more cost-effective, minimizes environmental disturbance, and can be applied and treating contaminants directly at the pollution site without excavation or transport (Omokhagbor et al. 2020).

There are three types of bioremediation techniques that are generally employed for contaminated environmental media, namely natural attenuation, biostimulation, and bioaugmentation.

- Natural attenuation (NA) refers to processes by which contaminants in the environment are reduced or degraded without human intervention. This can occur through various mechanisms such as microbial degradation, volatilization, sorption, or chemical transformation. Essentially, natural attenuation harnesses existing biological, chemical, and physical processes in the environment to mitigate contaminant levels over time (Schnoor 2006, 356-88).
- Biostimulation (BS) is the addition of substrates to enhance the activity of indigenous microorganisms when they show little or no degradation activity, by creating conditions necessary for their activity (Omokhagbor et al. 2020).
- Bioaugmentation (BA) is the introduction of degrading microorganisms (or fungi, genes, enzymes) enriched from the same or another site to degrade target pollutants, if the microbial activity is insufficient for intrinsic degradation at the site (Reible 2014).

## 2.8. Modelling efforts on dehalogenation of halogenated POPs

Computer programs and modeling play a crucial role in environmental science, particularly in studying contaminant behavior, degradation pathways, and risk assessments. In the context of POPs such as PBDEs and PCBs, computational models provide a powerful tool for simulating the fate and transport of these compounds in various environmental media, such as air, water, soil, and sediments. By utilizing mathematical models and numerical simulations, researchers can predict how pollutants move through ecosystems, interact with environmental factors, and how long they persist (Sarigiannis, Stratidakis, and Karakitsios 2024).

Several types of modeling approaches can be employed, including kinetic models to describe degradation rates and compartmental models to simulate the distribution of pollutants among different environmental compartments (e.g., water, sediment, and biota) (Valerio 2014). These models often rely on input data from laboratory experiments, field measurements, and physicochemical properties of the pollutants, such as solubility, vapor pressure, and partition coefficients (Valerio 2014). In PBDE degradation studies, models such as quantitative structure-activity relationship (QSAR) models can help predict the biodegradability of different congeners by relating their molecular structure to their environmental fate. By combining laboratory data with computer-based models, researchers can optimize remediation strategies, assess long-term ecological risks, and guide environmental policies more effectively (Peter et al. 2019).

Similar to PBDEs, PCBs degrade through reductive dehalogenation mechanism. Anaerobic dehalogenation models for PCBs and PBDEs, often rely on kinetic data from laboratory experiments and numerical simulations to predict the transformation rates of PCB congeners under anaerobic conditions. For instance, models developed for PCBs use degradation pathways and microbial community dynamics to simulate the dehalogenation process of highly chlorinated congeners into less chlorinated and potentially less toxic forms (Karakas 2016, 36).

For dehalogenation of halogenated POPs, a model named “Anaerobic Dechlorination Model” (ADM) was developed by Imamoglu (2001) to simulate the reductive dehalogenation PCBs. The ADM model focuses on predicting the degradation pathways of PCBs and congener distributions in environmental samples. Over time, this

model has been modified and improved by various researchers, including (Demirtepe 2012; Karakas 2016), to enhance its accuracy and adaptability to different environmental conditions.

## **2.9. Description of Terminology**

Before explaining the anaerobic dehalogenation model-integrated and enhanced (ADM-IE), it is important to first clarify some key terms related to this subject.

### **2.9.1. Coeluting congener**

There are 209 different PBDE congeners, and during their analytical detection, they appear as peaks on a chromatogram. In these chromatograms, a peak can represent either a single congener or a group of congeners. When multiple congeners are detected within the same peak during chromatographic analysis, they are referred to as coeluting congeners. These coeluting congeners are indicated by slashes between their congener numbers.

### **2.9.2. Dehalogenation pathway**

Under anaerobic conditions, the process of converting one PBDE congener into another, known as dehalogenation pathways or reactions, involves the transformation of a congener into a product congener. These dehalogenation pathways generally do not happen individually but are observed to occur simultaneously in the environment.

### **2.9.3. Marker and non-marker congeners**

Although there are theoretically 209 possible PBDE congeners, approximately 100 are actually released into the environment based on the specific commercial PBDE mixtures utilized. Not all these 100 congeners are detectable in environmental samples. Therefore, researchers often choose specific PBDE congeners for analysis. These selected congeners, which are analyzed in a given sample, are referred to as marker congeners. The ones which were not analyzed in a sample are named non-marker congeners. Accordingly, the dehalogenation pathways involving marker congeners as both mother and daughter are called marker pathways. If a non-marker congener appears in a dehalogenation pathway, it is called a non-marker pathway.

### **2.9.4. Mother/daughter**

‘Mother-Daughter’ concept in organic chemistry refers to a parent compound (mother) and its transformation products (daughters). This terminology is often used in environmental chemistry and bioremediation studies, particularly when analyzing the degradation pathways of organic pollutants (Karakas 2016, 57).

- Mother compound: This is the original or primary chemical compound, typically a pollutant or contaminant, before it undergoes chemical, biological, or environmental transformation.
- Daughter compounds: These are the products formed when the mother compound degrades or transforms through various processes such as oxidation, reduction, hydrolysis, or microbial degradation. Daughter compounds can sometimes be more or less toxic or persistent than the mother compound.

In the context of bioremediation, monitoring both the degradation of mother compounds and the formation of daughter compounds is critical. While bioremediation efforts aim to reduce the toxicity and environmental persistence of pollutants, the incomplete degradation of mother compounds can result in the accumulation of harmful

daughter compounds, necessitating careful management of the remediation process (Karakas and Imamoglu 2016).

### 2.9.5. Linear Regression

Linear regression is a simple model that works well when the relationship between the input features and the target variable is approximately linear (Schneider, Hommel, and Blettner 2010). Moreover, a statistical method that models the relationship between a dependent variable and one or more independent variables is shown by a linear equation:

$$k_{value} = \beta_0 + \beta_1 x Mother + \beta_2 x Daughter + \beta_3 x React + \epsilon \quad (2.1)$$

" $\beta_0$ " is the intercept, " $\beta_1, \beta_2, \beta_3$ " are the coefficients that measure the contribution of each feature to the k-value, " $\epsilon$ " represents the error term or residual. The goal of the linear regression model is to find the values of " $\beta_0, \beta_1, \beta_2, \beta_3$ " that minimize the sum of squared residuals.

### 2.9.6. Model Training

Using data, a linear regression model was trained with the following input matrix shown in Equation 2-2 and the corresponding vector is shown in Equation 2.3.

$$X = \begin{matrix} mother_1 & daughter_1 & react_1 \\ mother_2 & daughter_2 & react_2 \\ \vdots & \vdots & \vdots \\ mother_n & daughter_n & react_n \end{matrix} \quad (2.2)$$

$$Y = \begin{matrix} kvalue_1 \\ kvalue_2 \\ \vdots \\ kvalue_n \end{matrix} \quad (2.3)$$

The model uses MATLAB's function, which fits a linear regression model to the data. During the training phase, the model estimates the coefficients " $\beta_0, \beta_1, \beta_2, \beta_3$ " that best describe the relationship between the features and the k-values.

### 2.9.7. Reaction Amount

In the context of the model, reaction amounts refer to the quantities of a substance that participate in or are transformed during a chemical reaction. Specifically, in processes such as anaerobic dehalogenation, reaction amounts represent the difference between the initial concentration of a congener (either a mother or daughter compound) and its concentration after the reaction has occurred. These values are crucial for understanding the extent of the reaction and are used in the model to calculate reaction rate constants (Demirtepe 2017, 52).

## 2.10. Anaerobic Dehalogenation Model

### 2.10.1. Description of Model

ADM model was developed by Imamoglu (2001). The original model was based on the minimization of the objective function of the sum of squares of differences between predicted and sample congener profiles. The model is based on two fundamental principles. First, it assumes that a mass balance exists between dehalogenated (mother) congeners and the accumulated (daughter) congeners. Second, only dehalogenation

pathways that have been confirmed by studies in the literature are considered (Karakas and Imamoglu 2016).

### 2.10.2. Model Development and History

The first version of the program was written in Fortran language by Imamoglu in 2001. It was later converted to MATLAB, with modifications by Bzdusek, who also updated the model in 2005 to calculate pathways simultaneously (Bzdusek 2005). In 2012, Demirtepe introduced further modifications, which considered all possible reactions and allowed for the evaluation of the results produced by the model. The most recent modification, carried out by Karakas in 2016, involved separately investigating the degradation rate constants. This improvement enabled a better evaluation of model results, especially when the overall congener profile changes were not significant. Moreover, the last version of the model calculated the first-order reaction rate constants for the dehalogenation reactions. The chronology of ADM development is shown in Figure 2.3.

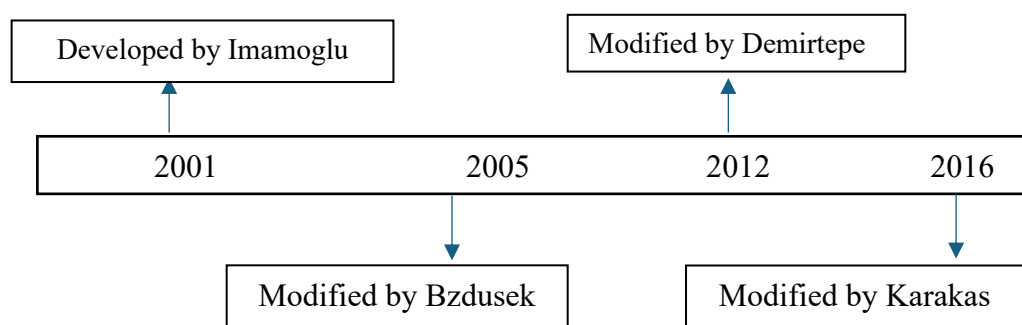


Figure 2.3. The chronology of ADM development and modification.

Table 2.6. Examination of models.

Status	Author	Year	Program	Enhancement	Limitations
Developed	Imamoglu	2001	Fortran	-	1.Old Computer Program 2.Degradation Rates 3.Pathway Quantification 4.Evaluating
Modification	Bzdusek	2005	MATLAB	Pathways Quantification	1.Degradation Rates 2.Evaluating
Modification	Demirtepe	2012	MATLAB	Evaluation of Results	1.Degradation Rates
Modification	Karakas	2016	MATLAB	First Order Degradation Rates Developed Evaluating	1.Degradation rates only for marker congeners

The modifications to ADM were made primarily due to certain limitations identified in earlier versions (Table 2.6). For instance, the Imamoglu model initially had four limitations, but Bzdusek's approach effectively addressed two of them. Similarly, Bzdusek's model was constrained by two limitations, one of which was later eliminated by Demirtepe's model, which also streamlined the process of evaluating results. Finally, Demirtepe's model had a remaining limitation that was successfully addressed in Karakas's model, leading to further refinement. The last version of the model also lacked the prediction of reaction rate constants for pathways involving non-marker congeners, which can actually occur in the environment.

## 2.11. Support Vector Machine Model

Support Vector Machines (SVMs) are a set of supervised machine learning algorithms used for classification and regression tasks. Originally designed for classification problems, SVMs can also be adapted for regression through a variant called Support Vector Regression (SVR), which is implemented in MATLAB with a function.

The model works by finding a hyperplane (or a decision boundary) that best separates data points into different categories, or in the case of regression, fits the data as closely as possible while remaining within a defined margin of error.

SVMs were first introduced by Vladimir Vapnik and Alexey Chervonenkis in the 1960s, but gained popularity in the 1990s as they were found to be effective for various practical problems in pattern and data perception. The core idea is to find an optimal hyperplane that separates data points in such a way that the margin between different classes (or the margin from the predicted line in regression) is maximized. The points that lie closest to the hyperplane and influence its position are known as support vectors (Smola and Schölkopf 2004).

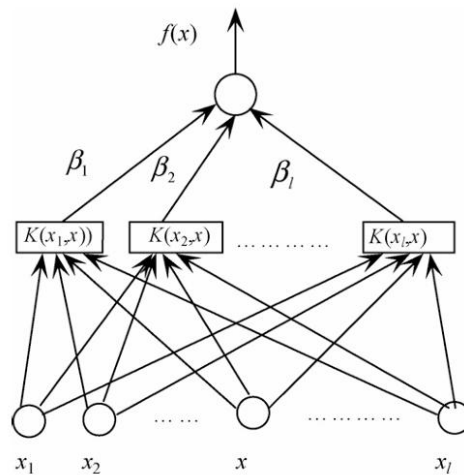


Figure 2.4. The structure of SVM (Source: Raghavendra N. and Deka 2014).

SVMs work with two main methods, classification, and regression. In classification, SVMs aim to find the hyperplane that separates two classes of data with the maximum margin. In cases where the data is not linearly separable, SVMs use a technique known as the kernel trick to transform the data into a higher-dimensional space where a linear separator can be found. For regression, SVMs are adapted into Support Vector Regression (SVR), where the goal is not to find a hyperplane that separates classes, but rather to find a function that approximates the output variable within a certain tolerance ( $\epsilon$ -margin). The model tries to fit the data points within a tube around the predicted function, and the support vectors are the data points that lie outside this tube

(Cortes and Vapnik 1995). Previous SVM studies for environmental applications are listed in Table 2.7.

Table 2.7. The application of SVM for the prediction of pollutants removal.

<b>Aim of study</b>	<b>Evaluation</b>	<b>Input</b>	<b>Output</b>	<b>Reference</b>
P, N pol.	$R^2 = 0.97-0.74$	pH, TN, TP	TN, TP Re.	(Xu et al. 2024)
Methylene - blue pollutant	$R = 0.99-0.97$	$C_{16}H_{18}ClN_3S$ , Conc. pH	$C_{16}H_{18}ClN_3S$ Removal	(Kooh, Dahri, and Lim 2018)
Biowastes	$R^2 = 0.87$	food waste	Biogas	(De Clercq et al. 2019)
Food waste	$R^2 = 0.74$	FS, COD, TN	Biogas	(C. Li et al. 2022)
Vegetable W.	$R^2 = 0.92$	pH, C°, VW	Biogas	(Yildirim and Ozkaya 2023)

$R^2$ : Coefficient of determination, R: Correlation coefficient, COD: Chemical Oxygen demand

TN: Total Nitrogen, TP: Total Phosphorus, VW: Vegetable waste, FS: Feedstock

SVMs offer several advantages. They are highly effective in dimensional spaces, making them particularly suitable for problems involving a large number of features. Additionally, SVMs are memory-efficient because they only utilize support vectors during the training process. Another key advantage is that SVMs perform well when the relationship between data is non-linear, allowing them to capture complex patterns in the dataset (Cortes and Vapnik 1995). SVMs have a wide range of applications across different fields. For instance, they are commonly used in text categorization and sentiment analysis, as well as image classification and face recognition tasks. In finance and bioinformatics, SVMs are employed for predictive modeling. Furthermore, SVMs are used for regression tasks, especially in cases where the data exhibits complex, non-linear relationships (Cortes and Vapnik 1995).

## 2.12. Neural Network Model

Neural networks are computational models inspired by the structure and functioning of the human brain. They consist of layers of interconnected nodes that process information through a series of mathematical transformations (Figure 2.5). Originally developed in the early 1940s, neural networks gained prominence in the 1980s and have since become a powerful tool in machine learning for a variety of tasks, such as classification, regression, image recognition, and natural language processing (Goodfellow, Bengio, and Courville 2016).

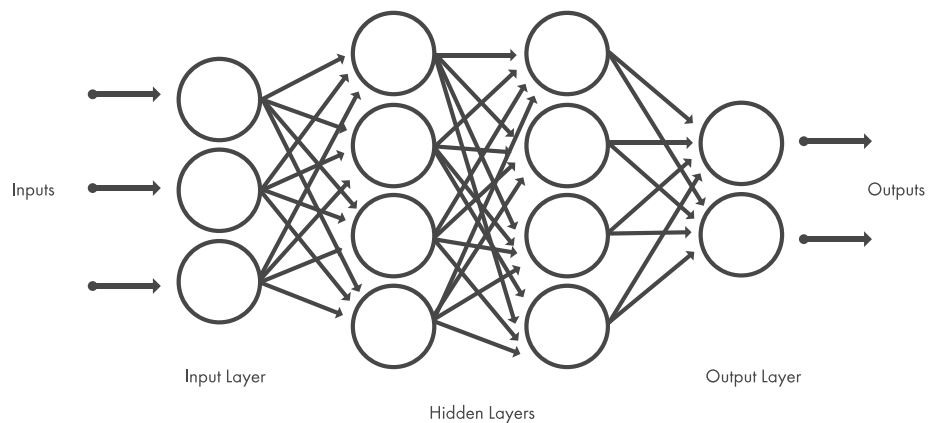


Figure 2.5. Typical neural network architecture (Source: The MathWorks 2024).

A neural network typically consists of three types of layers as a structure:

- **Input Layer:** Receives the input data
- **Hidden Layer(s):** Performs computations and feature extraction. These layers are fully connected, meaning each neuron in one layer is connected to every neuron in the next layer.

- **Output Layer:** Produces the final prediction or classification.

Each neuron in these layers processes data in the following way:

- **Weights:** Each input is multiplied by a weight.
- **Bias:** A bias term is added to the weighted input.

- **Activation Function:** The sum of the weighted inputs and bias is passed through an activation function that introduces non-linearity to the system.

Neural networks learn from data through a process called training. The workflow generally follows these procedures:

- **Forward Propagation:** The input data is passed through the layers of the network, where each neuron processes the data and passes it to the next layer. At the output layer, a prediction is made.
- **Loss Function:** After the network makes a prediction, the difference between the prediction and the true value (the error) is calculated using a loss function. In regression problems, this is the mean squared error (MSE).
- **Backpropagation:** The error is propagated backward through the network, and the weights and biases are adjusted using optimization techniques like gradient descent. This allows the network to "learn" by minimizing the error over time.
- **Updating Weights and Biases:** The weights and biases are adjusted iteratively during training to minimize the error between predicted and actual values. The goal is to reduce the error as much as possible, so the network can make accurate predictions.

#### Key Components of a Neural Network Model:

- **Neurons (Nodes):** Neurons are the building blocks of a neural network. Each neuron receives input from one or more neurons in the previous layer, applies a transformation (weight, bias, activation function), and passes the result to neurons in the next layer.
- **Weights:** Weights determine the strength of the connections between neurons. In a fully connected neural network, every neuron in one layer is connected to every neuron in the next layer, and each connection has an associated weight. These weights are learned during the training process and play a critical role in how the network processes input data.
- **Bias:** A bias term is added to the weighted sum of inputs before applying the activation function. This allows the model to better fit the data by adjusting the output independently of the input.
- **Activation Function:** The activation function introduces non-linearity into the model, which allows it to learn complex patterns. Common activation functions include:
  - a. **ReLU (Rectified Linear Unit),** which outputs 0 for negative inputs and passes positive inputs as they are. This is a popular activation function for hidden layers.

- b. Sigmoid maps the output to a value between 0 and 1. This is often used in the output layer for binary classification.
- c. Tanh is similar to sigmoid but outputs values between -1 and 1.
- Loss Function: The loss function is used to evaluate the effectiveness of neural networks. For regression tasks, equation 2.4 commonly used as the MSE (The MathWorks 2024e).

$$MSE = \sum_{i=1}^n (y_i - \hat{y}_i)^2 \quad (2.4)$$

Where  $y_i$  is the actual value and  $\hat{y}_i$  is the predicted value.

Backpropagation and gradient descent:

- Backpropagation is the process of computing the gradient of the loss function with respect to the weights and biases of the network.
- Gradient descent is then used to update these weights and biases in the direction that reduces the error. This is done iteratively until the error converges to a minimum.

There are many types of neural networks, but a few common ones are:

- Deep Neural Network (DNN): A neural network with many layers (often more than two hidden layers). These are sometimes referred to as deep learning models because of the depth of the network.
- Feedforward Neural Network (FNN): This is the simplest type of neural network, where the information flows in one direction—from input to output. There are no loops or any feedback. This is the type of network used in the present study.

Aim of using the neural networks model:

- Complexity: Neural networks are capable of modeling very complex relationships in data. In the present study, the relationship between mother, daughter, reaction amount, and reaction rate constant might be non-linear and difficult to capture using simple models like linear regression.
- Scalability: Neural networks can scale well with more data and features. If more input features are to be added in the future (such as temperature, pH, etc.), the neural network can accommodate them.
- Automatic Feature Learning: Instead of manual engineering features, neural networks can learn the important relationships between inputs and outputs during training.

### Challenges of Neural Networks:

- **Overfitting:** Neural networks can sometimes overfit the training data, especially if the network is very complex or the dataset is small. Regularization techniques such as dropout can help prevent overfitting.
- **Computation:** Neural networks, especially deep ones, require significant computational power. However, for smaller problems, like regression tasks, MATLAB should handle the computations efficiently.

The example structures of studies using the neural network method can be seen in Figure 2.6 and Figure 2.7 below.

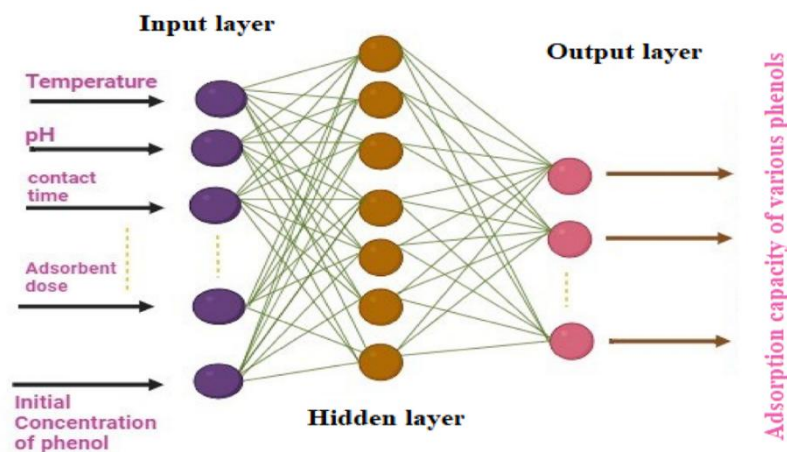


Figure 2.6. Structure of Neural Network (Source: Hafeez et al. 2024).

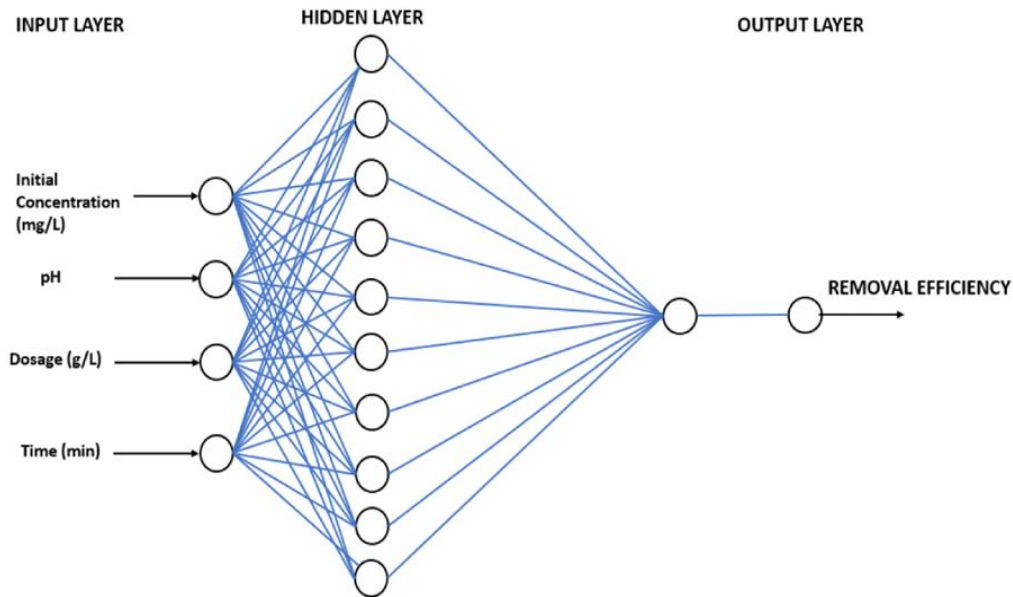


Figure 2.7. Structure of neural network (Source: Isah et al. 2024).

A Neural Network Model is a powerful tool for learning complex relationships in data. For specific cases of predicting degradation rate constants, it is well-suited because it can obtain non-linear relationships between the input variables, and the output (The MathWorks 2024e). It automatically adjusts its internal parameters to make accurate predictions and can be trained to improve its performance over time.

Applications of neural networks are widely used in various fields due to their flexibility and ability to model complex relationships. Some common applications include image and speech recognition, predictive modelling in finance and healthcare, language processing for text analysis and scientific research for regression tasks, such as predicting physical or chemical properties, which aligns with predicting degradation (Yadav et al. 2024). Previous studies on the degradation of contaminants in the environment using the neural network method are listed in Table 2.8.

Table 2.8. Previous studies on contaminant degradation using the neural network.

<b>Study</b>	<b>Location</b>	<b>Type</b>	<b>Pollutant</b>	<b>Input Parameters</b>
(Gardner 1999)	London	Air	$NO_x$ and $NO_2$	C°, visibility, PA
(Kukkonen 2003)	Helsinki	Air	$PM_{10}$ and $PM_{2.5}$	Air pollutant
(Mishra, Goyal, and Upadhyay 2015)	Delhi	Air	$PM_{2.5}$	$O_3$ , $NO_2$ , $SO_2$ , $CO$ , $PM_{2.5}$
(Ragosta, D'Emilio, and Giorgio 2015)	Italy	Air	CO and $SO_2$	Atm pressure
(Dunea, Pohoata, and Iordache 2015)	Romania	Air	$O_3$ , $NO_2$ , $PM_{10}$ , $PM_{2.5}$	Air pollutant
(Azid et al. 2014)	Malaysia	Air	$O_3$ , $CH_4$ , $PM_{10}$ , THC	Air pollutant
(Hafeez et al. 2024)	Pakistan	Water	$C_6H_6O$	C°, pH, $C_6H_6O$ conc.
(Isah et al. 2024)	India	Water	$C_6H_6O$	C°, pH, $C_6H_6O$ conc.

PM: Particulate matter, THC: Total Hydrocarbon

## CHAPTER 3

### METHOD

#### 3.1. PBDE data set

##### 3.1.1. Artificial data sets

Two small artificial datasets were generated to test the ADM-IE model. For the first artificial data set, the selection of congeners was based on their abundance in original mixtures, and relevant dehalogenation pathways. Congener concentrations were created randomly for the first dataset. Nine congeners were chosen as the measured inputs for the model (Table 3.1). These congeners are defined as markers. Input pathways were generated to represent different dehalogenation positions, and to assure appearance of some of the congeners more than once, and as a mother and daughter. For example, marker BDE-196 used as a daughter in the first pathway, was then used as a mother in the second pathway. Also, some markers are used twice as mothers and daughters. The dataset was selected in a computable quantity and hypothetically generated to evaluate the accuracy of the model. Hence, the concentration data and compounds did not represent real environmental data; however, the pathways were selected in accordance with the literature. The obtained reaction amounts were calculated by subtracting the difference between the initial and final concentrations after each degradation, corresponding to the amount directed to the subsequent compound. At certain points, multiple pathways necessitated estimation-based calculations for determining reaction amounts.

Table 3.1. First artificial data set input.

<b>Marker Congener</b>	<b>Initial Marker Conc. Mole ‰</b>	<b>Final Marker Conc. Mole ‰</b>
207	850	250
196	75	200
183	45	195
154	30	220
153	0	75
99	0	55
66	0	15
47	0	10
28	0	5
	T:1000	T:1000

T: Total amount.

Table 3.2 shows the pathways generated for the first artificial data set. The pathways among these congeners were generated to represent different dehalogenation positions. According to the input concentrations and dehalogenation pathways, the reaction amounts were calculated manually. Table 3.2 involves the reaction amounts, the initial and final PBDE congener concentrations, and the calculation method of first-order degradation rate constants (k-values). A specific lettering system has been used to make the calculations on the table easier to understand. The time ( $\Delta t$ ) used for the k-value calculation was assumed as 100 days. Table 3.2 also involves the degradation rate constants calculated manually.

Table 3.2. The first artificial data set calculations.

Marker congeners	Initial concentration (mole‰)	Final concentration (mole‰)	Pathway		
			Mother	→Daughter	
207	850	250	207	→196	625
196	75	200	196	→183	500
183	45	195	183	→154	200
154	30	220	183	→153	150
153	0	75	154	→99	10
99	0	55	153	→99	75
66	0	15	99	→66	20
47	0	10	99	→47	10
28	0	5	66	→28	3
			47	→28	2

A second artificial data set was generated using the same congeners and pathways as in the first data set, but with assumed congener concentrations based on the experimental microcosm data set. Hence, this dataset can be considered a more representative one to the experimental system conditions. Similar manual calculations were performed for this dataset, which can be seen in Table 3.3.

Table 3.3. The second artificial data set calculations.

Marker congeners	Initial concentration (mole‰)	Final concentration (mole‰)	Pathway		
			Mother	→Daughter	
207	1000	958	207	→196	42
196	0	6.14	196	→183	36
183	0	0.26	183	→154	18.4
154	0	0.56	183	→153	17.3
153	0	0.55	154	→99	18
99	0	18.64	153	→99	17
66	0	0.90	99	→66	16
47	0	14.6	99	→47	15
28	0	0.35	66	→28	0.15
			47	→28	0.20

### 3.1.2. Microcosm data set

Microcosm setups are experimental systems that simulate natural sediment conditions and often include treatments such as biostimulation or bioaugmentation to monitor the degradation of specific contaminants. This study used the data set of a microcosm setup aimed at investigating the biodegradation of PBDEs (Demirtepe and Imamoglu 2019b).

The sediments collected from Camkoru, National Park near Ankara, Turkey were artificially contaminated by BDE-209 in the laboratory. Then, they were used in the microcosms, designed to investigate three bioremediation scenarios, namely biostimulation (BS), bioaugmentation (BA), natural attenuation (NA) along with their control sets, i.e. negative, and sterile controls (Demirtepe and Imamoglu 2019b).

In the natural attenuation set, the sediments were supplied with only distilled water, while the biostimulation set used an organic medium to enhance the microbial activity in the sediments. In the bioaugmentation setup, a microorganism culture, grown in a liquid medium, was introduced into the sediments (Demirtepe 2017, 56). The negative control set was established to serve as a control for bioaugmentation set so that the effects of adding a culture medium without the cells can be observed. Hence, a spent growth medium was formed by passing the microorganism culture through 0.22  $\mu\text{m}$  filter so that no cells will remain in the medium. For the sterile control set, the microcosms were autoclaved at 120°C at 1.1 atm pressure for 20 min on three consecutive days to hinder any microbial activity in sediments. The details of the setup can be found in Table 3.4, which outlines the conditions for each reactor type and the corresponding treatment methods.

Table 3.4. Details of PBDE sediment microcosm sets (Source: Demirtepe 2017, 61).

<b>Reactor Type</b>	<b>Reactor Name</b>	<b>Liquid Ingredients</b>
Test	Natural Attenuation	DI water <sup>a</sup> (3.5mL.)
Microcosm	Biostimulation	e-donor & C source, organic medium (3.5mL) <sup>b</sup>
	Bioaugmentation	DF-1 culture <sup>c</sup> (0.5mL) + DI water <sup>a</sup> (3.0mL)
Control Microcosm	Negative Control	Spent growth medium (0.5mL) <sup>d</sup>
		+DIwater <sup>a</sup> (3.0mL)
	Sterile	DI water (3.5mL)

a: Distilled water.

b: Prepared as given in Berkaw et al. (1996) and supplied with sodium formate and ethanol.

c: Dehalobium chlorocoercia strain DF-1 culture.

d: DF-1 medium with no DF-1 cells, obtained by passing the culture medium through 0.22 µm filter.

Microcosms were prepared and operated under anaerobic conditions in dark. After the addition of sediments and the corresponding liquid ingredients to the 20 mL serum bottles, they were capped with crimped caps. Then, the bottles were flushed with high-purity nitrogen gas while allowing the headspace oxygen to be released into the atmosphere. This operation led to the establishment and maintenance of anaerobic conditions in microcosm bottles. During six months of incubation, periodic sampling was done on days 0, 20, 40, 60, 90, 120, 152, and 180 (Demirtepe 2017, 61-4). At each time point, only sediments were analyzed for PBDE congeners using gas chromatography-mass spectrometry. Nineteen PBDE congeners/congener groups (23 congeners with coelution) were analyzed.

Tables 3.5 to 3.9 presents the PBDE concentration changes during the operation of natural attenuation, biostimulation, bioaugmentation, negative control, and sterile set, respectively. They represent the average of parallel reactors for each time point. The concentrations were obtained in ng/g during the experiment; however, the model was based on mole per thousand (mole‰) concentration values. Therefore, the datasets were converted to mole‰, using as example calculation in Equation 3.1. The mole‰ concentrations are presented in Appendix B. The PBDE profiles of bioremediation microcosms are also illustrated in Figures 3.1., 3.2, and 3.3. Additionally, BDE congeners

198,199,200, and 203 coeluted in the microcosm dataset. For normalization and model calculations, the total concentration of these congeners were distributed equally among the coeluting ones. This method assumed that coeluting congeners were treated fairly within the model, distributing the detected concentration in a way that reflected the equal contribution of each congener to the peak.

$$\text{BDE 209}_{\text{mole}\%} = \left( \frac{\text{BDE}_{209} \left( \frac{\text{ng}}{\text{g}} \right) / \text{MW}_{\text{BDE}_{209}}}{\sum(\text{PBDEs in moles})} \right) * 10^3 \quad (3.1)$$

Table 3.5. Natural attenuation microcosm PBDE concentrations with time (ng/g).

<b>Time(day)</b>	<b>0</b>	<b>20</b>	<b>40</b>	<b>60</b>	<b>90</b>	<b>120</b>	<b>152</b>	<b>180</b>
<b>BDE-209</b>	628.30	636.25	625.20	632.66	409.31	426.04	418.43	434.06
<b>206</b>	5.01	8.81	15.92	20.77	11.34	17.29	16.43	28.90
<b>207</b>	2.79	3.31	6.49	8.05	4.82	21.23	16.37	14.65
<b>208</b>	0.00	1.76	3.02	6.76	2.57	10.12	6.70	8.75
<b>195</b>	0.00	0.00	0.63	0.42	0.46	0.00	0.35	0.00
<b>194</b>	0.00	0.00	0.98	0.27	1.34	0.00	0.70	0.00
<b>205</b>	0.00	0.00	0.00	0.00	0.00	0.00	0.00	0.00
<b>196</b>	0.00	0.00	0.56	0.75	0.66	2.19	1.53	0.74
<b>198<sup>a</sup></b>	0.00	0.00	0.58	0.36	0.72	0.39	0.49	0.83
<b>197<sup>b</sup></b>	0.00	0.00	0.37	0.14	0.50	1.44	0.58	0.72
<b>201</b>	0.00	0.00	0.25	0.33	0.44	0.21	0.34	0.56
<b>202</b>	0.00	0.00	0.23	0.64	0.92	0.04	0.27	0.52
<b>183</b>	0.00	0.00	0.00	0.00	0.00	0.00	0.00	0.00
<b>153</b>	0.00	0.00	0.00	0.00	0.26	0.00	0.00	0.16
<b>154</b>	0.00	0.00	0.00	0.00	0.16	0.00	0.24	2.26
<b>99</b>	0.00	0.00	0.00	0.00	0.14	0.51	0.00	0.57
<b>100</b>	0.00	0.00	0.00	0.00	0.20	0.48	0.00	0.31
<b>47</b>	0.00	0.00	0.00	0.00	0.00	0.00	0.00	0.00
<b>28</b>	0.00	0.00	0.00	0.00	0.00	0.00	0.00	0.00

a: BDE-198 coeluted with BDE-199, BDE-200, BDE-203.

b: BDE-197 coeluted with BDE-204.

Table 3.6. Biostimulation microcosm PBDE concentrations with time (ng/g).

Time(day)	0	20	40	60	90	120	152	180
<b>BDE-209</b>	725.46	657.88	612.68	535.20	422.45	368.98	359.68	324.50
<b>206</b>	8.86	17.98	15.87	15.99	10.90	17.98	10.34	24.45
<b>207</b>	3.07	21.60	5.63	5.49	3.89	21.60	8.82	11.06
<b>208</b>	0.00	11.76	2.78	2.55	2.21	11.76	3.90	6.03
<b>195</b>	0.00	0.00	0.00	0.12	0.00	0.00	0.00	0.00
<b>194</b>	0.00	0.00	0.70	0.17	0.27	0.00	0.00	0.08
<b>205</b>	0.00	0.00	0.00	0.00	0.00	0.00	0.00	0.00
<b>196</b>	0.00	2.66	0.39	0.15	0.20	2.66	0.40	0.44
<b>198<sup>a</sup></b>	0.00	0.28	0.38	0.19	0.25	0.28	0.27	0.57
<b>197<sup>b</sup></b>	0.00	0.11	0.18	0.30	0.00	0.11	0.12	0.16
<b>201</b>	0.00	0.05	0.18	0.46	0.24	0.05	0.00	0.05
<b>202</b>	0.00	0.00	0.29	0.00	0.00	0.00	0.00	0.00
<b>183</b>	0.00	0.00	0.25	0.00	0.11	0.00	0.00	0.00
<b>153</b>	0.00	0.00	0.08	0.00	0.08	0.00	0.55	0.09
<b>154</b>	0.00	0.00	0.22	0.00	0.08	0.00	0.22	0.02
<b>99</b>	0.00	0.51	0.00	0.00	0.11	0.51	0.39	0.30
<b>100</b>	0.00	0.40	0.13	0.14	0.23	0.40	7.80	0.27
<b>47</b>	0.00	0.00	0.20	0.00	0.11	0.00	6.25	0.00
<b>28</b>	0.00	0.00	0.00	0.00	0.00	0.00	0.00	0.00

Table 3.7. Bioaugmentation microcosm PBDE concentrations with time (ng/g).

Time(day)	0	20	40	60	90	120	152	180
<b>BDE-209</b>	675.83	628.14	605.06	575.75	490.07	474.69	467.55	404.25
<b>206</b>	8.84	8.90	18.93	16.83	11.77	24.96	8.65	25.55
<b>207</b>	5.27	3.34	7.71	5.78	4.38	23.43	7.77	11.91
<b>208</b>	0.00	0.00	3.65	2.80	2.30	12.45	3.53	6.23
<b>195</b>	0.00	0.00	0.00	0.00	0.00	0.00	1.31	0.00
<b>194</b>	0.00	0.00	0.15	1.36	0.77	0.00	0.47	0.67
<b>205</b>	0.00	0.00	0.00	0.00	0.00	0.00	0.00	0.00
<b>196</b>	0.00	0.00	0.19	0.93	0.38	1.39	0.58	0.74
<b>198<sup>a</sup></b>	0.00	0.00	0.24	0.58	0.50	0.80	0.35	0.82
<b>197<sup>b</sup></b>	0.00	0.00	0.05	0.35	0.36	1.05	0.34	0.90
<b>201</b>	0.00	0.00	0.12	1.13	0.28	0.36	0.11	0.46
<b>202</b>	0.00	0.00	0.12	0.37	0.33	0.47	0.05	0.08

(cont. on next page)

**Table 3.7 (cont.)**

<b>183</b>	0.00	0.00	0.00	0.00	0.00	0.00	0.00	0.00
<b>153</b>	0.00	0.00	0.12	0.00	0.00	0.00	0.78	0.00
<b>154</b>	0.00	0.00	0.00	0.00	0.00	0.00	1.42	0.04
<b>99</b>	0.00	0.00	0.00	0.00	0.13	0.58	2.20	0.00
<b>100</b>	0.00	0.00	0.22	0.24	0.18	0.40	4.58	0.13
<b>47</b>	0.00	0.00	0.17	0.10	0.00	0.00	2.02	0.00
<b>28</b>	0.00	0.00	0.00	0.20	0.00	0.00	0.00	0.15

Table 3.8. Negative control microcosm PBDE concentrations with time (ng/g).

<b>Time(day)</b>	<b>0</b>	<b>20</b>	<b>40</b>	<b>60</b>	<b>90</b>	<b>120</b>	<b>152</b>	<b>180</b>
<b>BDE-209</b>	680.06	556.02	552.75	548.85	533.46	525.25	516.34	468.31
<b>206</b>	7.35	8.51	15.68	11.64	10.31	26.16	9.75	21.78
<b>207</b>	1.33	4.50	5.79	4.29	4.09	30.16	11.39	11.14
<b>208</b>	0.00	1.12	2.68	2.25	2.07	16.36	4.91	6.02
<b>195</b>	0.00	0.00	0.00	0.00	0.00	0.00	0.00	0.00
<b>194</b>	0.00	0.00	0.00	0.00	0.00	0.00	0.00	0.00
<b>205</b>	0.00	0.00	0.00	0.00	0.00	0.00	0.00	0.00
<b>196</b>	0.00	0.00	0.22	0.31	0.22	1.41	0.41	0.36
<b>198<sup>a</sup></b>	0.00	0.00	0.00	0.32	0.26	1.06	0.48	0.67
<b>197<sup>b</sup></b>	0.00	0.00	0.21	0.00	0.26	1.79	0.45	0.74
<b>201</b>	0.00	0.00	0.00	0.29	0.25	0.61	0.00	0.50
<b>202</b>	0.00	0.00	0.00	0.00	0.00	0.00	0.00	0.00
<b>183</b>	0.00	0.00	0.00	0.00	0.11	0.00	0.00	0.18
<b>153</b>	0.00	0.00	0.00	0.00	0.21	0.00	0.00	0.00
<b>154</b>	0.00	0.00	0.00	0.00	0.00	0.28	0.33	0.28
<b>99</b>	0.00	0.00	0.00	0.00	0.11	0.54	0.36	0.14
<b>100</b>	0.00	0.00	0.00	0.27	0.15	0.46	2.92	0.00
<b>47</b>	0.00	0.00	0.00	0.00	0.00	0.00	1.61	0.00
<b>28</b>	0.00	0.00	0.00	0.00	0.00	0.00	0.00	0.00

Table 3.9. Microcosm data set, sterile profile microcosm (ng/g).

<b>Time(day)</b>	<b>0</b>	<b>20</b>	<b>40</b>	<b>60</b>	<b>90</b>	<b>120</b>	<b>152</b>	<b>180</b>
<b>BDE-209</b>	640.86	582.38	571.52	601.34	564.95	593.62	626.15	613.06
<b>206</b>	7.48	7.11	9.33	9.68	9.38	0.85	9.61	7.00
<b>207</b>	0.00	0.00	0.00	0.00	0.00	0.00	0.00	0.00
<b>208</b>	0.00	0.00	0.00	0.00	0.00	0.00	0.00	0.00
<b>195</b>	0.00	0.00	0.00	0.00	0.00	0.00	0.00	0.00
<b>194</b>	0.00	0.00	0.00	0.00	0.00	0.00	0.00	0.00
<b>205</b>	0.00	0.00	0.00	0.00	0.00	0.00	0.00	0.00
<b>196</b>	0.00	0.00	0.00	0.00	0.00	0.00	0.00	0.00
<b>198<sup>a</sup></b>	0.00	0.00	0.00	0.00	0.00	0.00	0.00	0.00
<b>197<sup>b</sup></b>	0.00	0.00	0.00	0.00	0.00	0.00	0.00	0.00
<b>201</b>	0.00	0.00	0.00	0.00	0.00	0.00	0.00	0.00
<b>202</b>	0.00	0.00	0.00	0.00	0.00	0.00	0.00	0.00
<b>183</b>	0.00	0.00	0.00	0.00	0.00	0.00	0.00	0.00
<b>153</b>	0.00	0.00	0.00	0.00	0.00	0.00	0.00	0.00
<b>154</b>	0.00	0.00	0.00	0.00	0.00	0.00	0.00	0.00
<b>99</b>	0.00	0.00	0.00	0.00	0.00	0.00	0.00	0.00
<b>100</b>	0.00	0.00	0.00	0.00	0.00	0.00	0.00	0.00
<b>47</b>	0.00	0.00	0.00	0.00	0.00	0.00	0.00	0.00
<b>28</b>	0.00	0.00	0.00	0.00	0.00	0.00	0.00	0.00

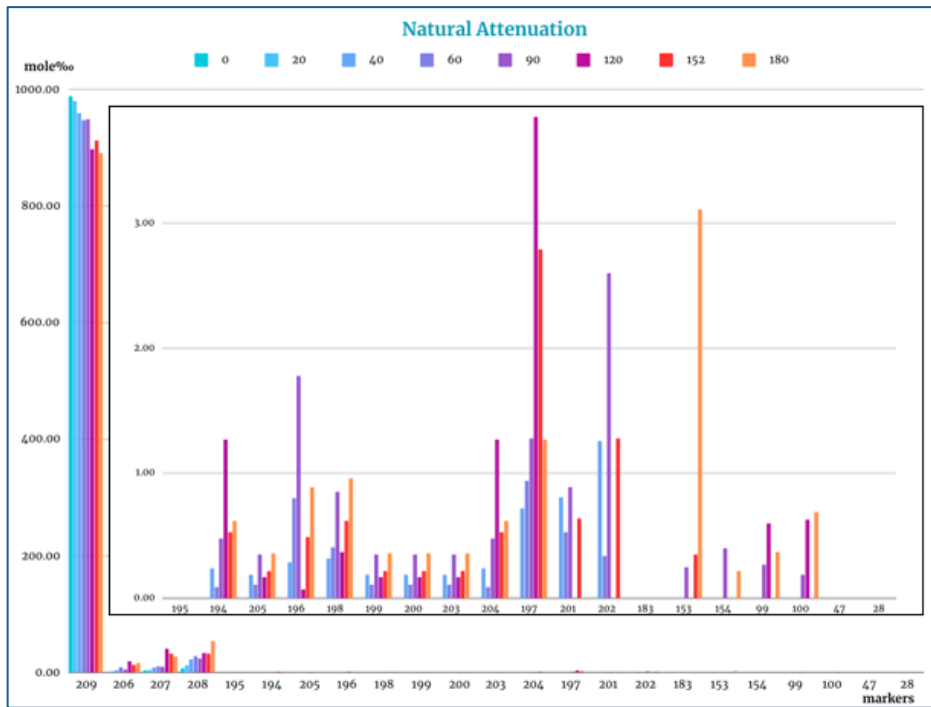


Figure 3.1. PBDE congener concentrations at sampling times in natural attenuation microcosm (mole%).

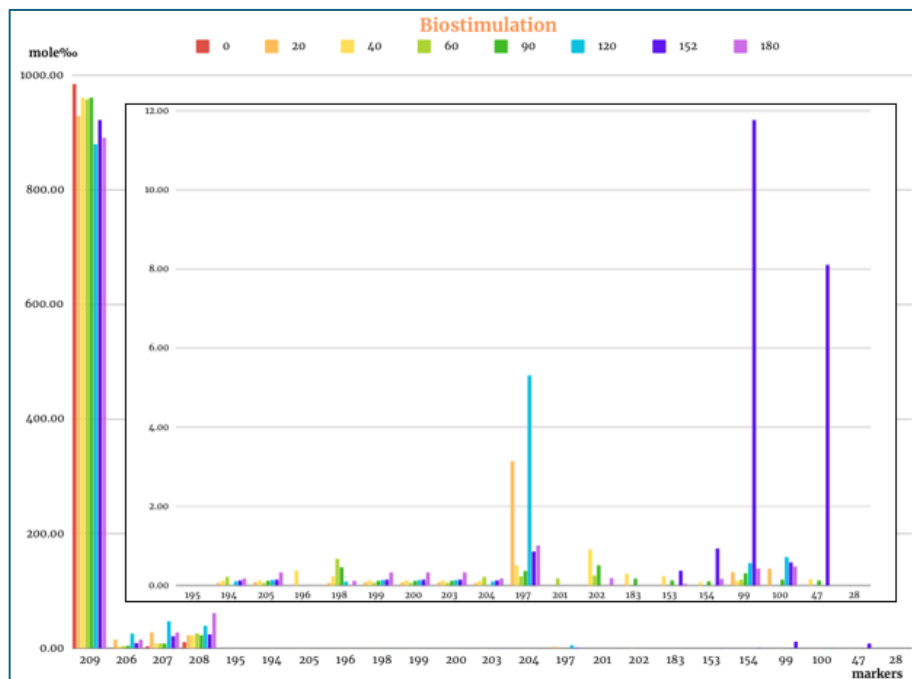


Figure 3.2. PBDE congener concentrations at sampling times in biostimulation microcosm (mole%).

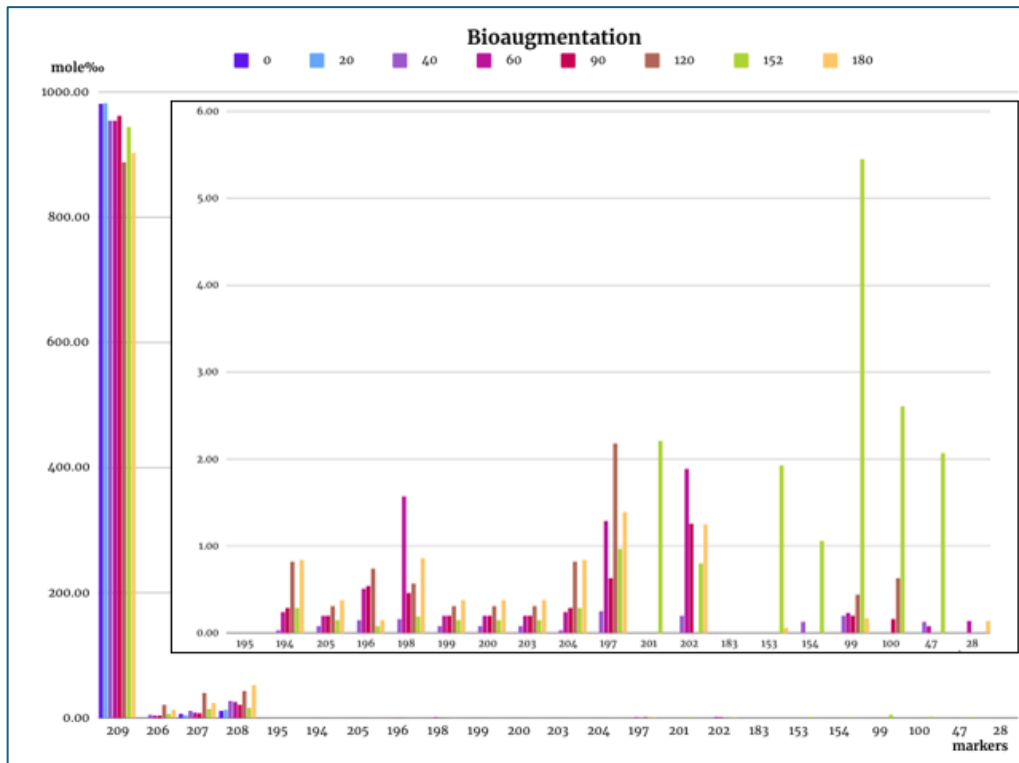


Figure 3.3. PBDE congener concentrations at sampling times in bioaugmentation microcosm (mole%).

## 3.2. Development and Evolution of the ADM

### 3.2.1. Anaerobic dehalogenation model

The anaerobic dehalogenation model aimed at altering a given sample contaminant profile with respect to dehalogenation pathways so that the resulting contaminant profile resembles the profile of known sample. In the previous version of the model, the given sample profile to be altered was PCB concentrations of a microcosm setup at the initial time point, or an Aroclor PCB profile, and the known profile was microcosm concentration at the final time point, or a measured environmental sample (Demirtepe 2012, 46-9).

The previous model included the execution of three distinct models, corresponding to three stages in the overall process. Each of these stages represented a step in the modeling framework, ultimately leading to the results. In the first stage, the process began by executing a MATLAB file initiating the modeling sequence to list the dehalogenation pathways. The algorithm is given in Figure 3.4. The inputs of this file were marker congeners, and the possible dehalogenation positions. As a result, the possible dehalogenation pathways among the given marker congeners were listed.

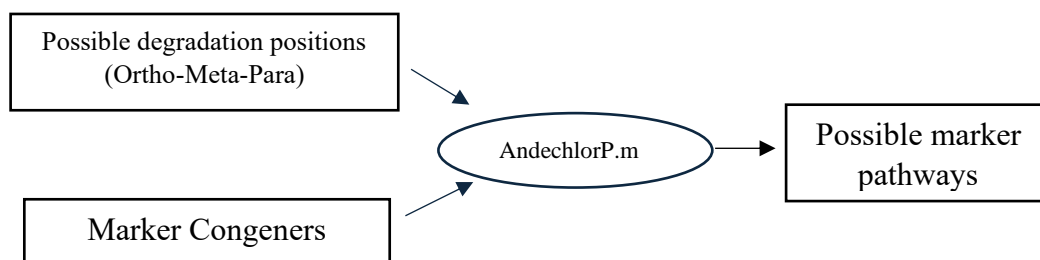


Figure 3.4. General algorithm in the first step of ADM (Source: Demirtepe 2012).

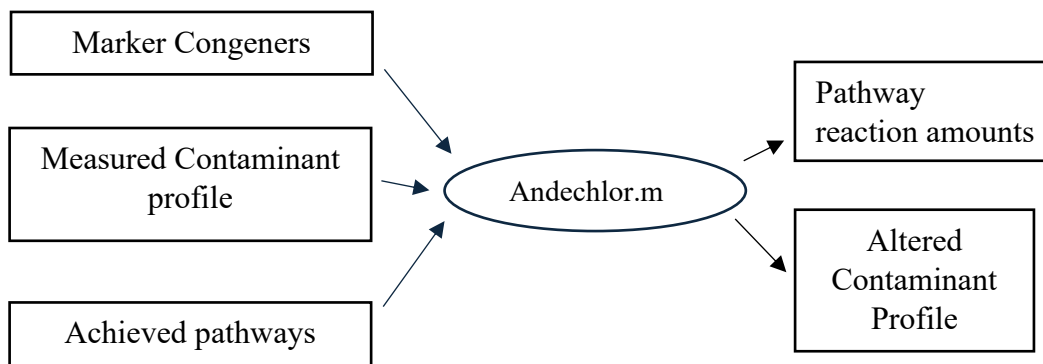


Figure 3.5. General algorithm in the second step of ADM (Source: Demirtepe 2012).

In the second stage, the process continued by executing another MATLAB file where the initial and final marker congener concentrations, and dehalogenation pathways (the output of the first stage) were the inputs. As the outputs, altered (predicted) marker congener profile and the reaction amount of the pathways were obtained. The related algorithm is given in Figure 3.5.

The altered contaminant profile represented the result of an iterative approach to obtain a predicted concentration profile by considering the initial and final measured concentration values. Iterations were done among the dehalogenation pathway sequences, obtained from the first step. During a dehalogenation pathway, a mass balance existed between the mother congener and the daughter congener. Hence, the reaction amount was subtracted from the concentration of the mother and that amount was added to that of the daughter. This whole process involved the core working principle of the model, where the altered contamination profile was determined by applying the dehalogenation pathway to the initial concentration data to minimize the sum of square of differences between predicted and measured profiles, as demonstrated in Equation 3.2 (Karakas 2016, 174).

$$S = \sum_{j=1}^m (y_j - x_j)^2 \quad (3.2)$$

where  $y_j$  is predicted congener profile according to the dehalogenation pathway (mole%),  $x_j$  is the measured congener profile of at final day (mole%), and  $m$  is number of the congeners (Demirtepe 2012, 39).

In the last stage, the process ended by executing another MATLAB file, which completed the modeling sequence. The algorithm is given in Figure 3.6. Here predicted (altered) profile and the reaction amounts of the pathways were used to assess the accuracy of the model.

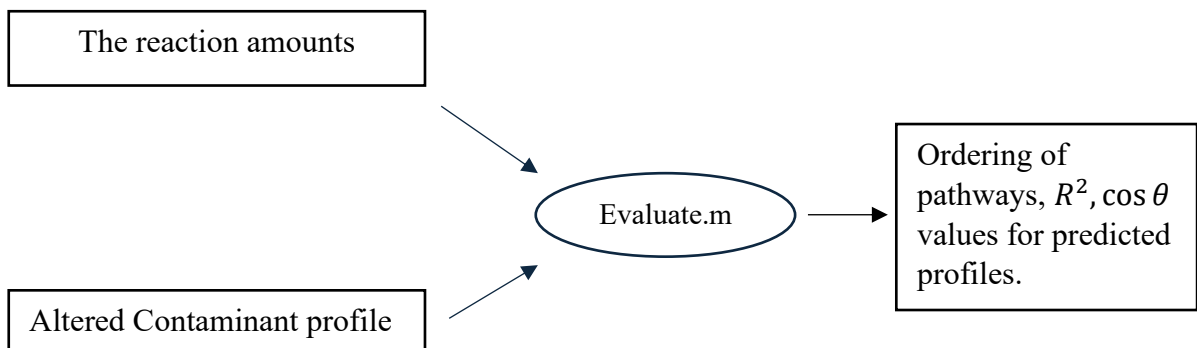


Figure 3.6. General algorithm in the last step of ADM (Source: Demirtepe 2012).

Model validation was assessed by using statistical goodness of fit criteria between measured and predicted contaminant concentrations. Under the scope of this algorithm, the coefficient of determination,  $R^2$ , was used for the evaluation of the ADM performance. The better the fit, the closer  $R^2$  approaches to “1”. In this model, when  $R^2$  was higher than 0.5, the fit was considered to be acceptable and satisfactory (Karakas and Imamoglu 2016). The  $R^2$  is an indicator of how well the predicted values approximated the measured data. It is defined in Equation 3.3, where  $x_i$  represented each congeners’ measured data,  $y_i$  represented each congeners’ predicted value from ADM,  $\bar{y}_i$  was the mean of the measured data (Davis 2002, 150-54).

$$R^2 = 1 - \frac{\sum (x_i - y_i)^2}{\sum (x_i - \bar{y})^2} \quad (3.3)$$

Another indicator used in the model was cosine  $\theta$ , coefficient of proportional similarity, given by Equation 3.4 (Davis 2002, 154-57).

$$\cos(\theta) = \frac{\sum_{i=1}^n (x_i \cdot y_i)}{\sqrt{\sum_{i=1}^n x_i^2 \cdot \sum_{i=1}^n y_i^2}} \quad (3.4)$$

For the  $\cos(\theta)$  coefficient,  $n$  is essentially the total number of data points, the cosine of the angle ( $\theta$ ) between predicted and measured concentrations vector. Each  $x_i$  and  $y_i$  corresponds to a single data point in the predicted and measured data sets.

### 3.2.2. Integrated model

The integrated model was developed by sequentially functionalizing three separate models and combining them into a single integrated model. The functions were executed in sequence, resulting in an integrated output. The algorithm of the integrated model is presented in Figure 3.7.

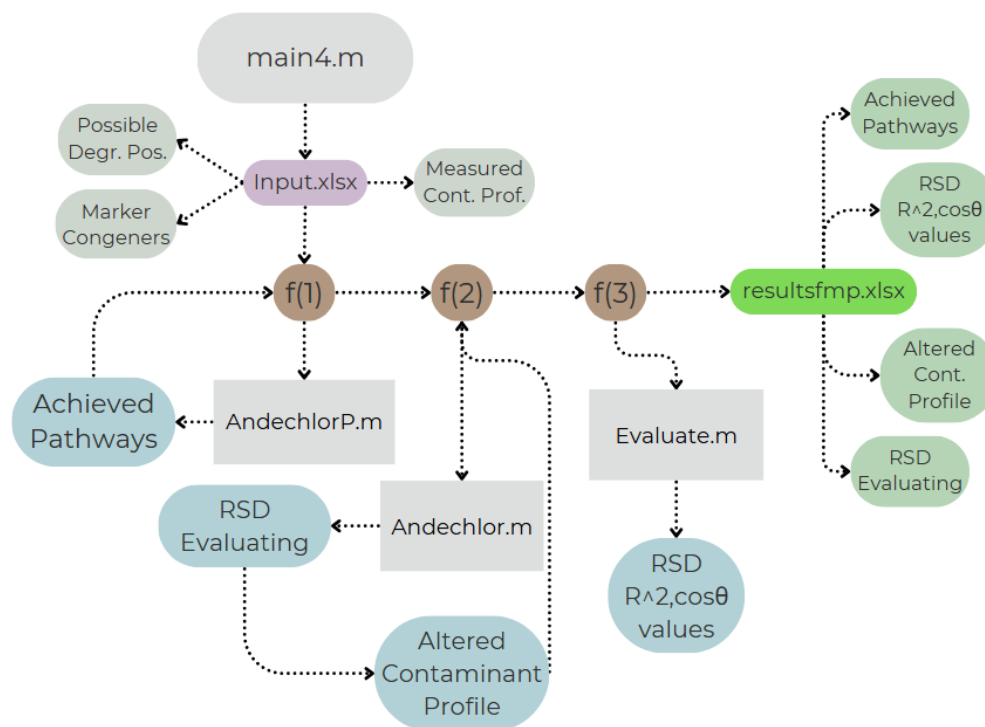


Figure 3.7. General algorithm of integrated anaerobic dehalogenation model.

The process began with the MATLAB script `main4.m`, which used an input file (`Input.xlsx`). This input file included the following data:

- i. Possible Degradation Positions: These might refer to the chemical position of degradation (e.g., ortho, meta, para positions in chemical structures).
- ii. Marker Congeners: The congeners measured during the GC-MS the analysis.
- iii. Measured Contaminant Profiles: The actual profile of contaminants measured from an experiment or sample.

Using these inputs, the first function ‘`f(1)`’ generated:

- The “Achieved Pathways”, which were the possible degradation pathways based on the given degradation positions.

The second function ‘`f(2)`’ processed the Marker Congeners and:

- Produced the Altered Contaminant Profile, which was the predicted contaminant profile based on the contaminant concentrations measured at the initial and final days, after considering the degradation pathways.
- Calculated the reaction amounts. The amount (in mole%) that was reacted in a dehalogenation pathway was calculated for each iteration. The iterations were

performed by shuffling the sequence of pathways since the dehalogenation pathways do not occur in the environment in a specific order. The model provided an average of the reaction amount found in the iterations, together with their standard deviation, and calculated the relative standard deviation (RSD).

The third function 'f(3)' processed the Measured Contaminant Profile and Altered Contaminant Profile. This step evaluated the results, calculating key performance criteria such as;

- $R^2$  (coefficient of determination): Measured how well the altered profile fitted the measured profile.
- Cosine theta coefficient of proportional similarity ( $\cos\theta$ ): Indicated the similarity between two profiles based on the angle between vectors.

All the results from these stages were compiled into an output file "resultsfmp.xlsx", which included:

- Achieved Pathways: The final list of potential pathways the contaminant might follow during degradation.
- Altered Contaminant Profile: The predicted profile after degradation.
- $R^2$  and cosine theta similarity values: Key metrics for evaluating the model's performance.

The process systematically ran these three functions in sequence, taking various inputs at each stage and producing consolidated outputs that evaluated the goodness of fit between measured and predicted profiles and the accuracy of the modeled pathways.

### **3.2.3. Integrated and Enhanced Model (ADM-IE)**

In the present study, the enhanced model, named as "Anaerobic dehalogenation model- integrated and enhanced (ADM-IE)", was built upon the previous structure by integrating additional functions and data points, leading to more comprehensive results.

The ADM-IE used the framework explained in Section 3.2.2 and integrated machine learning to further enhance model prediction capabilities and data visualization. This enhanced model aimed to deliver more precise and strong predictions for the

degradation rate constant and pathways, utilizing dynamic data sets. Figure 3.8 illustrates the ADM-IE.

ADM-IE was developed based on the previous model steps, and integrated the following principles:

- A new component in the enhanced model was kcalibration.m function, which estimated the degradation rate constants (k values) for each dehalogenation pathway which involved the marker congener as both mother and daughter. The dehalogenation reactions were assumed to follow the first-order reaction kinetics (Equation 3.5). In the equation, C is the concentration of the mother congener (mole%), t is the time (d) and k is the degradation rate constant ( $d^{-1}$ ).

$$\frac{dC}{dt} = -kC \quad (3.5)$$

Integrating the equation from time zero to time t, and from initial mother congener concentration to final, the rate constant is obtained as given in Equation 3.6:

$$k = \frac{\ln\left(\frac{C_{\text{initial}}}{C_{\text{final}}}\right)}{t} \quad (3.6)$$

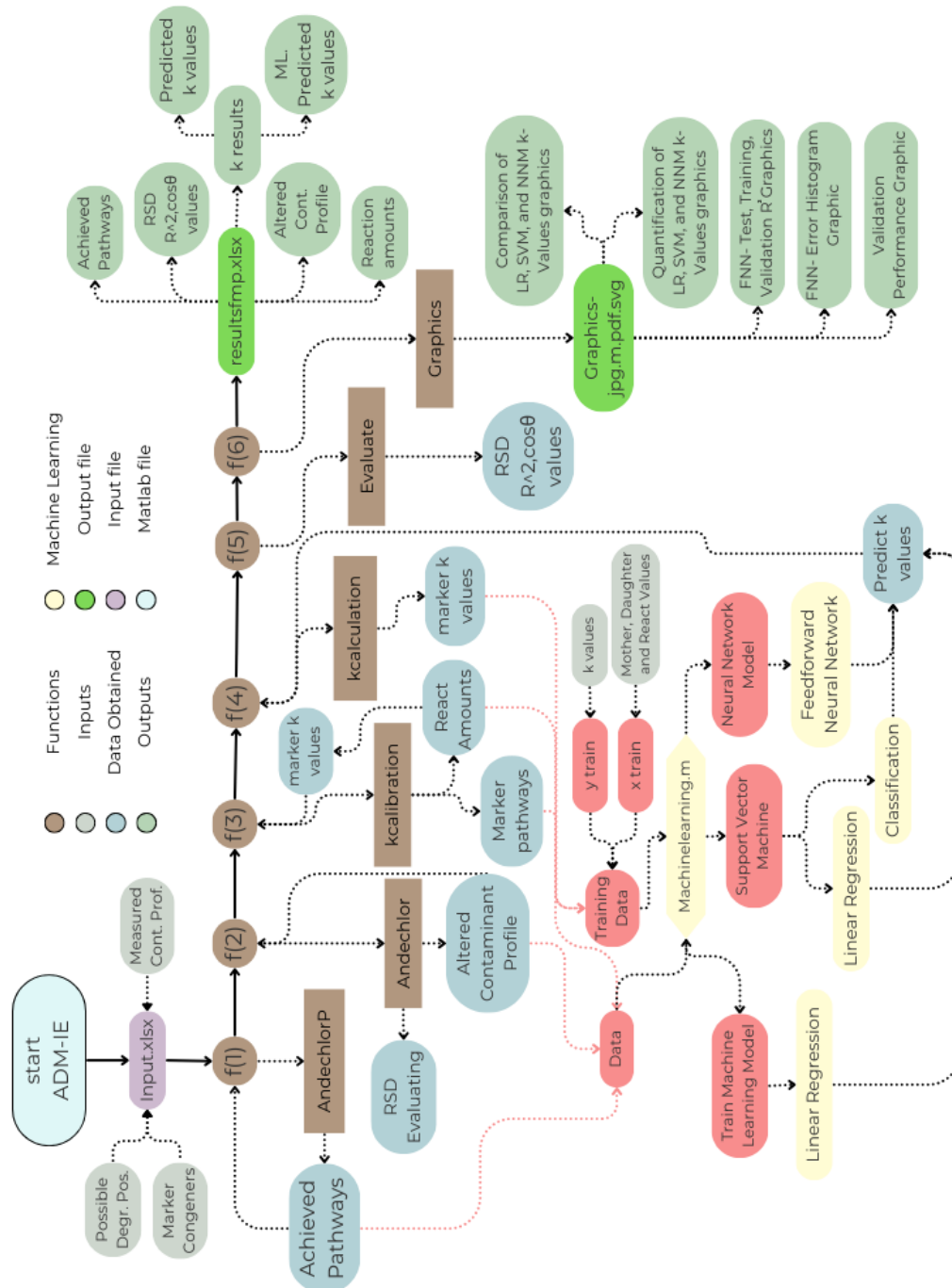


Figure 3.8. Integrated and enhanced anaerobic dehalogenation model algorithm.

- A key innovation in ADM-IE was the integration of a machine learning component, encapsulated within the `kcalculation.m` and `machinelearning.m` functions. The purpose of using machine learning was to predict  $k$  values for the pathways, which included non-marker congener either as a mother or daughter. This step proceeded as follows:
  - I. Data Preparation: The calculated  $k$  values, along with their corresponding mother, daughter, and reaction amounts, were extracted from the `resultsfmp.xlsx` file to form the training dataset ( $x$  train and  $y$  train).
  - II. Model Training: Machine learning model was employed to learn the relationships between the input variables (mother, daughter, and reaction amount) and the calculated  $k$  values. This training process enabled the model to generalize these relationships to predict  $k$  values for non-marker pathways.
  - III. Prediction of  $k$  values: The trained model was subsequently applied to predict  $k$  values for the dehalogenation pathways where the reaction amount was known. For data entries where the reaction amount was zero, the corresponding  $k$  value was set to zero, as no reaction was expected in such cases.

The results from all functions were consolidated into the `resultsfmp.xlsx` file, which contained the following plus the list presented in Section 3.2.2:

- The degradation rate constants for marker pathways
- The estimated degradation rate constants by machine learning analysis.

Through the integration of machine learning technique method, the ADM-IE offered a more comprehensive representation of anaerobic dehalogenation pathways.

### 3.3. Linear Regression Principles

The linear regression to predict  $k$ -values was based on the features of the dehalogenation pathways: mother, daughter, reaction amount, and  $k$ -values. It assumed that the relationship between the input features (mother, daughter, reaction amount) and the target variable ( $k$ -values) was linear. Hence, it developed a straight line (or hyperplane in higher dimensions) that best fitted the training data. The equation for linear regression can be written as seen below.

$$k_{\text{value}} = \beta_0 + \beta_1 x_{\text{Mother}} + \beta_2 x_{\text{Daughter}} + \beta_3 x_{\text{React}} \quad (3.7)$$

Where  $\beta_0, \beta_1, \beta_2, \beta_3$  are the parameters (coefficients) learned by the model during training. Once the model learned these coefficients, it was able to make predictions for new data in the test set (i.e., the k values of non-marker dehalogenation pathway).

### 3.4. Support Vector Machines Principles

SVMs were applied to predict the degradation rate constants using “fitrsvm” function in MATLAB. This methodology aimed to predict a continuous output (the degradation rate constant) based on several input features (mother, daughter, and reaction amount). In this regression task, SVR model found a function that best approximated the relationship between the input variables and the output (Cortes and Vapnik 1995). “fitrsvm” MATLAB function works with Kernel, Loss, and Regularization Parameter functions as mentioned in the literature section. In this study, the Kernel method has been selected to predict the k-values.

Training the SVR Model followed the steps of data preprocessing, model selection, fitting the model (fitrsvm in MATLAB), and making predictions. Data processing normalized or standardized the input features (mother, daughter, reaction amount) to ensure that all features contributed equally to the prediction. The “fitrsvm” function attempted to find the support vectors that defined the hyperplane (or regression function) that best fitted the data within the  $\varepsilon$ -margin. Once trained, the predict function was used to estimate the degradation rate constants for the new data.

Mathematical Formulation of SVR tries to find a function  $f(x)$  that has at most an  $\varepsilon$  deviation from the actual output  $y$  for all training data, while being as flat as possible (Smola and Schölkopf 2004), as given in the Equation 3.9.

$$f(x) = \omega^T \varphi(x) + b \quad (3.9)$$

$\omega$  is the weight vector,  $\varphi(x)$  represents the transformation applied by the kernel function,  $b$  is the bias term. The objective of optimization in SVR was to minimize equation shown in Equation 3.10.

$$\frac{1}{2} \|\omega\|^2 + C \sum_{i=1}^n L_{\epsilon}(y_i, f(x_i)) \quad (3.10)$$

$L_{\epsilon}$ : The epsilon-insensitive loss function.

$C$ : The regularization parameter that controls the trade-off between minimizing training error and maximizing margin.

$y_i$ : The target value for each observation in the dataset.

Then, the performance of the model was evaluated using metrics such as mean square error (MSE) or  $R^2$  to see how well the model predicts the degradation rate constants. Also, the hyperparameters, including the kernel type,  $C$ , and  $\epsilon$ , were tuned to improve the model's performance.

In summary, Support Vector Machines (using `fitrsvm`) provided a robust method for regression tasks by fitting a function that approximated the data within a certain margin of error (Smola and Schölkopf 2004). Through the use of kernel functions, SVMs can handle both linear and non-linear relationships. In this study, SVM can be particularly useful because it allowed for the flexibility in fitting the data while controlling the smoothness of the prediction function.

## 3.5. Neural network model

### 3.5.1. Neural network model principles

By neural network using “`feedforwardnet`” function of MATLAB, a feedforward neural network with 10 hidden neurons was created. The data was normalized before training because neural networks often perform better when the inputs are scaled.

MATLAB's "normalize" function was used for this purpose. Additionally, the network was trained using trains and predictions and these were made using the net.

Consistently, the same strategy was used to predict the k-values, and zero values for reaction amounts were handled as in the previous model. The FNN diagram illustrated in Figure 3.9 can be examined in four main steps.

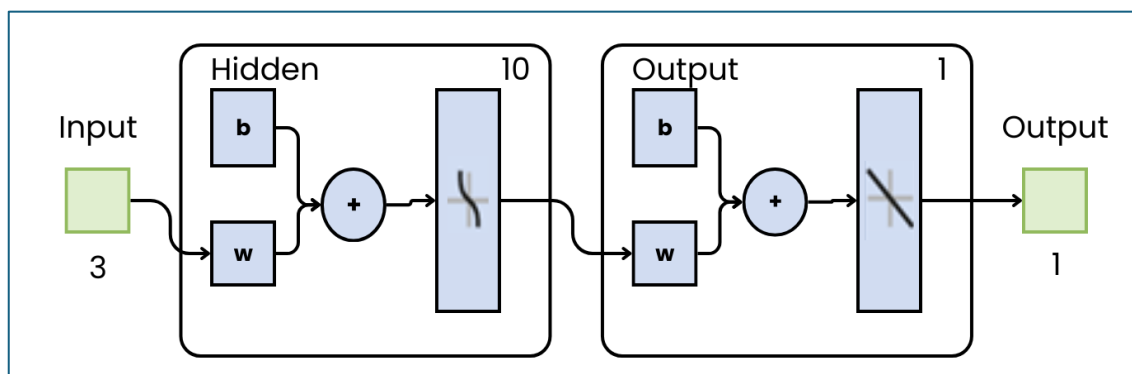


Figure 3.9. Feed-Forward neural network diagram.

In the first step input layer (green box labeled "Input"), the input layer had 3 nodes, representing the three input features used, mother, daughter, and reaction amounts. In the second step (labeled "Hidden"), the hidden layer contained 10 neurons. This was the intermediate layer where the network processes the input data. "w" represented the weight matrix for this hidden layer, and "b" represented the bias vector. The inputs were transformed by weights and biases, and then passed through an activation function (shown as a curve, likely a non-linear function).

In the third step (labeled "Output"), the output layer had 1 neuron, which corresponded to the single output of the network: the predicted k-value. Again, weight and biases were applied, and the output was passed through an activation function to produce the final prediction.

The last step involved the connections, i.e. the input layer connected to the hidden layer, which processed the information. The output from the hidden layer was passed to the output layer to make the final prediction. The two layers (hidden and output) used weights and biases to adjust how the input data was transformed.

### 3.5.2. FNN model graphics explanation

Upon running the FNN model, four main graphs were generated automatically to visualize the training process and evaluate the performance. Each graph offered insights into different aspects of the model's accuracy. After the model completed the model run, a command window appeared, displaying an overview of the FNN training results and providing access to the related graphs.

The example given in Figure 3.10 represents the results from running the ADM-IE on the natural attenuation microcosm dataset between days zero and 90. In this case, training was completed at 10 epochs out of a maximum of 1000, with displayed metrics for performance, gradient, and Learning Rate Parameter (Mu) showing their initial, stopped, and target values.

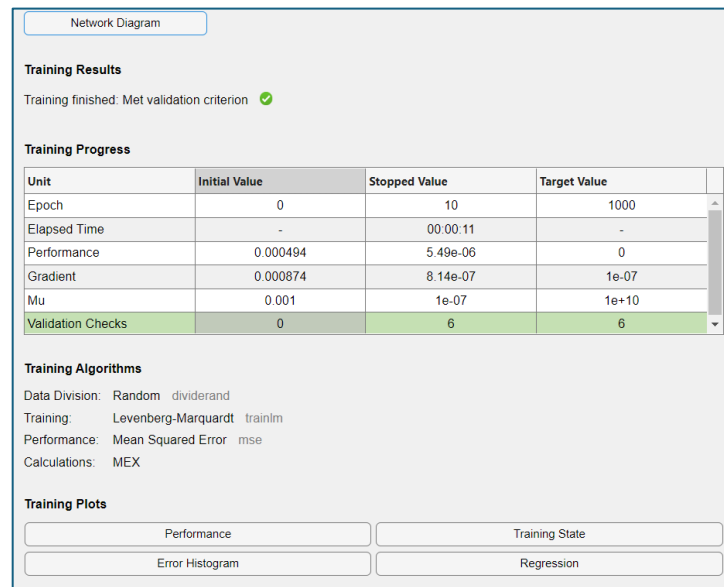


Figure 3.10. An example of the FNN command window.

As indicated in Figure 3.10 the training algorithm employed was the "Levenberg-Marquardt" algorithm, with MSE. MATLAB Executable (MEX) files in MATLAB was used to execute intensive computations more efficiently (The MathWorks 2024e).

Additionally, Figure 3.10 shows buttons for accessing the four previously mentioned graphs, which allow further examination of training outcomes.

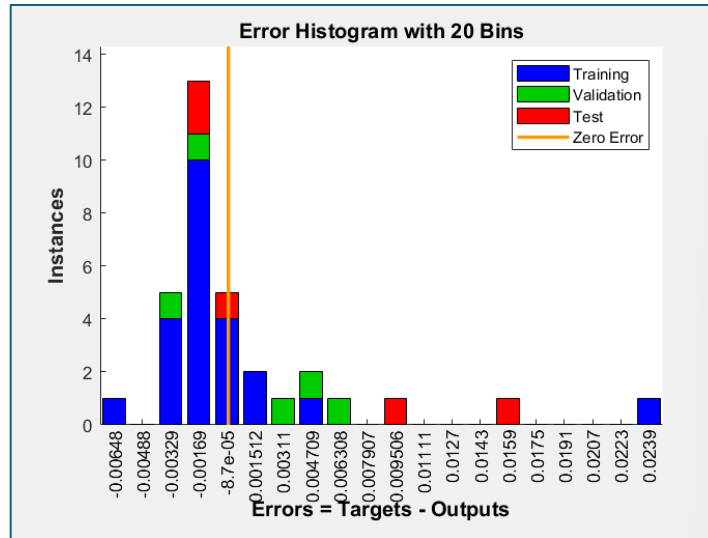


Figure 3.11. Error histogram training plots graph.

Figure 3.11 shows the distribution of errors between the target values and the model’s predictions across the training, validation, and testing datasets. The error values on the x-axis represented the difference between predicted and target outputs, while the y-axis showed the frequency of these error occurrences (The MathWorks 2024a). The graph also included a line for zero error, serving as a reference for how close the predictions were to the actual values. That error value was the lowest and can be evaluated as the point where optimal performance was expected.

Figure 3.12 demonstrates three parameters over the training epochs: the gradient, Mu, and the number of validation checks. The gradient plot showed the change in error gradient over time, indicating the model’s convergence during training (The MathWorks 2024c). The Mu plot represented the learning rate, which adjusted based on the gradient values to optimize learning (The MathWorks 2024c). The validation checks plot monitored the validation loss and indicated when early stopping occurs if the validation error did not improve after a set number of checks (The MathWorks 2024c).

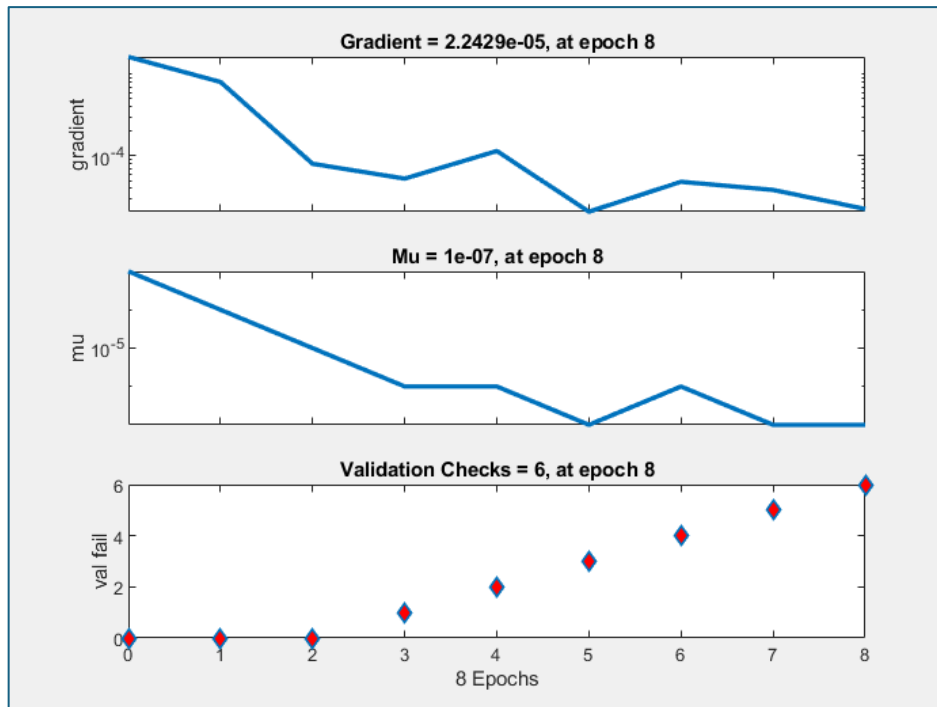


Figure 3.12. Training state graph.

To summarize, the term 'Epochs 6' indicated that the model was trained over a total of six epochs. This meant that the model passed through the entire dataset six times.

Four regression plots were provided for the training, validation, test, and overall datasets. These plots show the relationship between the target values and the predicted outputs, with each plot displaying a line fit and a reference line ( $Y=T$ ) where the prediction perfectly matches the target. The correlation coefficient ( $R$ ) in each plot serves as an indicator of the model's fit for each dataset, helping to visualize how closely predictions align with the true values across different phases of the dataset (The MathWorks 2024d).

The  $R$  measures the strength and direction of the linear relationship between the model predictions ( $\hat{y}$ ) and the actual values ( $y$ ). The value range is between -1 and 1. Perfect positive linear relationship in the  $R=1$ . The  $R$  is calculated using the Equation 3.10, where  $y_i$  is the actual values,  $\hat{y}_i$  is the predicted values from the model,  $\bar{y}$  is the mean of the actual values,  $\bar{\hat{y}}$  is the mean of the predicted values,  $n$  is the number of data points (A. Lee, Geem, and Suh 2016).

$$R = \frac{\sum_{i=1}^n (y_i - \hat{y})(\hat{y}_i - \hat{y})}{\sqrt{\sum_{i=1}^n (y_i - \hat{y})^2} \sqrt{\sum_{i=1}^n (\hat{y}_i - \hat{y})^2}} \quad (3.10)$$

The performance plot illustrates the model's MSE over each epoch for the training, validation, and test datasets as can be seen in Figure 3.13. The MSE calculation has been explained previously in the literature section. It provides a graphical view of the model's error reduction over time, showing how the error decreases and stabilizes as the model learns. A "best" line is typically indicated, highlighting the epoch with the lowest validation error, which helps determine the optimal stopping point for training (The MathWorks 2024b).

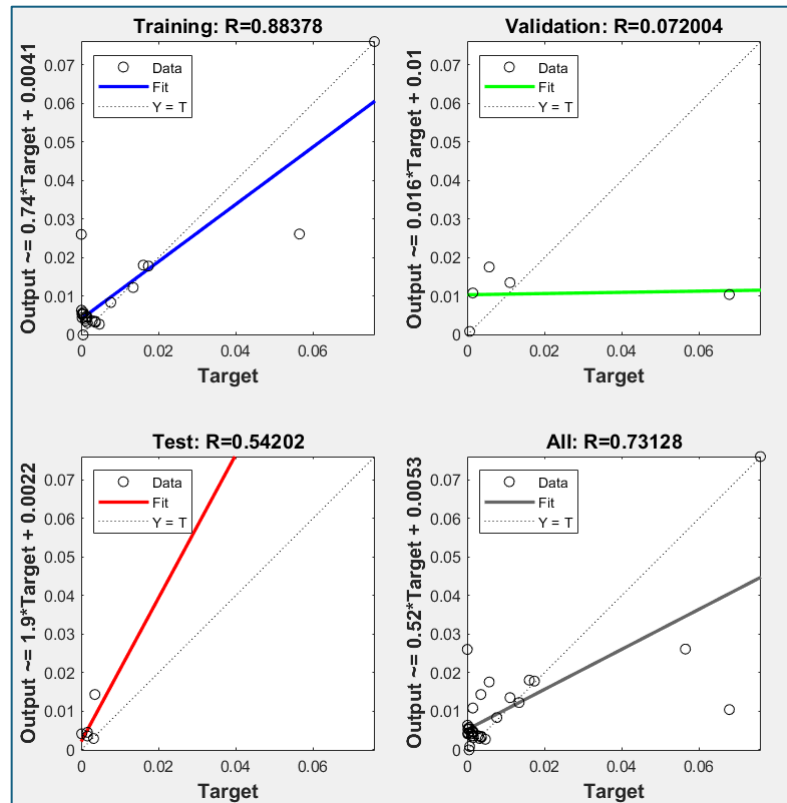


Figure 3.13. Regression graph for training, validation, and test.

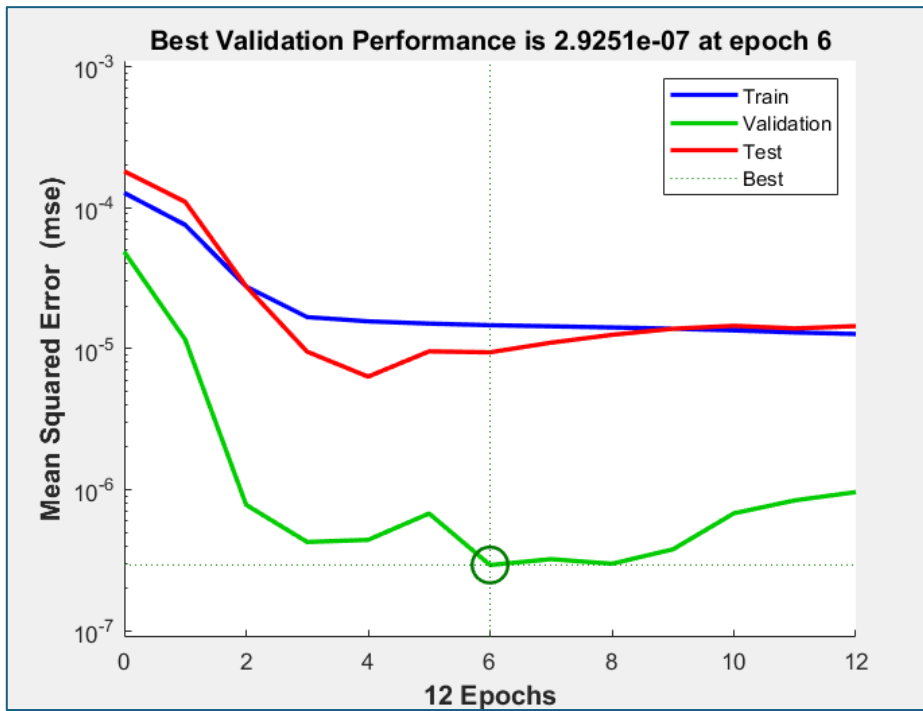


Figure 3.14. MSE performance graph.

## CHAPTER 4

### RESULT AND DISCUSSION

#### 4.1. Validation of ADM-IE using artificial data set

The purpose of model validation was to test the “enhanced and integrated” version of ADM whether it successfully proposed possible dehalogenation pathways and estimated the reaction rate constants. For this purpose, two artificial data sets were generated manually. Since ADM-IE provided a more comprehensive list of pathways, the model input was manipulated to obtain a limited number of pathways for the validation study so that the manual calculation of the reaction rates would be less challenging. The first artificial data set input and manual calculation of the reaction amounts to obtain the final congener concentrations are presented in Table 4.1.

Table 4.1. ADM-IE first artificial data set input.

<b>Marker Congeners</b>	<b>Initial Conc. Mole‰</b>	<b>Final Conc. Mole‰</b>	<b>Pathway M →D</b>	<b>Reaction Amount</b>
207	850	225	207→196	625
196	75	200	196→183	500
183	45	195	183→154	200
154	30	220	183→153	150
153	0	75	154→99	10
99	0	55	153→99	75

(cont. on next page)

**Table 4.1 (cont.)**

66	0	15	99→66	20
47	0	10	99→47	10
28	0	5	66→28	3
			47→28	2

The results of the first validation run are provided in Table 4.2. The model successfully processed the input data to produce the rate constants at the same order of magnitude with the manual calculations in six out of ten pathways. The rate constants obtained by manual vs model calculations and measured vs predicted congener profiles were compared in the scatter plots of Figure 4.1. As can be observed, the coefficient of determination ( $R^2$ ) of both plots were greater than 0.92. An important observation was that ADM-IE predicted the congeners with higher concentrations and their relevant pathways better than the ones with lower concentrations. For instance, the pathways producing BDE-28 were quantified as zero and their rate constants were zero, while BDE-207, 196, 183 were predicted better by the model. Overall, the validation study demonstrated the capability of ADM-IE to predict effectively the congener profile after dehalogenation and estimate the rate constants of dehalogenation pathways in complex environmental data scenarios.

Table 4.2. First validation comparison of manually calculated and ADM-IE k-values.

<b>M→D</b>	<b><i>k values</i> calculated (d)</b>	<b><i>k values</i> ADM-IE (<math>d^-</math>)</b>
207→196	0.01329	0.01188
196→183	0.01253	0.01092
183→154	0.00457	0.00525
183→153	0.00571	0.00395
154→99	0.00044	0.00085
153→99	0.00693	0.00334
99→66	0.00310	0.00074
99→47	0.00201	0.00013
66→28	0.00163	0
47→28	0.00223	0

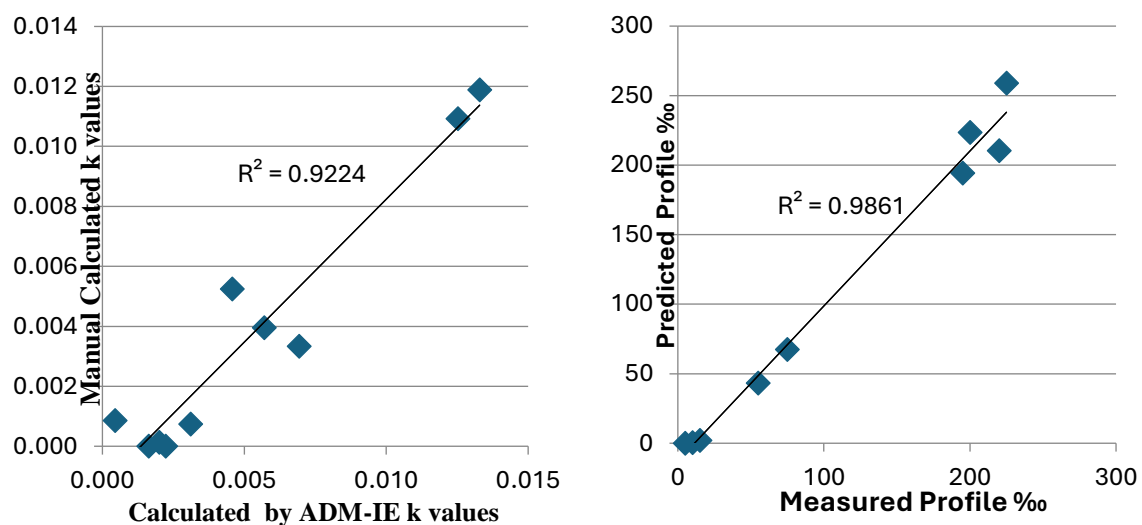


Figure 4.1. Manual/ADM-IE k values and measured/predicted profile plots.

The second artificial data set input and manual calculation of the reaction amounts to obtain the final congener concentrations are presented in Table 4.3.

Table 4.3. ADM-IE second artificial data set input.

<b>Marker Congeners</b>	<b>Initial Conc. Mole%</b>	<b>Final Conc. Mole%</b>	<b>Pathway M → D</b>	<b>Reaction Amount</b>
207	1000	958	207→196	42
196	0	6.14	196→183	36
183	0	0.26	183→154	18.4
154	0	0.56	183→153	17.3
153	0	0.55	154→99	18
99	0	18.64	153→99	17
66	0	0.9	99→66	16
47	0	14.6	99→47	15
28	0	0.35	66→28	0.15
			47→28	0.2

The results of the second validation run are summarized in Table 4.4. The model demonstrated an ability to predict rate constants within the same order of magnitude as manual calculations for eight out of ten pathways. However, deviations were observed for pathways associated with lower concentrations, where the model's predicted rate constants were zero. In contrast, pathways involving higher concentrations, such as BDE-207, 196, and 183, were better simulated by the model. The regression analysis of manual versus model-calculated rate constants yielded a  $R^2$  of 0.7168, as shown in Figure 4.2.

Overall, the validation of the ADM-IE proved that a more user-friendly version of the model was developed, allowing for a single run to obtain all the outputs. It was also shown that enhancement of the model was achieved by the calculation of rate constants for each dehalogenation pathway. This validation study further supports the model's capability to estimate dehalogenation rate constants and predict congener profiles, particularly for dominant pathways in complex environmental scenarios.

Table 4.4. Second validation comparison of manual and ADM-IE k-values.

<b>M→D</b>	<b><i>k values</i> calculated</b>	<b><i>k values</i> ADM-IE</b>
<b>Pathway</b>	<b>(<i>d</i><sup>-</sup>)</b>	<b>(<i>d</i><sup>-</sup>)</b>
207→196	0.00043	0.00030
196→183	0.01923	0.01242
183→154	0.00720	0.00616
183→153	0.04692	0.02190
154→99	0.03829	0.02509
153→99	0.04055	0.02547
99→66	0.02833	0.0
99→47	0.01558	0.01123
66→28	0.00009	0.0
47→28	0.00013	0.0

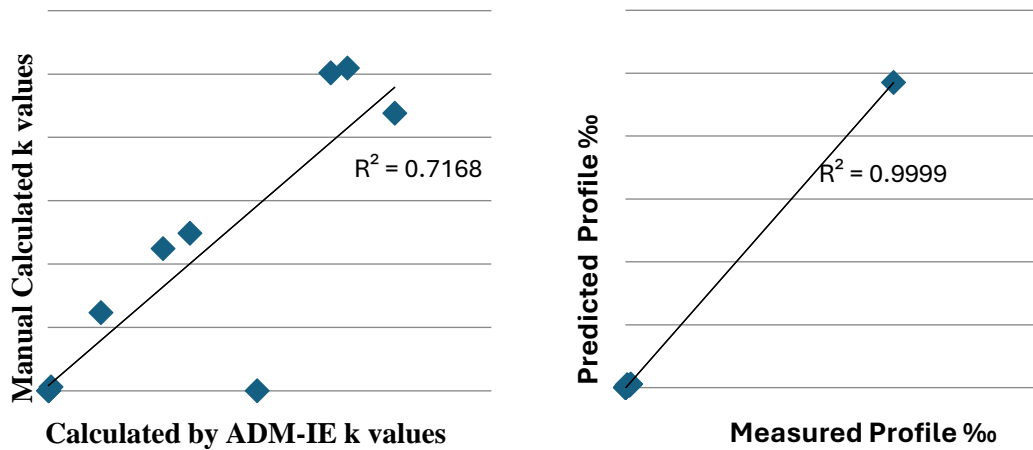


Figure 4.2. Manual/ADM-IE k values and measured/predicted profile plots.

## 4.2. ADM-IE application to PBDE bioremediation scenarios

### 4.2.1. Evaluation of PBDE dehalogenation after 180 days

The dehalogenation was observed in microcosms over 180 days with periodic sampling. Initially, the model was applied to the concentration data of day 0 and day 180 for three bioremediation scenarios and their control sets. Hence, the input data involved the PBDE concentrations at day 0 and 180, the marker congeners, and the bromine positions available for dehalogenation.

The aim of the model was to accurately predict the congener profile at 180 days, using the possible dehalogenation pathways in microcosm sediments. Then, the predicted profiles were compared with the measured (180 days) profiles to evaluate the success of the model, using the  $\cos \theta$ , and  $R^2$ . After the execution of ADM-IE, these model performance criteria were obtained for microcosms, as shown in Table 4.5. The measured and predicted PBDE congener profiles for each bioremediation scenario are presented in Table 4.6 and shown as scatter plots in Figure 4.3. The model performance criteria were found very close to 1, revealing a very good fit of the model results with the measured profiles for every microcosm set. When the predicted and measured concentrations were

compared (Table 4.6), it was observed that the model predicted the congeners with higher concentrations better than the ones with comparably lower concentrations. The results revealed that the model successfully predicted the congeners with high concentrations in the data set. The microcosm experiment was conducted by spiking BDE-209 to the sediments. Hence, BDE-209 and its first products were continuously observed at high concentrations in the bioremediation microcosms. The good fit for the profiles of these congeners was due to experimental conditions maintained during the microcosm operation. The microcosms were prepared by flushing the serum bottles with high-purity nitrogen to allow for the deoxygenation of sediments and the overlying liquid content, creating an anaerobic environment (Demirtepe and Imamoglu 2019b). Hence, the only mechanism of PBDE degradation was anaerobic dehalogenation in the microcosms.

The observation of better prediction of higher-concentration-congeners was similarly found in the validation study. This situation generated a bias in  $R^2$  calculation in microcosm data set, resulting in very high  $R^2$  values. Hence, the congeners BDE-209, 208, 207, and 206 were excluded from the scatter plots of measured vs predicted profiles, and  $R^2$  was calculated based only on the remaining congeners (Figure 4.3 D, E, F). As a result,  $R^2$  values ranged between 0.35 and 0.78 for the lower concentration congeners. The congeners that were not predicted very well varied among the bioremediation microcosms. For natural attenuation, BDE-154, for biostimulation BDE-201, 198, 199, and 200, and for bioaugmentation, BDE-196, 194, and 202 were predicted below or above the measured concentrations, and several congeners were quantified although they were measured as zero in the data set. This discrepancy might result from the reaction amounts of dehalogenation pathways. When the dehalogenation pathways were examined, it was observed that almost all pathways were predicted to occur with very high relative standard deviation (RSD) values, i.e. greater than 100% in each microcosm. The reaction amounts for each dehalogenation pathway are presented in Table 4.7, as the average, the standard deviation, and RSD. The model provided a total of 124 different pathways for 23 marker compounds. The reaction amounts of the dehalogenation pathways were obtained from 100 shuffles of the reaction sequences; hence their standard deviations and RSDs were also calculated.

Table 4.5. ADM-IE performance for 0-180 day microcosm data set.

<b>Method</b>	<b><math>\cos \theta</math></b>	<b><math>R^2</math></b>
Natural attenuation	0.99999	0.99998
Biostimulation	0.99998	0.99997
Bioaugmentation	0.99999	0.99997
Negative Control	0.99999	0.99999
Sterile Control	0.99999	0.99999

Table 4.6. Results of ADM-IE predicted and measured mole% profiles.

<b>m</b>	<b>NA 0-180</b>		<b>BS 0-180</b>		<b>BA 0-180</b>		<b>NC 0-180</b>		<b>SC 0-180</b>	
	<b>BDE</b>	<b>M</b>	<b>P</b>	<b>M</b>	<b>P</b>	<b>M</b>	<b>P</b>	<b>M</b>	<b>P</b>	<b>M</b>
28	0.00	0.16	0.00	0.20	0.14	0.40	0.00	0.18	0.00	0.00
47	0.00	0.13	0.00	0.22	0.00	0.33	0.00	0.19	0.00	0.00
99	0.69	0.68	0.48	0.64	0.00	0.40	0.16	0.34	0.00	0.00
100	0.37	0.18	0.43	0.46	0.17	0.44	0.00	0.15	0.00	0.00
153	0.22	0.32	0.17	0.33	0.00	0.39	0.00	0.21	0.00	0.00
154	3.11	1.66	0.04	0.20	0.06	0.37	0.37	0.40	0.00	0.00
183	0.00	0.09	0.00	0.16	0.00	0.29	0.27	0.25	0.00	0.00
194	0.00	0.16	0.19	0.21	1.25	0.52	0.00	0.13	0.00	0.00
195	0.00	0.42	0.00	0.28	0.00	0.36	0.00	0.08	0.00	0.00
196	1.27	1.01	1.01	0.78	1.39	0.86	0.59	0.30	0.00	0.00
197	0.62	0.41	0.18	0.19	0.84	0.49	0.61	0.29	0.00	0.00
198	0.36	0.77	0.33	0.64	0.38	0.67	0.28	0.33	0.00	0.00
199	0.36	0.67	0.33	0.63	0.38	0.68	0.28	0.35	0.00	0.00
200	0.36	0.55	0.33	0.70	0.38	0.77	0.28	0.37	0.00	0.00
201	0.96	1.04	0.12	0.53	0.86	1.01	0.83	0.70	0.00	0.00
202	0.89	1.13	0.00	0.59	0.15	0.79	0.00	0.39	0.00	0.00
203	0.36	0.31	0.33	0.30	0.38	0.38	0.28	0.16	0.00	0.00
204	0.62	0.59	0.18	0.25	0.84	0.52	0.61	0.29	0.00	0.00
205	0.00	0.19	0.00	0.18	0.00	0.19	0.00	0.10	0.00	0.00
206	54.46	54.02	61.63	59.57	52.38	50.05	39.48	38.90	10.37	10.38
207	27.61	26.53	27.87	26.38	24.41	23.19	20.19	19.65	0.00	0.00
208	16.49	16.01	15.19	13.65	12.77	11.40	10.91	10.02	0.00	0.00
209	891.2	892.9	891.1	892.9	903.2	905.5	924.8	926.2	989.6	989.6

m: marker, M: measured, P: predicted

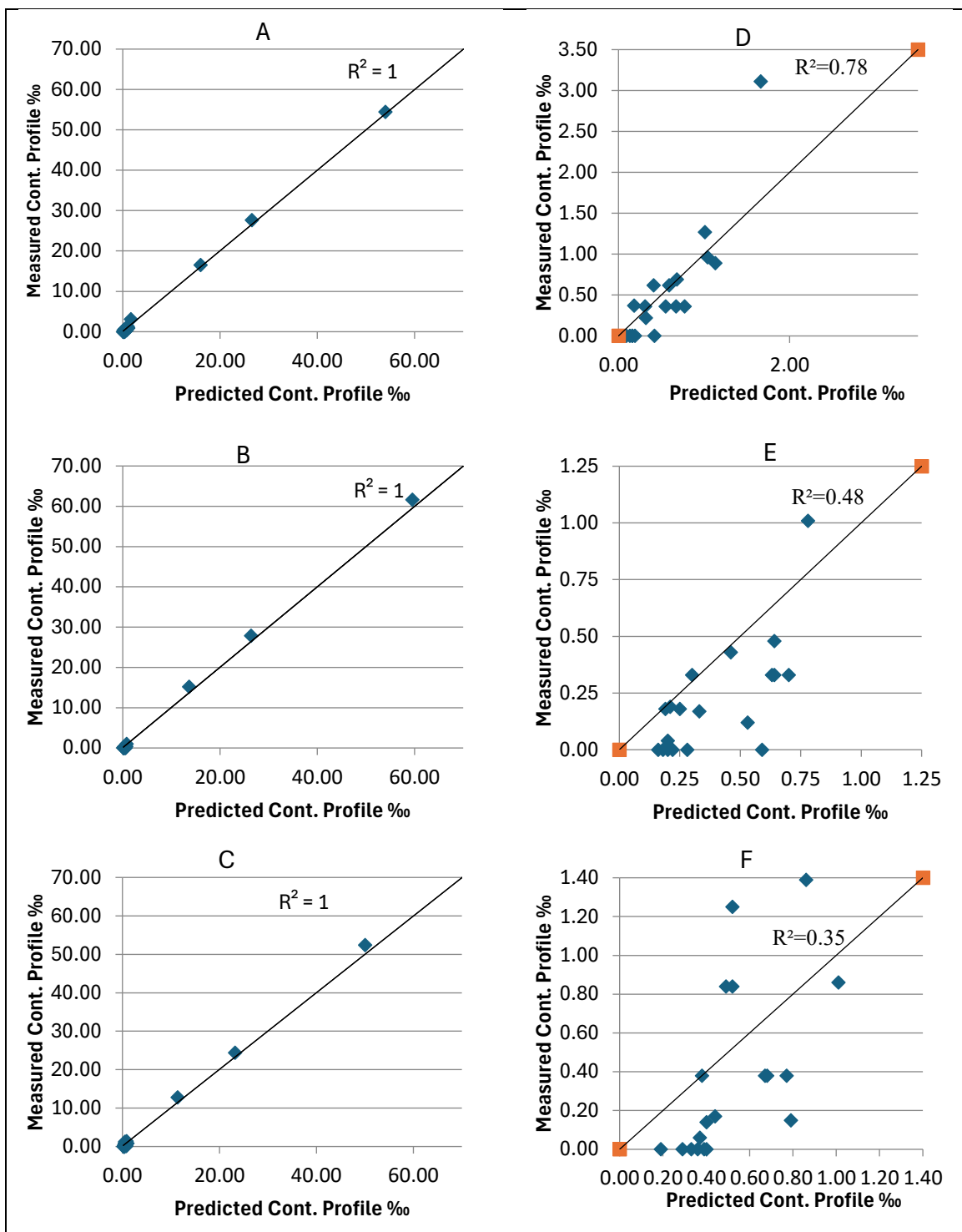


Figure 4.3. Measured vs predicted concentrations of all marker PBDE congeners for A) NA, B) BS, C) BA, except octa, nona, and deca-BDEs for D) NA, E) BS, F) BA.

Table 4.7. All possible pathways for 23 marker congeners.

0-180day			Natural Attenuation			Biostimulation			Bioaugmentation		
Pathway			Avg react	STD	RSD	Avg react	STD	RSD	Avg react	STD	RSD
<b>28</b>	→	15	0.004	0.023	630.7	0.016	0.126	803.1	0.000	0.000	0
<b>28</b>	→	7	0.002	0.012	556.1	0.003	0.016	602.9	0.002	0.018	1000
<b>28</b>	→	8	0.010	0.055	538.0	0.008	0.049	576.0	0.001	0.009	838
<b>47</b>	→	<b>28</b>	0.111	0.151	136.5	0.142	0.190	133.6	0.337	0.296	88
<b>47</b>	→	17	0.009	0.042	451.8	0.008	0.074	936.7	0.020	0.149	733
60	→	<b>28</b>	0	0	0	0	0	0	0	0	0
66	→	<b>28</b>	0	0	0	0	0	0	0	0	0
74	→	<b>28</b>	0.033	0.112	334.7	0.061	0.200	328.5	0.048	0.207	435
75	→	<b>28</b>	0.010	0.103	1000	0.015	0.139	922.7	0.006	0.036	637
85	→	<b>47</b>	0	0	0	0	0	0	0	0	0
<b>99</b>	→	<b>47</b>	0.231	0.311	134.9	0.286	0.388	135.6	0.481	0.486	101
<b>99</b>	→	74	0.085	0.311	365.3	0.116	0.397	341.8	0.055	0.263	474
<b>99</b>	→	48	0.058	0.258	444.6	0.081	0.324	399.0	0.023	0.158	693
<b>99</b>	→	49	0.023	0.103	448.5	0.070	0.329	472.1	0.049	0.188	385
<b>100</b>	→	<b>47</b>	0.029	0.119	410.4	0.075	0.153	205.4	0.203	0.336	166
<b>100</b>	→	75	0.023	0.166	707.7	0.019	0.174	936.7	0.007	0.041	601
<b>100</b>	→	50	0.031	0.311	997.4	0.019	0.134	706.8	0.009	0.083	904
<b>100</b>	→	51	0.028	0.131	476.0	0.050	0.181	362.5	0.025	0.132	534
137	→	<b>99</b>	0	0	0	0	0	0	0	0	0
138	→	<b>99</b>	0.130	0.412	316.7	0.189	0.605	319.5	0.105	0.436	416
139	→	<b>100</b>	0.052	0.356	686.7	0.065	0.226	345.5	0.130	0.438	336
139	→	<b>99</b>	0.075	0.332	443.7	0.141	0.515	365.7	0.086	0.357	413
140	→	<b>100</b>	0	0	0	0	0	0	0	0	0
<b>153</b>	→	<b>99</b>	0.643	0.667	103.7	0.509	0.664	130.5	0.508	0.633	125
<b>153</b>	→	101	0.107	0.362	337.5	0.195	0.706	361.0	0.095	0.328	346
<b>154</b>	→	<b>100</b>	0.256	0.496	193.9	0.546	0.537	98.3	0.540	0.609	113
<b>154</b>	→	<b>99</b>	0.214	0.543	253.5	0.329	0.455	138.3	0.301	0.472	157
<b>154</b>	→	102	0.144	0.749	521.4	0.031	0.136	442.7	0.051	0.441	861
<b>154</b>	→	103	0.168	0.836	496.6	0.126	0.525	415.4	0.086	0.475	554
155	→	<b>100</b>	0	0	0	0	0	0	0	0	0
180	→	<b>153</b>	0.502	0.897	178.6	0.331	0.723	218.4	0.473	0.905	191
182	→	<b>154</b>	0.757	1.858	245.4	0.328	0.748	228.3	0.354	0.845	239
<b>183</b>	→	139	0.170	1.023	602.0	0.282	0.978	347.1	0.240	0.797	333
<b>183</b>	→	<b>154</b>	1.392	1.556	111.8	0.636	0.863	135.8	0.766	1.081	141
<b>183</b>	→	138	0.166	0.528	318.3	0.317	1.020	321.6	0.163	0.841	517
<b>183</b>	→	<b>153</b>	0.560	0.706	126.2	0.690	1.093	158.4	0.511	0.736	144
<b>183</b>	→	144	0.226	0.920	407.1	0.197	0.735	372.4	0.095	0.650	681
<b>183</b>	→	149	0.206	0.714	346.7	0.266	0.872	328.3	0.165	0.963	583
184	→	<b>154</b>	0.317	0.941	296.4	0.260	0.690	265.6	0.223	0.715	321
<b>194</b>	→	170	0.266	1.132	425.7	0.171	0.820	479.6	0.178	0.828	465
<b>194</b>	→	180	0.235	1.197	509.2	0.065	0.355	544.9	0.156	0.685	440
<b>194</b>	→	189	0.202	1.183	586.2	0.075	0.510	683.7	0.017	0.166	954
<b>194</b>	→	172	0.205	1.152	563.0	0.040	0.253	637.5	0.212	0.913	431
<b>195</b>	→	171	0.356	1.149	322.5	0.220	0.819	372.3	0.324	1.265	391
<b>195</b>	→	181	0.310	1.241	400.7	0.773	2.756	356.4	0.412	1.715	417
<b>195</b>	→	170	0.601	2.028	337.7	0.321	1.433	446.2	0.226	1.072	474
<b>195</b>	→	190	0.471	1.258	267.2	0.440	2.011	457.5	0.240	1.180	493
<b>195</b>	→	173	0.422	1.562	370.4	0.250	0.859	343.6	0.244	0.815	334
<b>195</b>	→	177	0.505	1.939	384.2	0.691	2.640	381.9	0.371	1.403	378
<b>196</b>	→	171	0.306	1.248	408.0	0.478	2.001	418.9	0.319	1.194	375
<b>196</b>	→	182	0.648	1.974	304.8	0.522	1.750	335.3	0.277	1.010	364
<b>196</b>	→	<b>183</b>	0.893	1.747	195.6	0.905	1.942	214.5	0.488	1.128	231
<b>196</b>	→	170	0.390	1.724	441.7	0.461	1.719	373.3	0.323	1.112	345

(cont. on next page)

**Table 4.7 (cont.)**

<b>196</b>	→	180	0.208	0.754	362.6	0.150	0.716	478.2	0.224	0.850	379
<b>196</b>	→	191	0.363	1.220	335.7	0.548	1.797	327.6	0.318	1.351	425
<b>196</b>	→	174	0.205	0.722	352.3	0.584	1.739	297.8	0.279	1.649	590
<b>196</b>	→	175	0.362	1.242	342.9	0.286	0.783	274.3	0.423	1.758	416
<b>197</b>	→	184	0.236	1.258	534.3	0.234	1.078	461.6	0.151	0.631	418
<b>197</b>	→	171	0.365	0.919	251.8	0.400	1.767	441.9	0.081	0.352	433
<b>197</b>	→	<b>183</b>	0.711	1.476	207.8	0.652	1.531	234.7	0.755	1.767	234
<b>197</b>	→	176	0.199	0.677	340.6	0.269	1.077	400.5	0.707	2.348	332
<b>198</b>	→	173	0.477	2.266	475.1	0.495	1.558	314.9	0.598	2.231	373
<b>198</b>	→	175	0.322	1.735	539.0	0.750	2.919	389.0	0.525	2.124	405
<b>198</b>	→	185	0.884	2.614	295.6	0.996	3.312	332.7	0.459	1.550	338
<b>198</b>	→	172	0.448	1.564	348.9	0.985	2.758	280.1	0.751	2.292	305
<b>198</b>	→	192	0.734	1.991	271.5	0.622	2.618	420.9	0.421	1.586	376
<b>198</b>	→	178	0.312	1.073	344.1	0.576	2.407	417.7	0.241	1.112	462
<b>199</b>	→	174	0.646	2.645	409.6	0.943	3.169	335.9	0.307	1.370	446
<b>199</b>	→	177	1.243	3.716	298.9	0.336	1.122	333.8	0.838	2.754	329
<b>199</b>	→	187	0.802	2.895	360.9	0.874	2.596	297.1	0.219	0.781	357
<b>199</b>	→	172	0.339	1.077	317.5	0.373	1.304	349.8	0.357	1.265	354
<b>199</b>	→	193	0.738	2.913	394.9	0.503	1.580	314.2	0.567	1.748	309
<b>199</b>	→	178	0.483	2.197	454.6	0.619	2.677	432.6	0.472	1.581	335
<b>200</b>	→	176	0.676	2.211	327.3	0.809	2.678	331.1	0.584	2.191	375
<b>200</b>	→	186	0.969	3.375	348.5	0.543	1.637	301.5	0.709	2.365	334
<b>200</b>	→	173	0.518	1.837	354.4	1.008	3.256	323.1	0.472	1.599	339
<b>200</b>	→	174	0.975	2.950	302.4	1.189	3.758	316.2	0.400	1.336	334
<b>200</b>	→	185	1.199	3.658	305.2	0.665	2.468	370.9	0.575	1.954	340
<b>200</b>	→	179	0.377	1.355	359.1	0.558	1.987	355.8	0.586	2.222	379
<b>201</b>	→	176	0.339	1.674	493.4	0.824	2.908	352.7	0.800	2.987	373
<b>201</b>	→	188	0.763	2.390	313.2	0.898	2.851	317.6	0.490	2.050	418
<b>201</b>	→	175	1.033	3.393	328.5	0.746	2.822	378.4	0.561	1.925	343
<b>201</b>	→	177	0.521	2.028	388.9	0.880	2.816	320.0	0.504	1.695	336
<b>201</b>	→	187	1.519	4.156	273.6	0.872	2.784	319.4	1.144	3.485	305
<b>202</b>	→	179	0.901	3.509	389.6	1.356	3.397	250.6	1.266	3.898	308
<b>202</b>	→	178	1.909	5.007	262.2	2.021	4.676	231.3	0.970	2.859	295
<b>203</b>	→	181	0.407	1.399	343.7	0.723	2.407	332.9	0.391	1.405	359
<b>203</b>	→	<b>183</b>	1.201	2.000	166.5	0.988	1.791	181.4	0.984	1.969	200
<b>203</b>	→	180	0.485	1.764	363.8	0.446	1.575	353.1	0.461	1.351	293
<b>203</b>	→	185	0.187	0.610	326.5	0.455	1.753	385.6	0.246	0.855	347
<b>203</b>	→	187	0.621	2.048	329.8	0.626	2.254	359.9	0.213	1.165	548
<b>204</b>	→	184	0.200	0.905	453.1	0.269	1.117	414.6	0.294	1.499	509
<b>204</b>	→	181	0.604	2.223	368.2	0.103	0.382	371.6	0.189	1.020	541
<b>204</b>	→	182	0.646	2.603	403.2	0.084	0.412	491.2	0.447	1.780	398
<b>204</b>	→	186	0.221	0.922	417.0	0.577	2.431	421.1	0.326	1.383	424
<b>204</b>	→	188	0.439	1.957	446.1	0.213	1.039	487.6	0.443	1.537	347
<b>205</b>	→	190	0.121	0.589	488.6	0.090	0.643	714.8	0.222	1.115	502
<b>205</b>	→	191	0.118	0.878	742.5	0.122	0.746	610.6	0.026	0.204	792
<b>205</b>	→	189	0.424	1.487	350.4	0.069	0.374	545.5	0.180	0.815	454
<b>205</b>	→	192	0.101	0.364	359.2	0.200	1.059	529.2	0.058	0.464	806
<b>205</b>	→	193	0.171	1.013	591.6	0.334	1.402	419.8	0.083	0.434	523
<b>206</b>	→	<b>195</b>	1.395	3.101	222.3	0.802	1.918	239.2	0.805	2.008	249
<b>206</b>	→	<b>196</b>	1.574	2.545	161.7	1.274	2.595	203.7	1.222	2.446	200
<b>206</b>	→	<b>203</b>	1.090	2.507	229.9	0.848	2.232	263.3	0.773	1.993	258
<b>206</b>	→	<b>194</b>	1.186	2.699	227.6	0.560	1.557	277.8	1.078	1.992	185
<b>206</b>	→	<b>205</b>	1.089	2.695	247.5	0.988	2.281	231.0	0.753	2.199	292
<b>206</b>	→	<b>198</b>	0.906	2.327	256.8	0.771	2.069	268.3	0.727	1.947	268
<b>206</b>	→	<b>199</b>	1.144	2.495	218.0	1.121	2.513	224.1	0.801	2.119	264
<b>207</b>	→	<b>197</b>	1.860	3.070	165.1	1.736	3.350	192.9	2.172	3.987	184
<b>207</b>	→	<b>204</b>	2.572	5.010	194.8	1.484	3.039	204.8	2.209	4.147	188

(cont. on next page)

**Table 4.7 (cont.)**

<b>207</b>	→	<b>195</b>	1.617	3.510	217.1	2.163	4.563	211.0	1.362	3.138	230
<b>207</b>	→	<b>196</b>	2.743	4.228	154.2	3.412	5.272	154.5	2.270	3.456	152
<b>207</b>	→	<b>203</b>	2.107	3.966	188.2	2.680	4.708	175.7	1.897	3.820	201
<b>207</b>	→	<b>200</b>	2.621	5.245	200.1	1.954	4.169	213.4	1.646	3.277	199
<b>207</b>	→	<b>201</b>	2.455	4.734	192.8	1.506	3.829	254.2	1.922	3.443	179
<b>208</b>	→	<b>200</b>	2.763	4.803	173.8	3.492	6.084	174.2	2.428	4.283	176
<b>208</b>	→	<b>201</b>	3.795	5.867	154.6	3.807	6.062	159.2	3.169	5.400	170
<b>208</b>	→	<b>198</b>	2.920	4.652	159.3	4.269	6.621	155.1	2.925	5.031	172
<b>208</b>	→	<b>199</b>	3.793	6.571	173.3	3.138	4.831	154.0	2.619	4.359	166
<b>208</b>	→	<b>202</b>	4.005	6.338	158.3	3.944	6.153	156.0	3.000	5.202	173
<b>209</b>	→	<b>207</b>	37.46	17.03	45.5	36.61	17.16	46.9	32.27	13.89	43
<b>209</b>	→	<b>206</b>	53.47	11.39	21.3	52.96	11.17	21.0	43.97	10.23	23
<b>209</b>	→	<b>208</b>	32.83	19.04	58.0	31.83	20.85	65.5	25.25	17.02	67

\*Bold are marker congeners.

Among the 124 pathways, 33 contained marker compounds as both mother and daughter, and their k-values were calculated based on the reaction amounts. For the remaining 91 pathways, no concentration data was available to determine k-values. Therefore, machine learning was employed to predict k-values by considering reaction amounts, pathway information, and calculated k-values, as discussed in section 4.2.3.

The calculated k-values for bioremediation scenarios are presented in Table 4.8, with the position of bromine atom removed in the relevant pathway. The position of bromine atoms on the PBDE structure—whether ortho, meta, or para—played a significant role in evaluating the possible dehalogenation pathways and the degradation rate. For instance, the least number of possible pathways were observed for the removal from para positions (only 5 pathways), whereas the removal from ortho and meta positions occurred much more frequently (Table 4.8). Furthermore, the average of the rate constants estimated for dehalogenation from meta position was higher than that of ortho position for every bioremediation scenario. Hence, it can be speculated that for the dehalogenation of PBDEs, meta and ortho bromine removal was favored in the sediments, regardless of the bioremediation method applied.

The degradation process was found to be significantly influenced by the number of bromine atoms in the PBDE molecule. As the number of bromine in the structure decreased, the degradation rates tended to increase. For example, in the transformation from deca-BDE 209 to nona-BDE 208 (ortho position), the degradation rates were 0.00032 d<sup>-1</sup>, 0.00032 d<sup>-1</sup>, and 0.00026 d<sup>-1</sup> for NA, BS, and BA, respectively. Ortho bromine removal in dehalogenation of penta-BDE 100 to tetra-BDE 47, the k-values were

notably higher at 0.00067 d<sup>-1</sup> for NA, 0.00082 d<sup>-1</sup> for BS, and 0.00262 d<sup>-1</sup> for BA. This trend suggested that lower-brominated congeners might be more prone to degradation, potentially due to their less stable molecular structures.

Table 4.8. Dehalogenation rate constants estimated by ADM-IE for microcosm data set between days zero and 180.

Position	Mother	Daughter	k-values					Homologs
			NA	BS	BA	NC	SC	
Para	209	208	0.00019	0.00018	0.00014	1.18E-04	0	deca-nona
Ortho	209	206	0.00032	0.00032	0.00026	2.01E-04	0	deca-nona
Meta	209	207	0.00021	0.00020	0.00018	1.49E-04	0	deca-nona
Para	208	202	0.00072	0.00073	0.00070	6.33E-04	0	nona-octa
Ortho	208	199	0.00078	0.00066	0.00070	6.77E-04	0	nona-octa
Ortho	208	198	0.00059	0.00089	0.00077	7.47E-04	0	nona-octa
Meta	208	201	0.00075	0.00083	0.00085	7.80E-04	0	nona-octa
Meta	208	200	0.00056	0.00074	0.00065	5.76E-04	0	nona-octa
Para	207	201	0.00034	0.00021	0.00030	2.98E-04	0	nona-octa
Para	207	200	0.00039	0.00029	0.00027	2.43E-04	0	nona-octa
Ortho	207	203	0.00031	0.00040	0.00031	2.60E-04	0	nona-octa
Ortho	207	196	0.00040	0.00053	0.00038	2.76E-04	0	nona-octa
Ortho	207	195	0.00024	0.00033	0.00023	1.89E-04	0	nona-octa
Meta	207	204	0.00037	0.00022	0.00037	3.18E-04	0	nona-octa
Meta	207	197	0.00027	0.00025	0.00037	3.26E-04	0	nona-octa
Meta	206	199	0.00011	0.00010	0.00008	1.10E-04	2.22E-05	nona-octa
Para	206	198	0.00009	0.00007	0.00008	1.04E-04	1.50E-05	nona-octa
Ortho	206	205	0.00010	0.00009	0.00008	1.03E-04	1.61E-05	nona-octa
Ortho	206	194	0.00011	0.00005	0.00011	1.17E-04	1.67E-05	nona-octa
Meta	206	203	0.00010	0.00007	0.00008	1.11E-04	1.39E-05	nona-octa
Meta	206	196	0.00015	0.00011	0.00013	1.37E-04	1.05E-05	nona-octa
Meta	206	195	0.00013	0.00007	0.00008	1.14E-04	1.67E-05	nona-octa
Meta	203	183	0.01269	0.01003	0.00721	1.39E-02	9.73E-04	octa-hepta
Ortho	197	183	0.00267	0.00262	0.00237	2.28E-03	0	octa-hepta
Meta	196	183	0.00465	0.00689	0.00284	3.18E-03	1.48E-04	octa-hepta
Ortho	183	153	0.00548	0.00798	0.01717	5.54E-03	2.81E-05	hepta-hexa
Meta	183	154	0	0	0	0	0	hepta-hexa
Ortho	154	99	0.00093	0.00405	0.00277	2.13E-03	0	hexa-penta
Meta	154	100	0.00136	0.00138	0.01013	4.29E-03	0	hexa-penta
Meta	153	99	0.01059	0.00743	0.02935	6.96E-03	3.85E-03	hexa-penta
Ortho	100	47	0.00067	0.00082	0.00262	3.97E-03	0	penta-tetra
Meta	99	47	0.00247	0.00458	0.01624	6.00E-03	3.85E-03	penta-tetra
Ortho	47	28	0.00363	0.00383	0.00672	4.69E-03	0	tetra-tri
Average±			0.0023±	0.0022±	0.0046±	0.0025±	0.0006±	
std.dev.meta			0.0039	0.0032	0.0081	0.0038	0.0013	
Average±			0.0012±	0.0017±	0.0027±	0.0016±	4.68E-06±	
std.dev.ortho			0.0016	0.0022	0.0046	0.0019	8.95E-06	
Average±			0.0003±	0.0003±	0.0003±	0.0003±	3.00E-06±	
std.dev.para			0.0002	0.0002	0.0002	0.0002	6.00E-06	

Across the three bioremediation scenarios, the degradation rates varied, with bioaugmentation generally showing the highest k-values for several pathways (Table 4.8). For example, the pathway, having the highest degradation rate, BDE-153 → BDE-99 showed a significant increase in the degradation rate, with BA reaching 0.02935 d<sup>-1</sup>, compared to 0.01059 d<sup>-1</sup> under NA conditions. This indicated that bioaugmentation enhanced the degradation process, likely due to the enhanced microbial activity introduced into the system. Hence, it can be suggested that bioaugmentation was the most effective method for improvement of the PBDE degradation process, followed by biostimulation and natural attenuation.

On the other hand, certain pathways, such as the BDE-196 → BDE-183, exhibited higher degradation rates under BS conditions, with a k value of 0.00689 d<sup>-1</sup> compared to 0.00465 d<sup>-1</sup> under NA conditions (Table 4.8). This variation demonstrated the effectiveness of different microcosm strategies in influencing the degradation of PBDEs depending on the pathways and the environmental conditions. Another observation was for the dehalogenation from hexa- to penta-BDEs. The results showed that meta bromine removal had higher rate constants under BS conditions. This suggested that the progress of degradation was highly dependent on both the bromine atom positions and the type of bioremediation method applied.

Additionally, when sorted from high to lower k values, the order of pathways differed among the bioremediation scenarios, although the first ten were almost the same for all scenarios. These findings indicated that preferential pathways occurred regardless of the addition of nutrients and microorganisms to the sediments.

The negative control and sterile microcosm data were also analyzed in the model based on the 0-180 day dataset (Table 4.8) To facilitate the comparison with the test microcosm data, the results are displayed in graphical form in Figure 4.4. As can be seen from Figure 4.4, sterile control microcosms exhibited zero or very low degradation rates for most of the pathways. For some of the pathways, especially the ones with high degradation rates in bioremediation microcosms, both negative control and sterile sets revealed high k values, for some cases even higher than bioremediation microcosms. In the sterile set, no congeners other than BDE-209 and 206 were detected at any time period. However, ADM-IE predicted some of the pathways to occur in the sterile set. When the reaction amounts in the sterile set were examined, it can be seen that they were very low compared to other microcosm sets and RSDs were very high. The negative control set resembled the natural attenuation set in terms of its liquid content, with a minor

addition of nutrients. Therefore, the k-values obtained for the dehalogenation pathways were expected to be similar to the natural attenuation set, and smaller than the bioaugmentation set. The k-values presented in Figure 4.4 supported this hypothesis for most of the pathways. Only in the pathways BDE-203 → BDE-183 and BDE-100 → BDE-47, negative control set revealed k-values greater than all microcosm sets. The reason for this observation was not understood clearly.

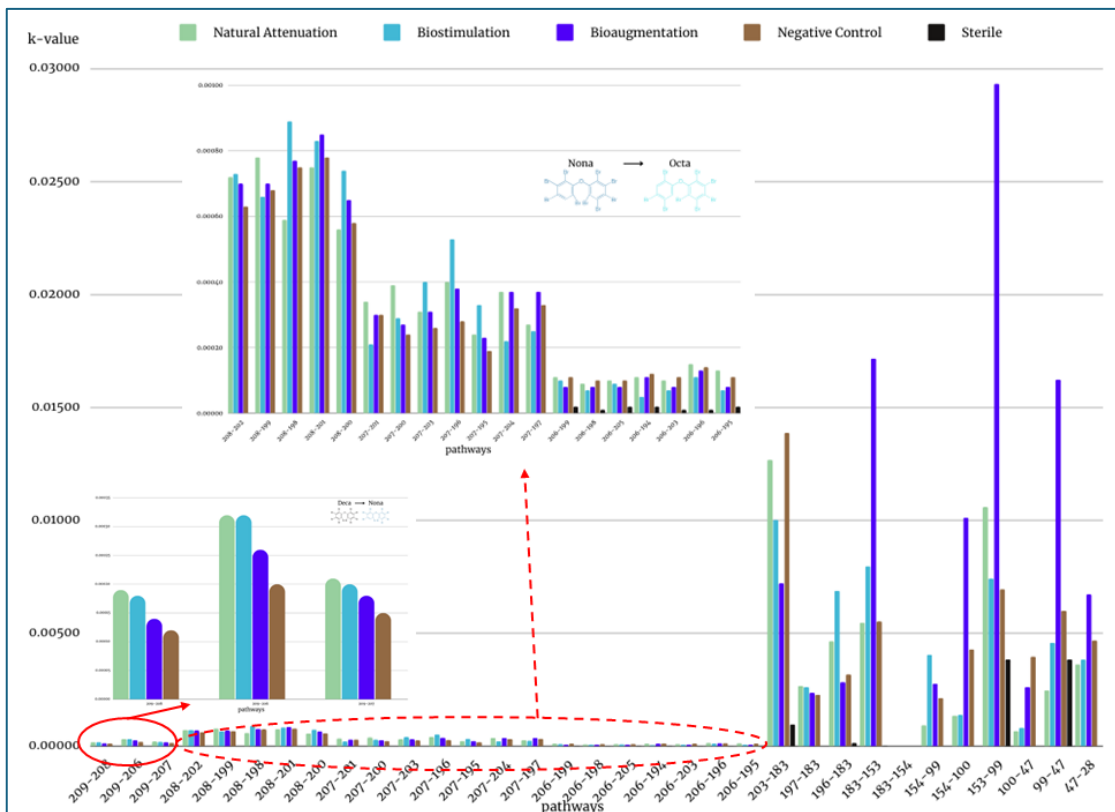


Figure 4.4. Marker pathways' k-values for all microcosm data between 0 and 180 days.

To evaluate possibly occurring dehalogenation pathways observed in each bioremediation scenario and better visualize them, Figure 4.5, 4.6, and 4.7 was prepared. When the figures were examined, several findings can be highlighted:

- a. A variation of preferential pathways for mother congeners having more than one daughter was observed in three bioremediation scenarios. For example, for bioaugmentation, BDE-206 → BDE-196 and BDE-206 → BDE-194 were favored when compared to other daughters of BDE-206. However, for BDE-207 and 208, no preference was observed for their pathways. On the other hand, in biostimulation

BDE-206 → BDE-196 and BDE-206 → BDE-199, BDE-207 → BDE-196 and BDE-207 → BDE-203, BDE-208 → BDE-198 and BDE-208 → BDE-201 were preferred. Lastly, for natural attenuation, BDE-206 had no preferential pathways, while BDE-207 → BDE-196 and BDE-207 → BDE-200, BDE-208 → BDE-199 and BDE-208 → BDE-201 were favored. For dehalogenation of BDE-154, BDE-100 was the dominant product in bioaugmentation and natural attenuation, while it was BDE-99 in biostimulation. Both BDE-99 and -100 were classified as bioaccumulative compounds, but no-observed effect level for aquatic species (NOEC) of BDE-99 is lower than that of BDE-100, which indicates that BDE-99 is more toxic than BDE-100 (“Comptox” 2024). To conclude, degradation of PBDEs can be tailored by applying different bioremediation methods to enhance the removal of specific congeners and to ensure that less harmful products were obtained.

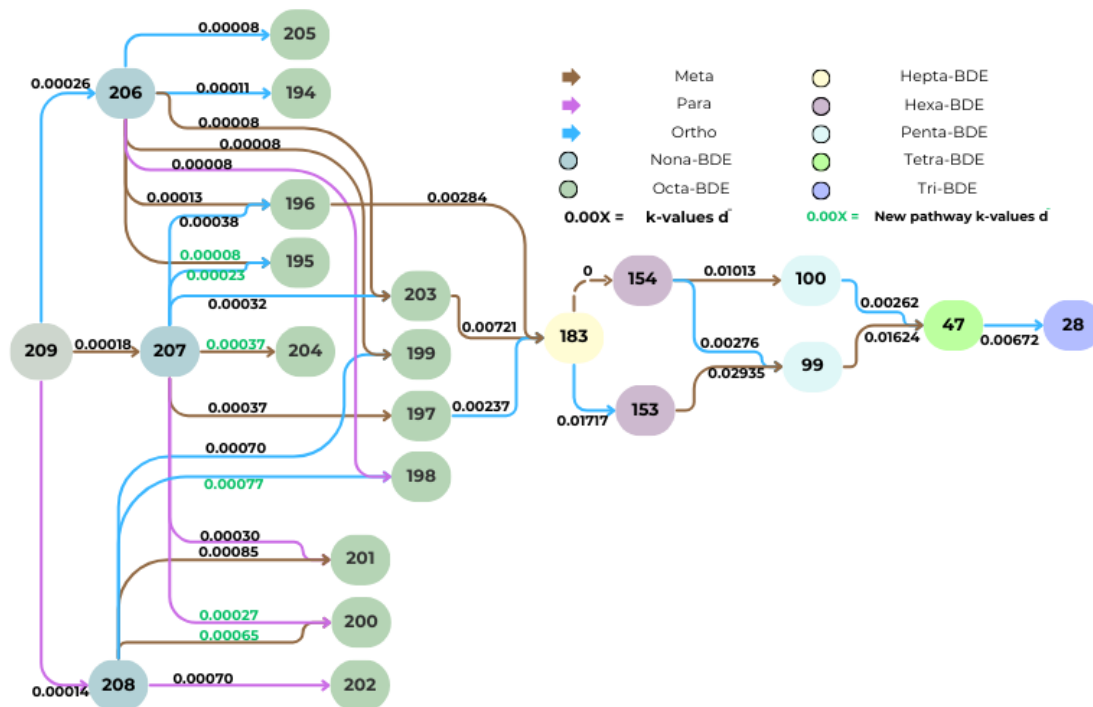


Figure 4.5. Degradation rate constants under bioaugmentation between 0 and 180 days.

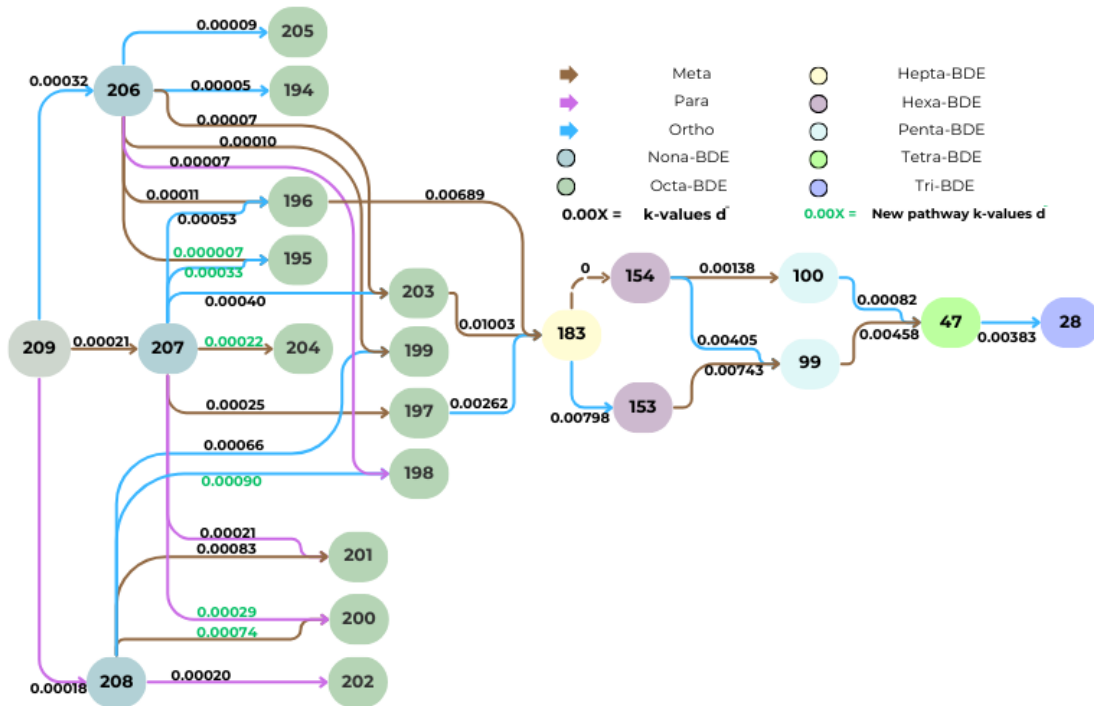


Figure 4.6. Degradation rate constant under biostimulation between 0 and 180 days.

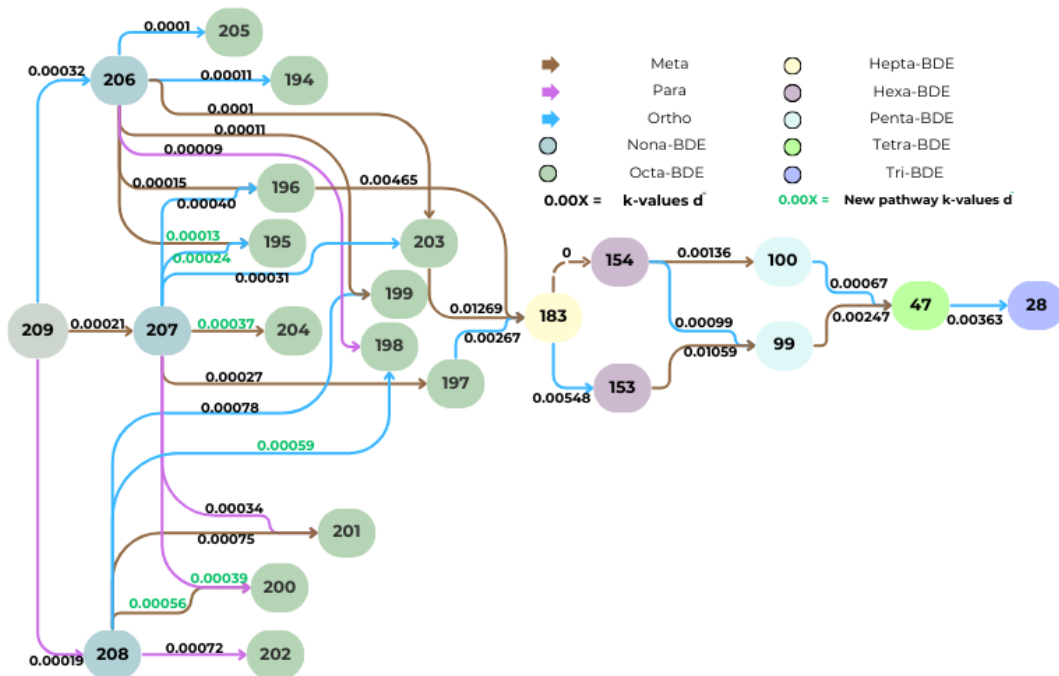


Figure 4.7. Degradation rate constant under natural attenuation between 0 and 180 days.

- b. The pathways for ortho bromine removal in all bioremediation scenarios displayed relatively consistent degradation rates but were often enhanced in bioaugmentation, indicating that bioaugmentation favored ortho degradation. The meta bromine removal pathways tended to show higher k-values in biostimulation and bioaugmentation, suggesting that both methods facilitated meta position degradation more effectively than natural attenuation. For the para removal pathways, the degradation rates remained moderate across all methods. This analysis highlighted that bioaugmentation generally yielded the highest degradation rates across multiple pathways, followed by biostimulation, with natural attenuation exhibiting the slowest degradation in most cases.
- c. Green-labeled k-values represented pathways not reported in previous studies. Hence, novel degradation routes under specific conditions could be proposed, highlighting the ADM-IE capability to detect pathways in PBDE anaerobic degradation. The newly identified degradation pathways, shown in Table 4.9, demonstrated moderate degradation rates and emphasized the diversity in dehalogenation potential depending on the position of bromine atoms in the molecule. The pathways also displayed clear differentiation in degradation rates based on bioremediation scenario. For instance, three out of six pathways showed the highest k-values under biostimulation, suggesting that biostimulation may enhance degradation rates for certain congeners. To sum up, the novel pathways identified here suggested potential additional degradation routes that had not been previously reported, adding new dimensions to understanding PBDE degradation in sediment environments.

Table 4.9. Novel pathways degradation rate constants under test microcosms.

<b>New Pathway</b>	<b>NA k-value (<math>d^{-1}</math>)</b>	<b>BS k-value (<math>d^{-1}</math>)</b>	<b>BA k-value (<math>d^{-1}</math>)</b>	<b>Pos.</b>
208-200	0.00056	0.00074	0.00065	Meta
208-198	0.00059	0.00090	0.00077	Ortho
207-200	0.00039	0.00029	0.00027	Para
207-204	0.00037	0.00022	0.00038	Meta
207-195	0.00024	0.00033	0.00023	Ortho
206-195	0.00013	0.00007	0.00008	Meta

## 4.2.2. Sequential degradation analysis in defined time intervals for microcosms

The microcosms were operated for 180 days with periodic sampling on days 20, 40, 60, 90, 120, 152, and 180. Examining the data revealed distinct changes in PBDE concentrations after 90 days. Hence, the ADM-IE was applied to the data structured in time intervals: 0-90, 90-120, 120-152, and 152-180 days, allowing for a detailed analysis of the degradation progress within each time period. Table 4.10 presents the degradation rate constants for the dehalogenation pathways in bioremediation microcosms. The results revealed that pathways occurred at their highest rates at various time intervals for different bioremediation scenarios. For example, BDE-153 → BDE-99 pathway occurred at its highest rate between 0 and 90 days for bioaugmentation, between 90 and 120 days for biostimulation, and between 120 and 152 for natural attenuation. Similar cases were observed for BDE-196 → BDE-183 and BDE-197 → BDE-183. This finding indicated the delayed dehalogenation of some pathways under natural sediment conditions when no treatment was applied. For a couple of pathways, e.g. BDE-183 → BDE-153, the opposite situation was observed. This specific pathway had high degradation rates almost at all time periods. This comprehensive analysis provided a valuable comparison of the degradation rates, highlighting the effectiveness of different microcosm conditions and specific time periods for enhanced degradation.

Table 4.10. Degradation rate constants for dehalogenation pathways in different time intervals.

Pos.	Hom.	M	D	Natural Attenuation				Biostimulation				Bioaugmentation				
				0(day) 90	90 120	120 152	152 180	0(day) 90	90 120	120 152	152 180	0(day) 90	90 120	120 152	152 180	
Para	deca- nona	209	208	0.000	0.001	0.000	0.000	0.000	0.001	0.000	0.000	0.000	0.000	0.001	0.000	0.000
Ortho	deca- nona	209	206	0.000	0.001	0.000	0.001	0.000	0.001	0.000	0.001	0.000	0.000	0.001	0.000	0.001
Meta	deca- nona	209	207	0.000	0.001	0.000	0.000	0.000	0.002	0.000	0.000	0.000	0.000	0.001	0.000	0.001
Para	nona- octa	208	202	0.002	0.001	0.003	0.001	0.001	0.002	0.005	0.002	0.002	0.002	0.003	0.005	0.003
Ortho	nona- octa	208	199	0.001	0.001	0.002	0.001	0.001	0.003	0.006	0.002	0.002	0.002	0.003	0.006	0.003
Ortho	nona- octa	208	198	0.002	0.002	0.002	0.001	0.001	0.002	0.005	0.003	0.002	0.002	0.003	0.006	0.004
Meta	nona- octa	208	201	0.002	0.002	0.002	0.001	0.002	0.003	0.005	0.003	0.002	0.002	0.003	0.005	0.005

(cont. on next page)

**Table 4.10 (cont.)**

Meta	nona-octa	208	200	0.002	0.003	0.002	0.001	0.001	0.002	0.005	0.003	0.002	0.002	0.005	0.004
Para	nona-octa	207	201	0.001	0.000	0.001	0.002	0.001	0.001	0.003	0.001	0.001	0.001	0.003	0.002
Para	nona-octa	207	200	0.001	0.000	0.001	0.002	0.000	0.001	0.003	0.001	0.001	0.001	0.003	0.001
Ortho	nona-octa	207	203	0.001	0.000	0.001	0.002	0.001	0.001	0.003	0.001	0.001	0.000	0.003	0.001
Ortho	nona-octa	207	196	0.001	0.001	0.002	0.001	0.001	0.002	0.003	0.001	0.001	0.001	0.004	0.002
Ortho	nona-octa	207	195	0.001	0.000	0.001	0.001	0.001	0.000	0.003	0.001	0.001	0.001	0.005	0.001
Meta	nona-octa	207	204	0.001	0.000	0.001	0.002	0.001	0.001	0.003	0.001	0.001	0.001	0.003	0.002
Meta	nona-octa	207	197	0.001	0.000	0.001	0.002	0.000	0.001	0.003	0.001	0.001	0.001	0.004	0.001
Meta	nona-octa	206	199	0.000	0.001	0.000	0.000	0.000	0.001	0.002	0.000	0.000	0.001	0.002	0.000
Para	nona-octa	206	198	0.000	0.001	0.000	0.000	0.000	0.001	0.002	0.000	0.000	0.001	0.003	0.000
Ortho	nona-octa	206	205	0.000	0.001	0.000	0.000	0.000	0.001	0.002	0.000	0.000	0.001	0.003	0.000
Ortho	nona-octa	206	194	0.001	0.001	0.001	0.000	0.000	0.001	0.002	0.000	0.000	0.001	0.004	0.001
Meta	nona-octa	206	203	0.000	0.001	0.000	0.000	0.000	0.001	0.002	0.000	0.000	0.001	0.003	0.000
Meta	nona-octa	206	196	0.000	0.002	0.001	0.000	0.000	0.003	0.002	0.000	0.000	0.002	0.003	0.000
Meta	nona-octa	206	195	0.000	0.001	0.000	0.000	0.000	0.001	0.002	0.000	0.000	0.001	0.004	0.000
Meta	octa-hepta	203	183	0.027	0.021	0.195	0.000	0.015	0.021	0.044	0.031	0.000	0.019	0.013	0.068
Ortho	octa-hepta	197	183	0.007	0.004	0.006	0.016	0.009	0.020	0.011	0.011	0.004	0.010	0.009	0.011
Meta	octa-hepta	196	183	0.007	0.002	0.001	0.027	0.021	0.003	0.005	0.004	0.038	0.007	0.007	0.004
Ortho	hepta-hexa	183	153	0.019	0.069	0.035	0.024	0.021	0.038	0.119	0.073	0.009	0.043	0.116	0.056
Ortho	hexa-penta	154	99	0.004	0.025	0.097	0.002	0.003	0.040	0.020	0.058	0.009	0.035	0.023	0.006
Meta	hexa-penta	154	100	0.016	0.005	0.000	0.004	0.016	0.000	0.000	0.000	0.000	0.000	0.000	0.016
Meta	hexa-penta	153	99	0.007	0.027	0.101	0.060	0.010	0.062	0.007	0.034	0.037	0.032	0.007	0.017
Ortho	penta-tetra	100	47	0.002	0.004	0.009	0.005	0.002	0.003	0.002	0.007	0.002	0.006	0.001	0.013
Meta	penta-tetra	99	47	0.014	0.011	0.014	0.010	0.018	0.013	0.093	0.001	0.013	0.015	0.019	0.008
Ortho	tetra-tri	47	28	0.009	0.023	0.025	0.025	0.005	0.024	0.000	0.044	0.010	0.026	0.000	0.076

### 4.3. Analysis of machine learning results

In this study, the ML methods were applied to estimate k-values for the dehalogenation pathways proposed with a non-marker congener as either mother or daughter. These ML methods were applied to natural attenuation, biostimulation and bioaugmentation data sets, only for the time interval 0-180 days. Three ML algorithms were tested and the results were compared in Appendix-C. The method with the highest performance, as indicated by the R value, was selected for further analysis. Hence, machine learning results with R-values averaging below 0.5 for linear regression and SVM were excluded from further evaluation. Since the neural network model demonstrated higher performance, machine learning analysis continued based on this method's results.

The neural network validation outcomes for NA, BS, BA are presented in Figure 4.8. These validation plots represented the performance of the Feedforward Neural Network under different conditions. The R-values greater than 0.76 indicated a strong correlation between the model's outputs and the targets, showing accurate prediction performance. The R values were converted to  $R^2$  for a more comprehensive analysis and are presented in Table 4.11.

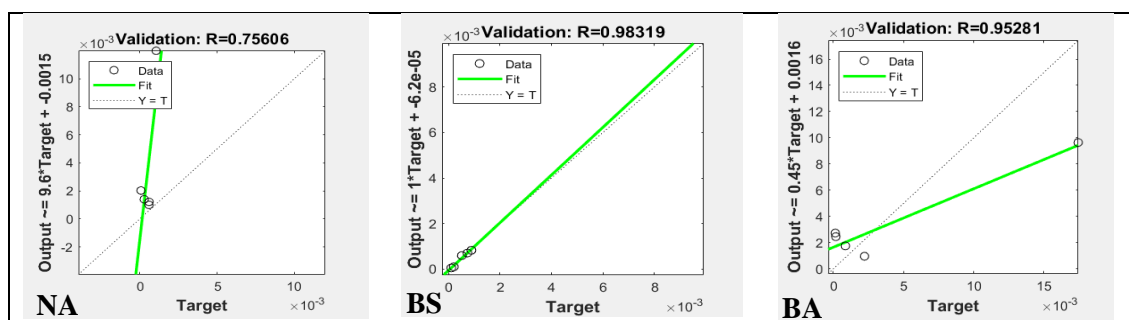


Figure 4.8. BS, NA and BA neural network model results.

Table 4.11. Neural network model performance results under 3 test microcosms.

Bioremediation Methods	Natural Attenuation	Biostimulation	Bioaugmentation
$R^2$	0.5716	0.9667	0.9078

### 4.3.1. Pathways and degradation rates estimated by machine learning

ADM-IE identified a total of 124 pathways, but using neural network model, the k-values for the 91 pathways were estimated and are provided in Table 4.12. As the number of possible pathways was high and the k-values ranged between 0 and 0.025  $d^{-1}$  (BDE-183  $\rightarrow$  BDE-138), the evaluation would be challenging. To help in evaluating and understanding the pathways, significant pathways were defined to distinguish them from others and were highlighted in the visual representation of pathway mechanisms created for this purpose.

Table 4.12. k-values of non-marker pathways for bioremediation microcosms between 0 and 180 days, predicted by neural network model.

<b>Homolog</b>	<b>Pathway</b>		<b>k-values (<math>d^{-1}</math>)</b>		
	<b>M</b>	<b>D</b>	<b>Natural attenuation</b>	<b>Biostimulation</b>	<b>Bioaugmentation</b>
octa-hepta	<b>205</b>	193	0.00415	0.00165	0.00134
octa-hepta	<b>205</b>	192	0.00397	0.00068	0.00129
octa-hepta	<b>205</b>	189	0.00512	0.00000	0.00096
octa-hepta	<b>205</b>	191	0.00400	0.00000	0.00123
octa-hepta	<b>205</b>	190	0.00400	0.00000	0.00104
octa-hepta	<b>204</b>	188	0.00510	0.00045	0.00116
octa-hepta	<b>204</b>	186	0.00416	0.00165	0.00078
octa-hepta	<b>204</b>	182	0.00630	0.00000	0.00062
octa-hepta	<b>204</b>	181	0.00593	0.00000	0.00023
octa-hepta	<b>204</b>	184	0.00409	0.00074	0.00056
octa-hepta	<b>203</b>	187	0.00629	0.00154	0.00092
octa-hepta	<b>203</b>	185	0.00402	0.00168	0.00073
octa-hepta	<b>203</b>	180	0.00505	0.00155	0.00057
octa-hepta	<b>203</b>	181	0.00469	0.00128	0.00046
octa-hepta	<b>202</b>	178	0.01869	0.00036	0.00294
octa-hepta	<b>202</b>	179	0.00828	0.00020	0.00303
octa-hepta	<b>201</b>	179	0.00981	0.00156	0.00145
octa-hepta	<b>201</b>	187	0.01396	0.00076	0.00444
octa-hepta	<b>201</b>	177	0.00504	0.00079	0.00066
octa-hepta	<b>201</b>	175	0.00917	0.00121	0.00077
octa-hepta	<b>201</b>	188	0.00748	0.00068	0.00154
octa-hepta	<b>201</b>	176	0.00427	0.00096	0.00232
octa-hepta	<b>200</b>	179	0.00437	0.00156	0.00142
octa-hepta	<b>200</b>	185	0.01109	0.00139	0.00182
octa-hepta	<b>200</b>	174	0.00848	0.00027	0.00002
octa-hepta	<b>200</b>	173	0.00487	0.00049	0.00018
octa-hepta	<b>200</b>	186	0.00924	0.00164	0.00277
octa-hepta	<b>200</b>	176	0.00594	0.00099	0.00113
octa-hepta	<b>199</b>	178	0.00474	0.00147	0.00082
octa-hepta	<b>199</b>	193	0.00742	0.00173	0.00228
octa-hepta	<b>199</b>	172	0.00415	0.00101	0.00000
octa-hepta	<b>199</b>	187	0.00763	0.00073	0.00121
octa-hepta	<b>199</b>	177	0.01099	0.00083	0.00287
octa-hepta	<b>199</b>	174	0.00557	0.00061	0.00000
octa-hepta	<b>198</b>	178	0.00405	0.00149	0.00045
octa-hepta	<b>198</b>	192	0.00723	0.00147	0.00180
octa-hepta	<b>198</b>	172	0.00444	0.00052	0.00200
octa-hepta	<b>198</b>	185	0.00821	0.00046	0.00145
octa-hepta	<b>198</b>	175	0.00406	0.00113	0.00090
octa-hepta	<b>198</b>	173	0.00456	0.00140	0.00115
octa-hepta	<b>197</b>	176	0.00376	0.00011	0.00229
octa-hepta	<b>197</b>	171	0.00411	0.00106	0.00000
octa-hepta	<b>197</b>	184	0.00386	0.00016	0.00111
octa-hepta	<b>196</b>	175	0.00406	0.00021	0.00064
octa-hepta	<b>196</b>	174	0.00373	0.00139	0.00023
octa-hepta	<b>196</b>	191	0.00437	0.00159	0.00171
octa-hepta	<b>196</b>	180	0.00373	0.00000	0.00082
octa-hepta	<b>196</b>	170	0.00412	0.00123	0.00000

(cont. on next page)

**Table 4.12 (cont.)**

octa-hepta	<b>196</b>	182	0.00571	0.00151	0.00103
octa-hepta	<b>196</b>	171	0.00392	0.00127	0.00000
octa-hepta	<b>195</b>	177	0.00458	0.00121	0.00079
octa-hepta	<b>195</b>	173	0.00418	0.00000	0.00020
octa-hepta	<b>195</b>	181	0.00392	0.00099	0.00124
octa-hepta	<b>195</b>	171	0.00398	0.00010	0.00005
octa-hepta	<b>194</b>	172	0.00364	0.00199	0.00017
octa-hepta	<b>194</b>	189	0.00370	0.00000	0.00170
octa-hepta	<b>194</b>	180	0.00369	0.00000	0.00099
octa-hepta	<b>194</b>	170	0.00374	0.00062	0.00000
hepta-hexa	184	<b>154</b>	0.00334	0.01413	0.00000
hepta-hexa	<b>183</b>	149	0.00320	0.02002	0.00000
hepta-hexa	<b>183</b>	144	0.00330	0.02173	0.00000
hepta-hexa	<b>183</b>	138	0.00333	0.02538	0.00000
hepta-hexa	<b>183</b>	139	0.00332	0.02424	0.00000
hepta-hexa	182	<b>154</b>	0.00445	0.00950	0.00000
hepta-hexa	180	<b>153</b>	0.00341	0.00998	0.00066
hexa-penta	155	<b>100</b>	0.00000	0.00000	0.00000
hexa-penta	<b>154</b>	103	0.00113	0.00215	0.00036
hexa-penta	<b>154</b>	102	0.00111	0.00281	0.00019
hexa-penta	<b>153</b>	101	0.00102	0.00184	0.00085
hexa-penta	140	<b>100</b>	0.00000	0.00000	0.00000
hexa-penta	139	<b>99</b>	0.00026	0.00403	0.00552
hexa-penta	139	<b>100</b>	0.00024	0.00468	0.00576
hexa-penta	138	<b>99</b>	0.00022	0.00384	0.00600
hexa-penta	137	<b>99</b>	0.00000	0.00000	0.00000
penta-tetra	<b>100</b>	51	0.00000	0.00751	0.02089
penta-tetra	<b>100</b>	50	0.00000	0.00756	0.02056
penta-tetra	<b>100</b>	75	0.00000	0.00801	0.01915
penta-tetra	<b>99</b>	49	0.00000	0.00742	0.02159
penta-tetra	<b>99</b>	48	0.00000	0.00735	0.02098
penta-tetra	<b>99</b>	74	0.00000	0.00783	0.02014
penta-tetra	85	<b>47</b>	0.00000	0.00000	0.00000
tetra-tri	75	<b>28</b>	0.00000	0.00638	0.01494
tetra-tri	74	<b>28</b>	0.00000	0.00631	0.01585
tetra-tri	66	<b>28</b>	0.00000	0.00000	0.00000
tetra-tri	60	<b>28</b>	0.00000	0.00000	0.00000
tetra-tri	<b>47</b>	17	0.00000	0.00509	0.01104
tri-di	<b>28</b>	8	0.00000	0.00437	0.01077
tri-di	<b>28</b>	7	0.00000	0.00430	0.01072
tri-di	<b>28</b>	15	0.00000	0.00487	0.00000

The estimation of k-values for these 91 non-marker pathways relies on the reaction amounts determined by the ADM-IE and their inferred relationships with previously calculated marker congener pathways. To make a classification and evaluate the important pathways, the distribution of k-values obtained for each bioremediation microcosm was investigated and their mean and standard deviations were calculated. Among the non-marker congener pathways, those with k-values exceeding the sum of the mean and one standard deviation were defined as significant pathways.

The term ‘Machine Learning Highest k-values’ marker pathways identified through machine learning that exhibit the highest degradation rates but do not belong to significant pathways.

### 4.3.2. Natural attenuation neural network results

The k-values estimated by ML for natural attenuation microcosms indicated a range of degradation rates, with some pathways exhibiting slower rates (e.g., around 0.0007 d<sup>-1</sup>) and others demonstrating relatively higher degradation rates (e.g., around 0.01869 d<sup>-1</sup>). Figure 4.9 highlights 10 significant pathways as non-marker congener significant pathways (NCSP), for the natural attenuation microcosm. In Table 4-13, the significant pathways and their corresponding k-values are presented.

Table 4.13. k-values of non-marker significant pathways for natural attenuation.

Pathway	k-value (d <sup>-1</sup> )	Pathway	k-value (d <sup>-1</sup> )
202→178	0.01869	201→188	0.00748
202→179	0.00828	200→185	0.01101
201→179	0.00981	200→174	0.00848
201→187	0.01396	200→186	0.00924
201→175	0.00917	198→185	0.00821
		Stdev+mean = 0.0074	

The non-marker congener significant pathways acted as indirect routes within the degradation network, providing supplementary pathways that contributed to the overall degradation process. These machine learning-predicted k-values extended the degradation network by estimating the rates of pathways that did not have a concentration data. Importantly, these pathways suggested a potential transfer of concentration within the network that would not be observed through traditional calculations alone.

According to the natural attenuation results, BDE-202 → BDE-178 pathway demonstrated the highest k-value and neural network predicted higher k values for higher brominated BDEs such as octa and hepta-BDE homologs.

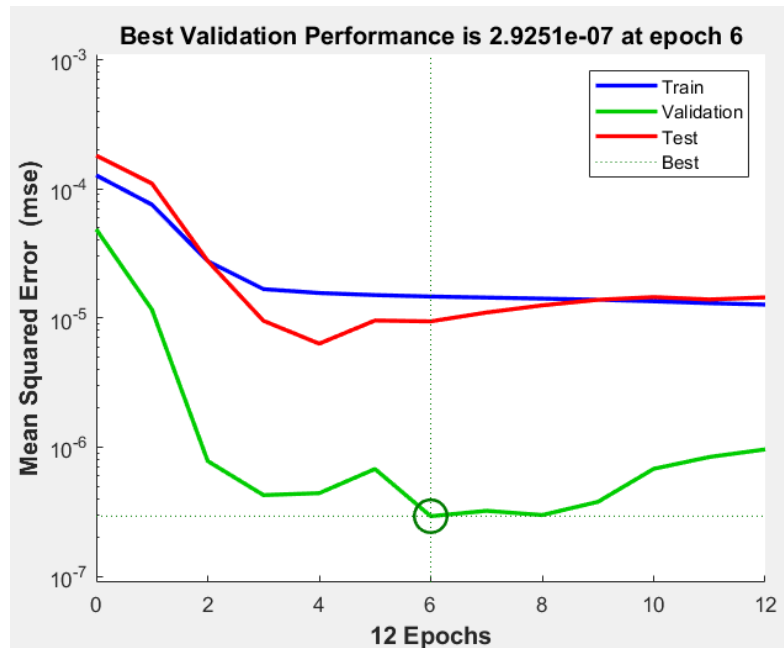


Figure 4.10. NA 0-180day MSE performance graph.

The performance plot for ML application to natural attenuation is given in Figure 4.10, demonstrating the MSE trend over 12 epochs for training, validation, and test sets as mentioned as in the methods section. The model achieved its lowest validation error at epoch 6, with an MSE of approximately  $2.93 \times 10^{-7}$ , indicating the optimal stopping point. Beyond this point, the validation error began to rise slightly, suggesting potential overfitting if training were to continue. The test and training errors stabilized at low values after epoch 6, further supporting that the model had effectively minimized errors by this epoch.



The training state graph shown in Figure 4.11 presents the gradient, Mu, and validation checks throughout the model's training, as detailed previously in the methodology section. According to this graph, the model completed its training at epoch 12 after six validation checks.

Figure 4.12 shows the distribution of errors between the target values and the model's predictions across the training. Based on this graph, the prediction errors for the training, validation, and test datasets were largely concentrated around zero. The error distribution indicated that most errors fell between  $-0.0001$  and  $0.0001$ , suggesting that the model's predictions were quite close to the target values. These values near the zero-error line represented points where the model achieved optimal performance.

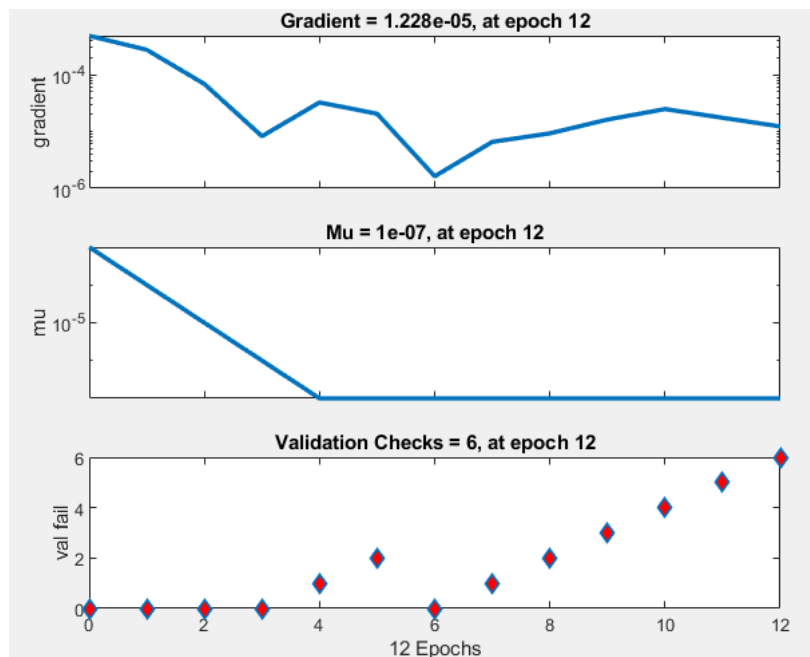


Figure 4.11. NA 0-180day training state graph.

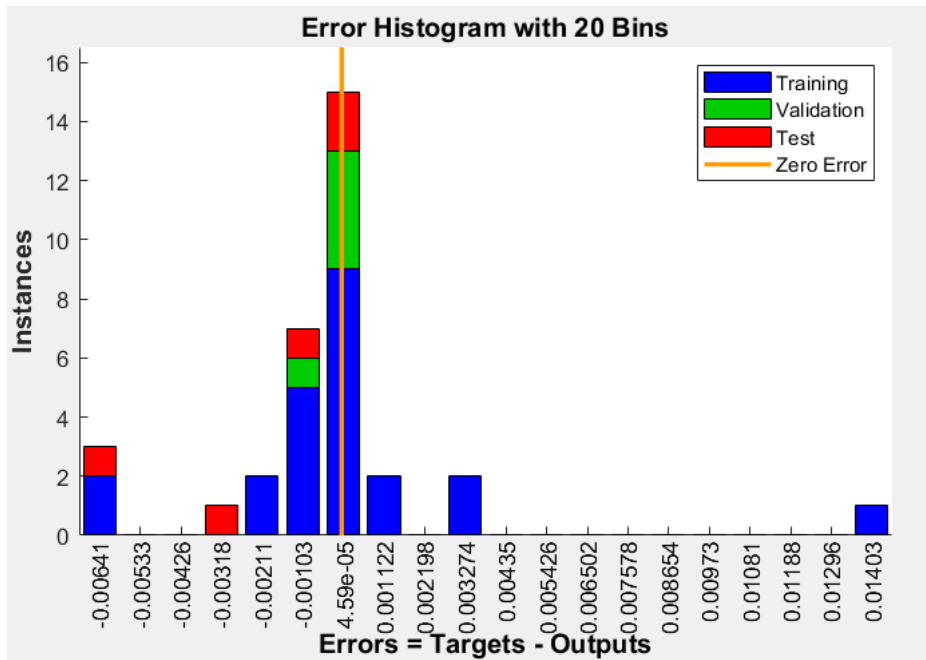


Figure 4.12. NA 0-180day error histogram training plots.

Lastly, the regression plots (Figure 4.13) showed the model's performance across training, validation, and test sets. The R-values varied, with the test set achieving the highest correlation at  $R = 0.94$ , indicating strong alignment with target values. However, the training and validation sets had lower R-values (0.57 and 0.76, respectively), suggesting some variability in model accuracy. The overall R-value of 0.35 reflected a moderate fit across all data.

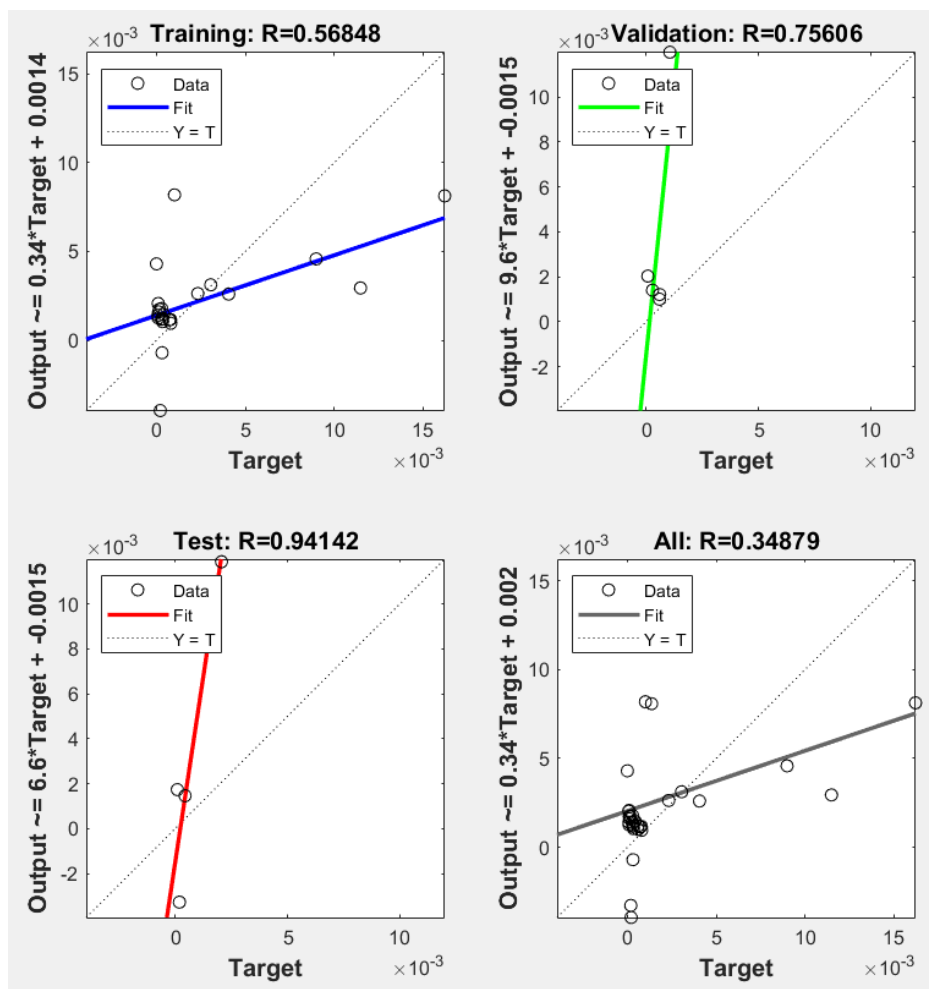


Figure 4.13. Regression graph for training, validation, and test.

### 4.3.3. Biostimulation 0-180day neural network results

Figure 4.14 highlights 7 non-marker congener significant pathways, each identified through machine learning to estimate degradation rates. In Table 4.14, the non-marker congener significant pathways and their corresponding k-values are presented.

Table 4.14. k-values of non-marker significant pathways for biostimulation.

<b>Pathway</b>	<b>k-value (<math>d^{-1}</math>)</b>	<b>Pathway</b>	<b>k-value (<math>d^{-1}</math>)</b>
184→154	0.01413	183→139	0.02424
183→149	0.02002	182→154	0.00949
183→144	0.02173	180→153	0.00998
183→138	0.02538	Stdev+mean=0.008	

These k-values indicated a range of degradation rates within the non-marker congener significant pathways, with a few pathways exhibiting slower rates such as BDE-182→BDE-154 ( $0.00949 d^{-1}$ ), and others demonstrating relatively higher degradation rates such as  $0.02538 d^{-1}$  in BDE-183→BDE-139 pathway. The significant pathways were observed only for dehalogenation of hepta-BDEs in biostimulation microcosm.

According to the results, BDE-182→BDE-154 and BDE-184→BDE-154 pathways were observed. These can be considered important pathways since the calculated k-value for the BDE-183→BDE-154 pathway is 0, which indicated that the mothers of BDE-154 were the congeners not measured commonly in environmental matrices. Additionally, significant degradation values were observed for the BDE-183→BDE-139 and BDE-183→BDE-138 pathways, whose daughters were the mothers of more toxic compounds such as BDE-100 and BDE-99 (“Comptox” 2024). Therefore, it can be concluded that while investigating PBDE contamination in sediments or their dehalogenation, BDE-182, BDE-184, BDE-138 and BDE-139 should be monitored to track their transformation into more toxic products. The bioremediation strategies would then be developed to direct the dehalogenation towards production of less harmful products.

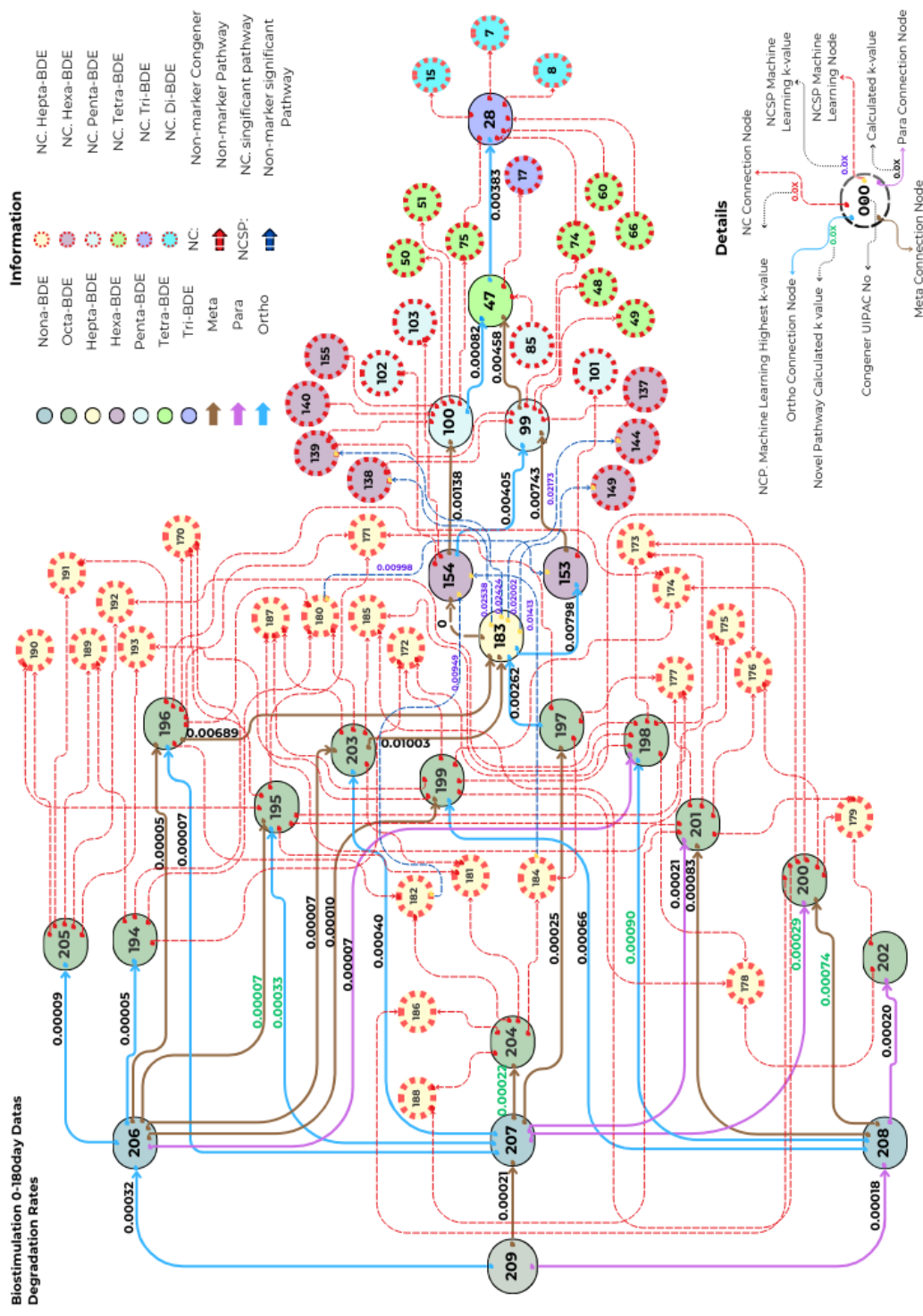


Figure 4.14. ADM-IE BS 0-180day ML and calculated degradation rate.

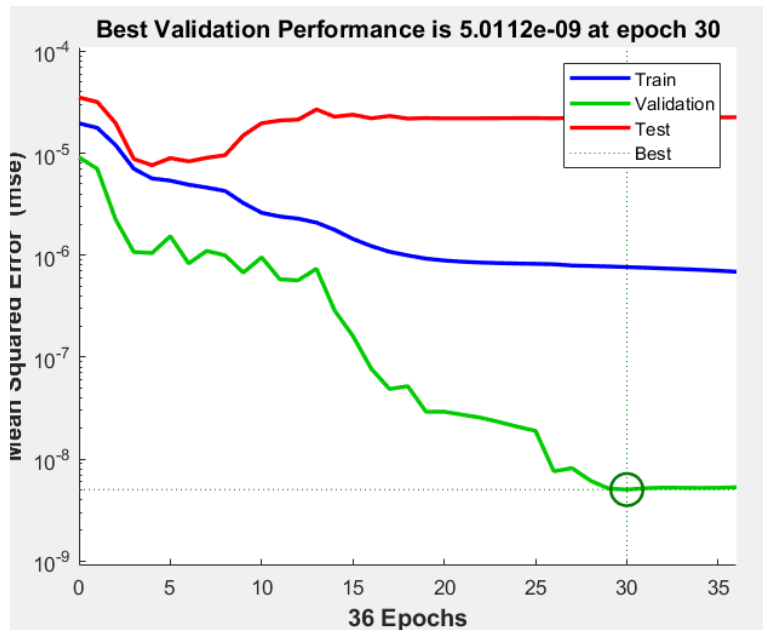


Figure 4.15. BS 0-180day MSE performance graph.

ML performance plots were examined for the results of the model run of biostimulation microcosm. Figure 4.15 demonstrates the MSE trend over 36 epochs for training. The model achieved its lowest validation error at epoch 30, with an MSE of approximately  $5.01 \times 10^{-9}$ , indicating the optimal stopping point.

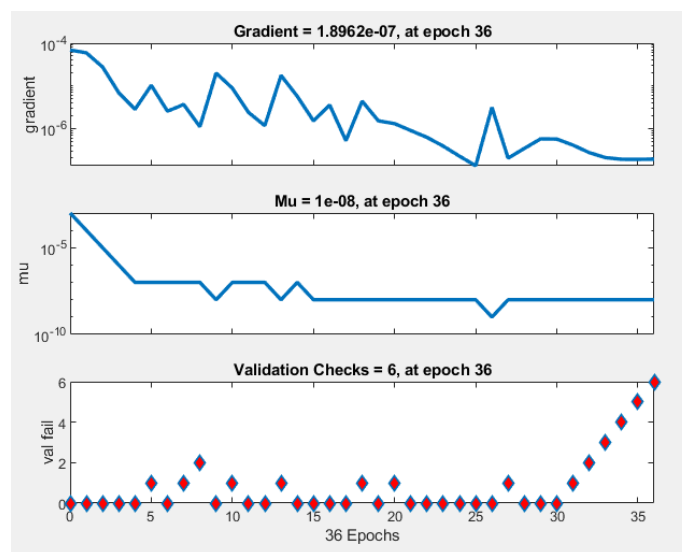


Figure 4.16. BS 0-180day training state graph.

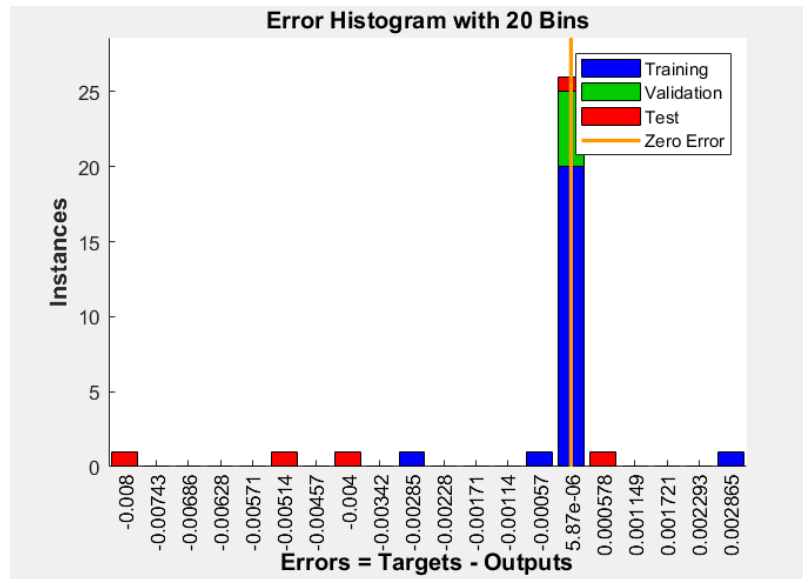


Figure 4.17. BS 0-180day Error histogram training plots.

Figure 4.16 indicates that the model completed its training at epoch 36 after six validation checks. Based on Figure 4.17, the error distribution indicated that most errors fell approximately  $5.87 \times 10^{-6}$ , suggesting that the model's predictions were quite close to the target values.

The R-values, with the validation set, achieved the highest correlation at  $R = 0.98$ , indicating strong alignment with target values. However, the testing set had lower R-values (0.51), suggesting some variability in model accuracy. The overall R-value of 0.77 reflected a high fit across all data.

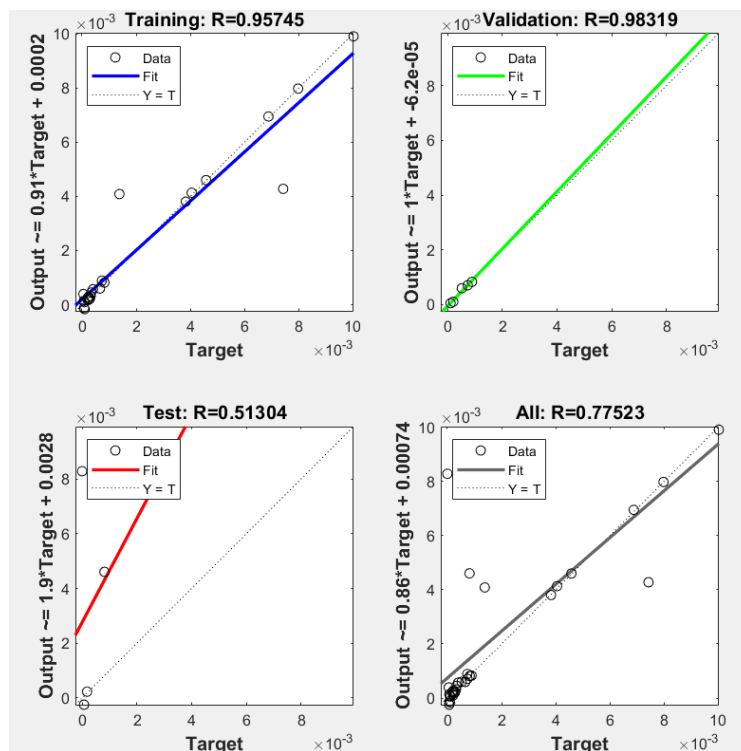


Figure 4.18. BS 0-180day regression graph for training, validation, and test.

#### 4.3.4. Bioaugmentation 0-180day neural network results

Figure 4.19 highlights 11 non-marker congener significant pathways, each identified through machine learning to estimate degradation rates. Table 4.15 shows the non-marker congener significant pathways and their corresponding k-values.

Table 4.15. k-values of non-marker significant pathways for bioaugmentation.

Pathway	k-value ( $d^{-1}$ )	Pathway	k-value ( $d^{-1}$ )
100→51	0.02089	75→28	0.01494
100→50	0.02056	74→28	0.01585
100→75	0.01915	47→17	0.01105
99→49	0.02159	28→8	0.01077
99→48	0.02098	28→7	0.01072
99→74	0.02014	Stdev + aver = 0.0085	

The k-values indicated a range of degradation rates within the non-marker congener significant pathways, with 5 pathways exhibiting higher rates BDE-100→BDE-51, BDE-100→BDE-50, BDE-99→BDE-49, BDE-99→BDE-48, and BDE-99→BDE-74. As seen in Table 4.14, significant pathways were observed for penta-, tetra-, and tri-BDE homolog groups. When compared, natural attenuation, biostimulation and bioaugmentation demonstrated significant pathways for homolog groups in descending order. Hence, bioaugmentation can be said to achieve dehalogenation towards less brominated congeners more effectively than other bioremediation scenarios. Particularly for dehalogenation of more toxic congeners (e.g. BDE-100 and BDE-99) or the ones with a defined NOEC value (e.g. BDE-28), ADM-IE estimated degradation rate constants for biostimulation and bioaugmentation microcosms, with bioaugmentation having higher rates. Therefore, it can be said that the end products of dehalogenation in these bioremediation scenarios were less harmful PBDE congeners, achieving the ultimate goal of remediation application.

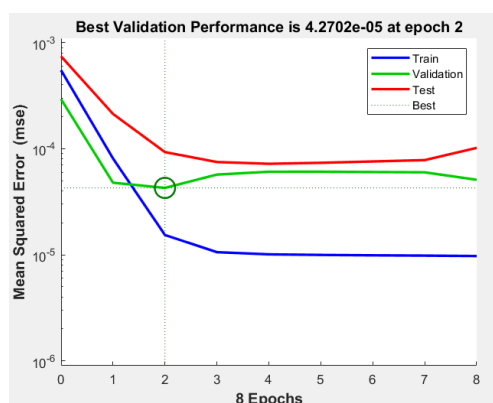


Figure 4.20. BA 0-180day MSE performance graph.

Model performance plots obtained for ML application to bioaugmentation yielded satisfactory results. Figure 4.20 demonstrates the MSE trend over 8 epochs for training. The model achieved its lowest validation error at epoch 2, with an MSE of approximately  $4.27 \times 10^{-5}$ , indicating the optimal stopping point. According to Figure 4.21, the model completed its training at epoch 8 after 6 validation checks. Based on Figure 4.22, the error distribution indicated that most errors fell  $-0.00014$ , suggesting that the model's predictions were quite close to the target values.

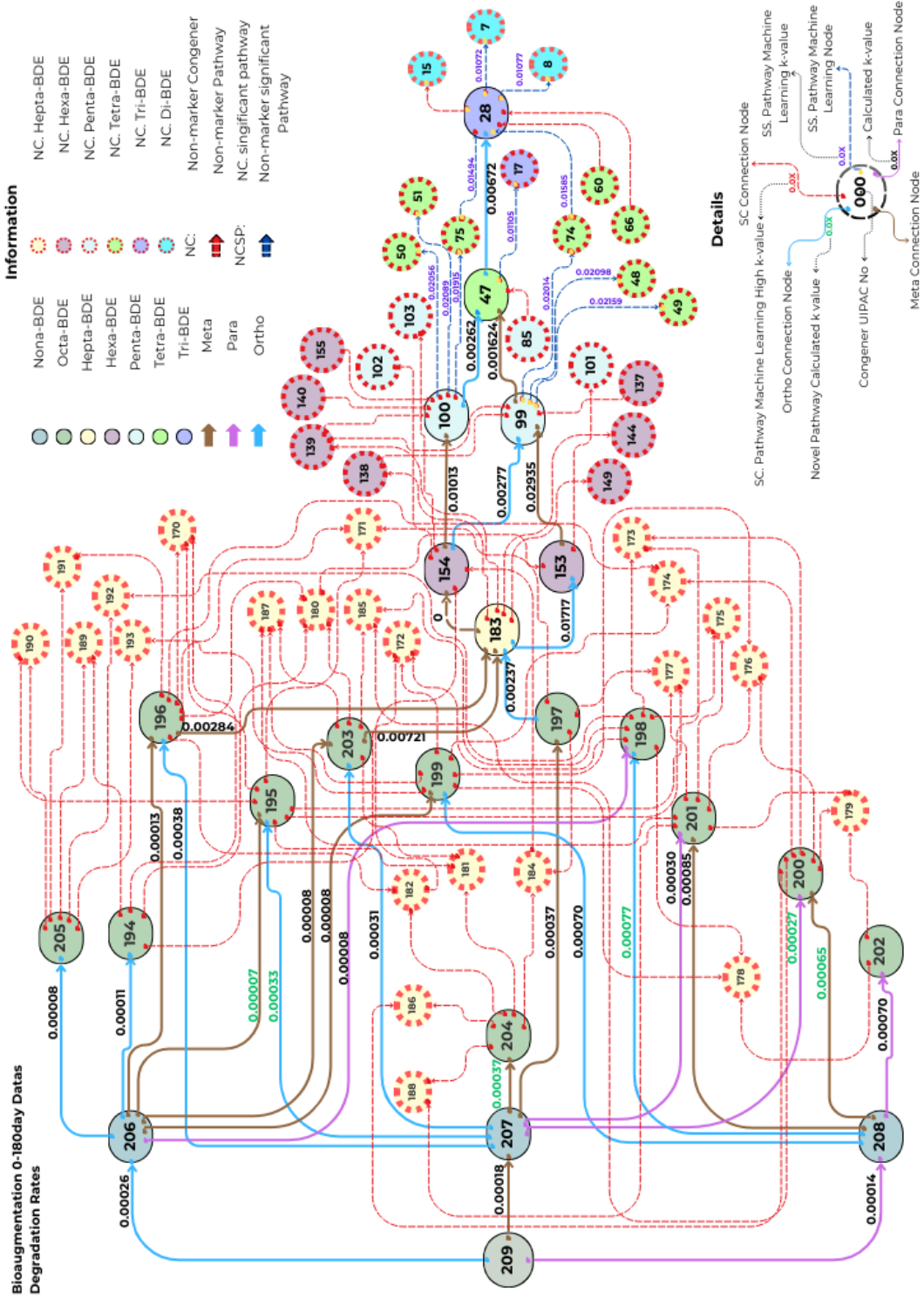


Figure 4.19. ADM-IE BA 0-180day ML and calculated degradation rate.

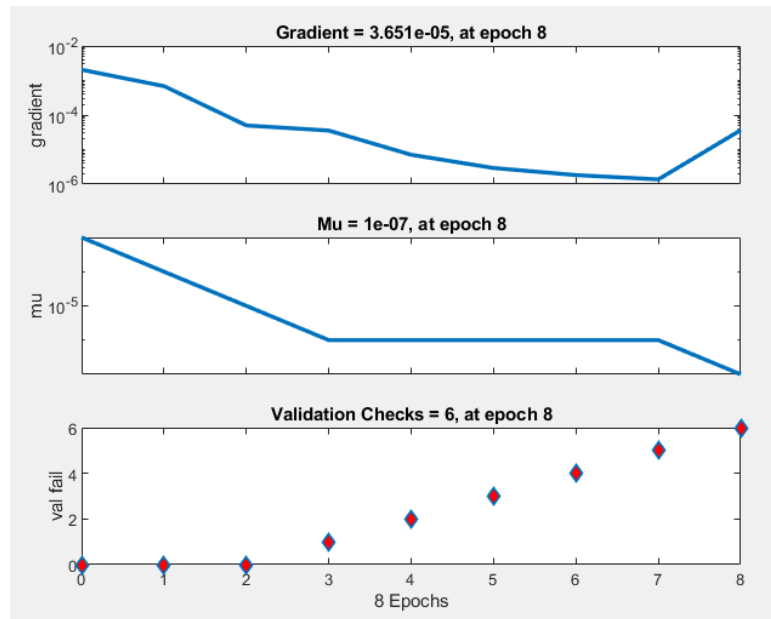


Figure 4.21. BA 0-180day training state graph.

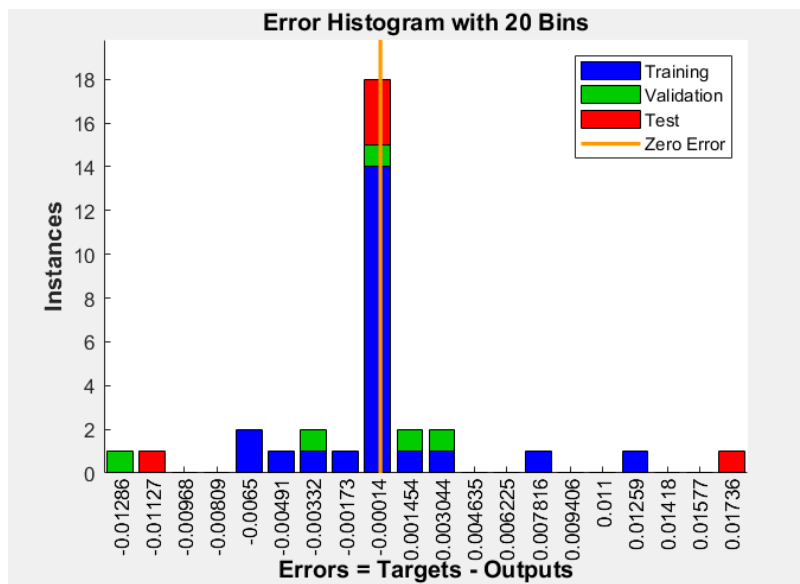


Figure 4.22. BA 0-180day Error histogram training plots.

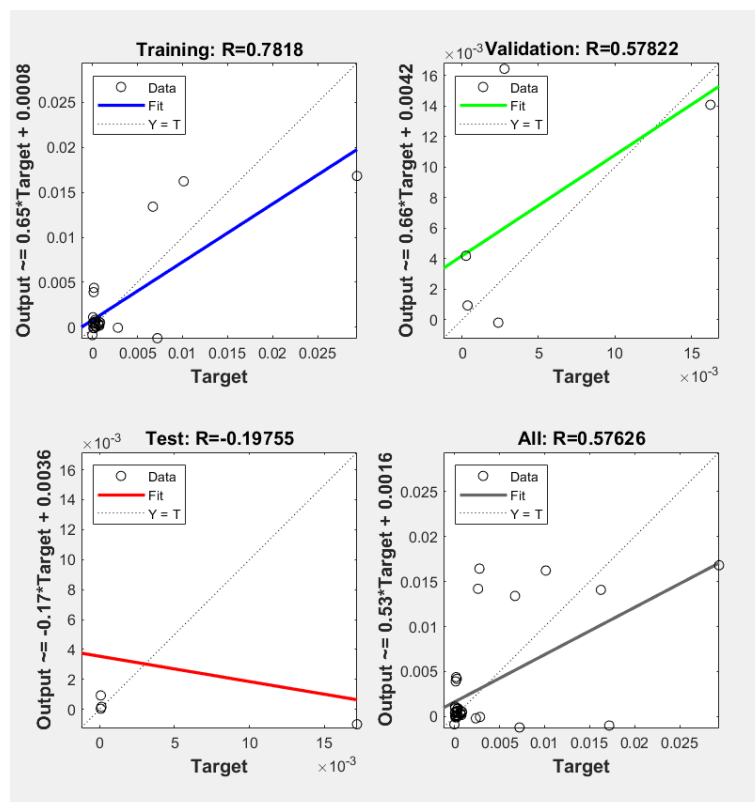


Figure 4.23. BA 0-180day regression graph for training, validation, and test.

The R-values, with the training set achieving the highest correlation at  $R = 0.78$ , indicated strong alignment. However, the testing set had lower R-values (0.19), suggesting some variability in model accuracy. The overall R-value of 0.57 reflected a moderate fit across all data.

#### 4.4. Discussion on the findings of ADM-IE

##### 4.4.1. Evaluation of model results and the experimental results

Previous research by Demirtepe (2017) investigated the degradation of PBDEs in sediment microcosms, focusing on the bromine per diphenyl ether (Br/dp) ratio changes over time across the experimental conditions. In that study, bioaugmentation

demonstrated the highest removal rates across bromine positions (para, meta, and ortho), with reported removal values of 1.02%, 1.27%, and 1.55%, respectively. Both natural attenuation and biostimulation followed similar patterns but at relatively lower removal percentages. Specifically, in the biostimulation set, para-Br removal was considerably lower at 0.82%, whereas meta and ortho removals were 2.11% and 2.08%, respectively, illustrating the influence of treatment type and bromine position on degradation efficiency. This finding was consistent with the ADM-IE model results.

Degradation rate was also evaluated using bromine per diphenyl ether (Br/dp) content of sediments (Equation 4.1) and calculated as shown in Equation 4.2.  $C_i$  is the concentration of each congener  $i$ . The number of bromines ( $n_i$ ) can be total number of bromines for each homolog group or number of ortho-/meta-/para-bromines for each congener. Furthermore, percent reduction in Br/dp was computed as ratio of the difference in Br/dp between days 0 and 180 to Br/dp at time zero (Demirtepe 2017, 85).

$$Br/dp = \frac{\sum_{i=1}^{10} C_i x n_i}{\sum_{i=1}^{10} C_i} \quad (4.1)$$

$$\frac{Br}{dp.day} = \frac{(Br/dp)_{t_1} - (Br/dp)_{t_2}}{|t_1 - t_2|} \quad (4.2)$$

In the current study, using the ADM-IE model, similar trends were observed, with degradation rates generally increasing as the bromine count decreased. This observation aligns with Demirtepe (2017)'s findings, suggesting that lower-brominated congeners are more susceptible to degradation due to their less stable molecular structures.

Additionally, both studies showed that biostimulation was particularly effective in removing bromine from meta and ortho positions. In the degradation pathway from hexa to penta-BDEs, meta positions exhibited higher k-values under BA, while ortho positions showed increased rates under BS. This finding was consistent with Demirtepe's results, reinforcing the role of biostimulation in targeting specific bromine positions effectively.

In summary, while Demirtepe (2017)'s study provided foundational insights into PBDE degradation by tracking Br/dp ratios across bromine positions, the ADM-IE

employed in the current study offered different perspective by estimating the degradation rates for each pathway. Both studies concluded that bioaugmentation was the most effective treatment method, yet the ADM-IE enabled a more detailed comparison of treatment efficacy across specific pathways and bromine positions.

#### 4.4.2. Previous usage of Machine learning in degradation of persistent organic pollutants

In many biodegradation studies, machine learning applications have been utilized. Examples of these studies are presented in Table 4.16. Overall, it has been suggested that machine learning could play a significant role in predicting biodegradation.

Table 4.16. Selected studies on machine learning applications.

Reference	Title	Key focus	Outcome
(Baker et al. 2004)	Evaluation of Artificial Intelligence-Based Models for Chemical Biodegradability Prediction	Explores the effectiveness of artificial intelligence methods, including neural networks, in predicting biodegradation.	Neural networks demonstrated reliable predictions, showcasing their potential in environmental studies.
(Goh et al. 2018)	Multimodal Deep Neural Networks Using Engineered and Learned Representations for Biodegradability Prediction	Combines engineered features and deep learning to predict the biodegradability of chemicals.	Deep neural networks successfully improved prediction accuracy, providing a robust modeling framework.

(cont. on next page)

**Table 4.16 (cont.)**

(Motamedi et al. 2023)	Comparison of Photocatalysis and Photolysis of BDE-47: Operational Parameters, Kinetic Studies, and Data Validation Using Three Modern Machine Learning Models	Applies learning (artificial neural network, Boosted Decision Tree, Symbolic Regression) to validate degradation kinetics and predict pollutant concentration.	machine models neural Gradient Boosted Decision Tree, Symbolic Regression) to validate degradation kinetics and predict pollutant concentration.	Differences among machine learning models were analyzed to assess their application in environmental remediation.
------------------------	--	--	--	---

Baker et al. (2004) highlighted the capacity of artificial intelligence, particularly neural networks, to predict the biodegradability of chemicals. Their analysis demonstrated that neural networks provide accurate predictions, making them a valuable tool for environmental modeling. This suggests that neural networks can bridge the gap between chemical complexity and predictive modeling, facilitating better decision-making in remediation efforts. Goh et al. (2018) extended the application of machine learning by integrating deep neural networks with both engineered and learned chemical features. This multimodal approach enhanced prediction performance, indicating that deep learning techniques can offer robust and scalable solutions for biodegradability assessment. Their findings underline the significance of combining feature engineering with advanced neural architecture to achieve higher accuracy. Motamedi et al. (2023) findings suggested that integrating machine learning models, particularly gradient boosted decision tree, can effectively validate and predict outcomes in the degradation processes of persistent organic pollutants like BDE-47. The study underscored the potential of combining experimental techniques with advanced computational tools to enhance the efficiency and understanding of environmental remediation strategies. As a result, the use of machine learning in biodegradation provided significant results and enabled more accurate predictions depending on the abundance of available data.

### 4.4.3. Comparison of the degradation rate constants with previous model applications

Table 4.17 presented k-values for certain pathways, calculated using the anaerobic dehalogenation model developed by Karakas (2016), which used previously conducted degradation studies' data. In Table 4.17, the k-values were shown as median values for the 0, 24, 40, 60, and 90-day intervals (Karakas 2016, 192-95). To enable a comparison with the ADM-IE k-values, the k-values for similar pathways were calculated and added to the table for all bioremediation scenarios.

Table 4.17. Degradation rate constants of eight pathways different studies.

Ortho 47-28	Meta 99-47	Ortho 100- 47	Meta 153-99	Ortho 154- 99	Meta 154-100	Ortho 183-153	Meta 183-154	Microcosm data	Model
0.002	0.002	-	0	0	-	-	-	(Tokarz et al. 2008)	
0.002	-	0	-	0	0	-	0.002	(H.-W. Huang, Chang, and Lee 2014)	ADM <sup>a</sup>
0.002	0.001	-	0	-	-	0	0.001	(Robrock et al., 2008)	
0.002	0.001	0	0	0	0.003	0	0.002	(Song et al. 2015)	
0.024/ 0.014/ 0.018	0.013/ 0.015/ 0.014	0.004/ 0.003/ 0.004	0.043/ 0.022/ 0.025	0.004/ 0/ 0	0.015/ 0.030/ 0.016	0.029/ 0.056/ 0.050	0/0/0	(Demirtepe and Imamoglu 2019b)	ADM – IE <sup>b</sup>

a: Karakas's anaerobic dehalogenation model k results.

b: The median of k-values under natural attenuation/biostimulation/bioaugmentation.

According to these results, the degradation rate of the BDE-183→153 pathway was higher than the results obtained in this study, highlighting its significance in other sediment conditions. Additionally, higher k-values were observed in the BDE-47→28, 153→99, and 154→100 pathways, in this study. This may be attributed to the effect of bioremediation techniques, particularly the BA and BS methods applied by Demirtepe & Imamoglu (2019), which were especially impactful on lower-brominated and medium-

brominated compounds. This outcome highlighted the effectiveness of these methods in affecting degradation rates, although the experimental conditions for previous studies were not examined in this comparison. Nevertheless, this comparison suggested that more experimental data is needed to be tested by ADM-IE to have a better understanding of dehalogenation efficiency.

## CHAPTER 5

### CONCLUSION

In this study, anaerobic dehalogenation of PBDEs in sediments was modeled using the experimental data of a microcosm study mimicking three bioremediation scenarios, namely natural attenuation, biostimulation and bioaugmentation. To do that, a previously developed anaerobic dehalogenation model was integrated and enhanced, resulting in a new model called “ADM-IE”. Different from the previous versions, ADM-IE was able to list all possible dehalogenation pathways for PBDE degradation, quantify the reaction amounts for these pathways, calculate the degradation rate constants for congeners measured in the data set, and estimate the rate constants for congeners not measured experimentally, by using machine learning algorithms.

The ADM-IE was first validated using artificial data sets, generated manually with a limited number of congeners and manipulated pathways. The model was successful in predicting the PBDE profile given as the input and calculated the degradation rate constants. When compared to manual calculations, the model was found more successful in predicting rate constants and concentrations for PBDEs with higher concentrations.

After validation, the ADM-IE was applied to the microcosm data set using the time zero and time 180 days’ concentrations of three bioremediation and two control microcosms. The resulting goodness of fit criteria comparing the measured and predicted PBDE concentrations showed very good fits overall, for all microcosms. However, when the results were further examined, it was observed that the model predicted the congeners with higher concentrations better than the ones with comparably lower concentrations, similar to the validation results. To understand the effect, the high concentration congeners were excluded from  $R^2$  calculation. As a result,  $R^2$  values ranged between 0.35 and 0.78 for the lower concentration congeners. The congeners that were not predicted very well varied among the bioremediation microcosms. The discrepancy was considered due to the very high relative standard deviations obtained for quantified pathway reaction amounts. As per the researchers’ knowledge, the model was applied to such a data set where there were large variations in concentrations of the measured congeners. Therefore,

the model may need further development on this issue. Overall, the model's ability to generate reaction amounts and pathways based on the input concentrations and markers provided a robust framework for understanding the degradation mechanisms occurring in the sediments.

Thirty three out of 124 dehalogenation pathways included the marker congeners both as a mother and daughter, hence the degradation rate constants for these pathways were calculated assuming first order reaction kinetics. The position of bromine atoms on the PBDE structure—whether ortho, meta, or para—played a significant role in evaluating the possible dehalogenation pathways and the degradation rate. It was observed that for the dehalogenation of PBDEs, meta and ortho bromine removal was favored in the sediments and para bromine removal was the least favored, regardless of the bioremediation method applied. The degradation process was found to be significantly influenced by the number of bromine atoms in the PDBE molecule. As the number of bromine in the structure decreased, the degradation rates tended to increase. Hence, lower-brominated congeners might be more prone to degradation, potentially due to their less stable molecular structures.

Among the three bioremediation scenarios, the degradation rates varied, with bioaugmentation generally showing the highest k-values for several pathways. However, for some specific pathways, biostimulation exhibited higher degradation rates. Furthermore, the dominant daughters of the same mother varied among the bioremediation scenarios. Hence, it can be speculated that bioremediation method applied had an influence on the PBDE dehalogenation, and that the dehalogenation could be tailored to obtain or prevent the formation of certain congeners. For example, the formation of BDE-99, a more toxic congener compared to others, was favored in biostimulation. Therefore, cautions must be taken when applying biostimulation for PBDE contaminated sites.

The application of ADM-IE revealed novel degradation routes under specific conditions. A total of six pathways among 33 were identified as the novel pathways, mostly favored by biostimulation.

The ADM-IE was also applied to the data set obtained from sequential time periods of microcosms, allowing for a detailed analysis of the degradation progress within each period. The results revealed that pathways occurred at their highest rates at various time intervals for different bioremediation scenarios. For some pathways, a delay in dehalogenation was observed under natural attenuation microcosms, although for a

couple of them the reverse case was observed. This comprehensive analysis provided a valuable comparison of the degradation rates, highlighting the effectiveness of different microcosm conditions and specific time periods for enhanced degradation.

ADM-IE employed machine learning algorithms to estimate the degradation rate constants for 91 pathways involving one non-marker congener either as a mother or a daughter. A significant pathway definition was introduced to evaluate the ones with the highest degradation rate in three microcosms. As a result, the significant pathways varied among bioremediation scenarios. The dehalogenation of octa-, hepta-, and less than penta-BDEs was significant for natural attenuation, biostimulation and bioaugmentation, respectively. Hence, bioaugmentation can be said to achieve dehalogenation towards less brominated congeners more effectively than other bioremediation scenarios. Furthermore, the preferential pathways could be observed when the rate constants were estimated by machine learning. For example, the dominant daughters of BDE-183 were found as BDE-138 and BDE-139, which were not monitored in the experimental microcosm study. These congeners were the mothers of BDE-100 and BDE-99, which are more toxic than their mothers. Hence, to monitor the toxicity change during bioremediation, these congeners should be measured in the environment. An important observation was that dehalogenation of toxic (e.g. BDE-99, -100) and bioaccumulative (e.g. BDE-47) congeners were observed and quantified in biostimulation and bioaugmentation microcosms, with bioaugmentation having higher rates.

To conclude, the results of ADM-IE helped to gather important and comprehensive information on the bioremediation of PBDEs in the sediments. The anaerobic dehalogenation model was applied for the first time to a data set where different bioremediation methods were applied. Using the results of this study, the bioremediation strategies would be developed to obtain degradation of halogenated compounds with higher degradation rates, and to direct the dehalogenation towards the production of less harmful products. Further improvements on the model are possible, such as the application of a non-linear relationship in machine learning algorithms. It can also be possible to combine the model with fate and transport models, so that a comprehensive analysis of the fate of halogenated compounds in various environmental compartments could be predicted. Furthermore, the model could be upgraded to a version where the dehalogenated contaminant profile could be estimated so that the outcome of bioremediation would be predicted before its application on-site.

## REFERENCES

- Azid, Azman, Hafizan Juahir, Mohd Ekhwan Toriman, Mohd Khairul Amri Kamarudin, Ahmad Shakir Mohd Saudi, Che Noraini Che Hasnam, Nor Azlina Abdul Aziz, et al. 2014. "Prediction of the Level of Air Pollution Using Principal Component Analysis and Artificial Neural Network Techniques: A Case Study in Malaysia." *Water, Air, & Soil Pollution* 225 (8): 2063. <https://doi.org/10.1007/s11270-014-2063-1>.
- Bzdusek, Philip A. 2005. "PAHs in Sediments of the Black River and the Ashtabula River, Ohio: Source Apportionment by Factor Analysis." *Water Research* 39 (4): 511–24. <https://doi.org/10.1016/j.watres.2004.11.016>.
- Cho, Young-Cheol, Roger C. Sokol, Robert C. Frohnhoefer, and G-Yull Rhee. 2003. "Reductive Dechlorination of Polychlorinated Biphenyls: Threshold Concentration and Dechlorination Kinetics of Individual Congeners in Aroclor 1248." *Environmental Science & Technology* 37 (24): 5651–56. <https://doi.org/10.1021/es034600k>.
- Clercq, Djavan De, Devansh Jalota, Ruoxi Shang, Kunyi Ni, Zhuxin Zhang, Areeb Khan, Zongguo Wen, Luis Caicedo, and Kai Yuan. 2019. "Machine Learning Powered Software for Accurate Prediction of Biogas Production: A Case Study on Industrial-Scale Chinese Production Data." *Journal of Cleaner Production* 218 (May):390–99. <https://doi.org/10.1016/j.jclepro.2019.01.031>.
- Cortes, Corinna, and Vladimir Vapnik. 1995. "Support-Vector Networks." *Machine Learning* 20 (3): 273–97. <https://doi.org/10.1007/BF00994018>.
- Davis, J. C. 2002. *Statistics and Data Analysis in Geology*. 3rd ed. New York: Wiley.
- Demirtepe, Hale. 2012. *Modeling Anaerobic Dechlorination of Polychlorinated Biphenyls*. M.S. - Master of Science, Middle East Technical University.
- Demirtepe, Hale, and Ipek Imamoglu. 2019a. "Biostimulation Enhanced the Biotic Degradation of Hexabromocyclododecane in Sediments." *Journal of Soils and Sediments*, 2859–2868. <https://hdl.handle.net/11511/43761>.
- Demirtepe, Hale, and Ipek Imamoglu. 2019b. "Degradation of Decabromodiphenyl Ether (BDE-209) in Microcosms Mimicking Sediment Environment Subjected to Comparative Bioremediation Strategies." *Journal of Environmental Management*, 120–130. <https://hdl.handle.net/11511/43533>.
- Dunea, Daniel, Alin Pohoata, and Stefania Iordache. 2015. "Using Wavelet–Feedforward Neural Networks to Improve Air Pollution Forecasting in Urban Environments." *Environmental Monitoring and Assessment* 187 (7): 477. <https://doi.org/10.1007/s10661-015-4697-x>.

- Eddy Y. Zeng. 2015. *Comprehensive Analytical Chemistry, Persistent Organic Pollutants (POPs) Analytical Techniques, Environmental Fate and Biological Effects*. Vol. 67. Elsevier.
- EPA. 2024. Comptox. Accessed October 10, 2024. <https://comptox.epa.gov/dashboard/>.
- Fennell, Donna E., and James M. Gossett. 2003. "Microcosms for Site-Specific Evaluation of Enhanced Biological Reductive Dehalogenation." *In Dehalogenation*, 385–420. Boston: Kluwer Academic Publishers. [https://doi.org/10.1007/0-306-48011-5\\_15](https://doi.org/10.1007/0-306-48011-5_15).
- Fromme, Hermann, Wolfgang Körner, Nabil Shahin, Antonia Wanner, Michael Albrecht, Sigrun Boehmer, Harun Parlar, Richard Mayer, Bernhard Liebl, and Gabriele Bolte. 2009. "Human Exposure to Polybrominated Diphenyl Ethers (PBDE), as Evidenced by Data from a Duplicate Diet Study, Indoor Air, House Dust, and Biomonitoring in Germany." *Environment International* 35 (8): 1125–35. <https://doi.org/10.1016/j.envint.2009.07.003>.
- Gardner, M. 1999. "Neural Network Modelling and Prediction of Hourly NO<sub>x</sub> and NO<sub>2</sub> Concentrations in Urban Air in London." *Atmospheric Environment* 33 (5): 709–19. [https://doi.org/10.1016/S1352-2310\(98\)00230-1](https://doi.org/10.1016/S1352-2310(98)00230-1).
- Gerecke, Andreas C., Paul C. Hartmann, Norbert V. Heeb, Hans Peter E. Kohler, Walter Giger, Peter Schmid, Markus Zennegg, and Martin Kohler. 2005. "Anaerobic Degradation of Decabromodiphenyl Ether." *Environmental Science and Technology* 39 (4): 1078–83. <https://doi.org/10.1021/es048634j>.
- Goh, Garrett B., Khushmeen Sakloth, Charles Siegel, Abhinav Vishnu, and Jim Pfaendtner. 2018. "Multimodal Deep Neural Networks Using Both Engineered and Learned Representations for Biodegradability Prediction," August.
- Gustafsson, Kerstin, Mikael Björk, Sven Burreau, and Michael Gilek. 1999. "Bioaccumulation Kinetics of Brominated Flame Retardants PBDEs in Blue Mussels." *Environmental Toxicology and Chemistry* 18 (6): 1218–24. <https://doi.org/10.1002/etc.5620180621>.
- Gwen O'Sullivan, and Court Sandau. 2014. *Environmental Forensics for Persistent Organic Pollutants*. Elsevier. <https://doi.org/10.1016/C2011-0-04340-5>.
- Hafeez, Shahzar, Ayesha Ishaq, Azeem Intisar, Tariq Mahmood, Muhammad Imran Din, Ejaz Ahmed, Muhammad Rizwan Tariq, and Muhammad Amin Abid. 2024. "Predictive Modeling for the Adsorptive and Photocatalytic Removal of Phenolic Contaminants from Water Using Artificial Neural Networks." *Heliyon* 10 (19): e37951. <https://doi.org/10.1016/j.heliyon.2024.e37951>.
- Hale, Robert C., Mark J. La Guardia, Ellen Harvey, Michael O. Gaylor, and T. Matt Mainor. 2006. "Brominated Flame Retardant Concentrations and Trends in Abiotic Media." *Chemosphere* 64 (2): 181–86. <https://doi.org/10.1016/j.chemosphere.2005.12.006>.

- Hu, Dingfei, and Keri C. Hornbuckle. 2010. "Inadvertent Polychlorinated Biphenyls in Commercial Paint Pigments." *Environmental Science & Technology* 44 (8): 2822–27. <https://doi.org/10.1021/es902413k>.
- Huang, Chengcheng, Xiaogu Zheng, Andrew Tait, Yongjiu Dai, Chi Yang, Zhuoqi Chen, Tao Li, and Zhonglei Wang. 2014. "On Using Smoothing Spline and Residual Correction to Fuse Rain Gauge Observations and Remote Sensing Data." *Journal of Hydrology* 508 (January):410–17. <https://doi.org/10.1016/j.jhydrol.2013.11.022>.
- Huang, Huang-Wen, Bea-Ven Chang, and Ching-Chang Lee. 2014. "Reductive Debromination of Decabromodiphenyl Ether by Anaerobic Microbes from River Sediment." *International Biodeterioration & Biodegradation* 87 (February):60–65. <https://doi.org/10.1016/j.ibiod.2013.10.011>.
- Ian Goodfellow, Yoshua Bengio, and Aaron Courville. 2016. *Deep learning. Genetic Programming and Evolvable Machines* 19, 305–307. <https://doi.org/10.1007/s10710-017-9314-z>
- Isah, Bello Abdu, Muthamilselvi Ponnuchamy, B. Senthil Rathi, P. Senthil Kumar, Ashish Kapoor, Manjula Rajagopal, Anjali Awasthi, and Gayathri Rangasamy. 2024. "Artificial Intelligence-Based Neural Network Modeling of Adsorptive Removal of Phenol from Aquatic Environment." *Desalination and Water Treatment* 319 (July). <https://doi.org/10.1016/j.dwt.2024.100564>.
- Ji, Kyunghye, Kyungho Choi, John P. Giesy, Javed Musarrat, and Shunichi Takeda. 2011. "Genotoxicity of Several Polybrominated Diphenyl Ethers (PBDEs) and Hydroxylated PBDEs, and Their Mechanisms of Toxicity." *Environmental Science and Technology* 45 (11): 5003–8. <https://doi.org/10.1021/es104344e>.
- Jones, K.C., and P. de Voogt. 1999. "Persistent Organic Pollutants (POPs): State of the Science." *Environmental Pollution* 100 (1–3): 209–21. [https://doi.org/10.1016/S0269-7491\(99\)00098-6](https://doi.org/10.1016/S0269-7491(99)00098-6).
- Karakas, Filiz. 2016. *Model Development for Evaluating Remediation of Contaminated Sediments: PCBs and PBDEs as Cases for Halogenated Hydrophobic Organics*. Ph.D. - Doctoral Program, Middle East Technical University.
- Karakas, Filiz, Aysegul Aksoy, and Ipek Imamoglu. 2020. "Development of a Fate and Transport Model for Biodegradation of PBDE Congeners in Sediments." *Environmental Pollution* 266 (November). <https://doi.org/10.1016/j.envpol.2020.115116>.
- Kooh, Muhammad Raziq Rahimi, Muhammad Khairud Dahri, and Linda Biaw Leng Lim. 2018. "Jackfruit Seed as Low-Cost Adsorbent for Removal of Malachite Green: Artificial Neural Network and Random Forest Approaches." *Environmental Earth Sciences* 77 (12). <https://doi.org/10.1007/s12665-018-7618-9>.
- Kukkonen, J. 2003. "Extensive Evaluation of Neural Network Models for the Prediction of NO<sub>2</sub> and PM<sub>10</sub> Concentrations, Compared with a Deterministic Modelling System and Measurements in Central Helsinki." *Atmospheric Environment* 37 (32): 4539–50. [https://doi.org/10.1016/S1352-2310\(03\)00583-1](https://doi.org/10.1016/S1352-2310(03)00583-1).

- Law, Robin J., Adrian Covaci, Stuart Harrad, Dorte Herzke, Mohamed A.-E. Abdallah, Kim Fernie, Leisa-Maree L. Toms, and Hidetaka Takigami. 2014. "Levels and Trends of PBDEs and HBCDs in the Global Environment: Status at the End of 2012." *Environment International* 65 (April):147–58. <https://doi.org/10.1016/j.envint.2014.01.006>.
- Lee, Anzy, Zong Geem, and Kyung-Duck Suh. 2016. "Determination of Optimal Initial Weights of an Artificial Neural Network by Using the Harmony Search Algorithm: Application to Breakwater Armor Stones." *Applied Sciences* 6 (6): 164. <https://doi.org/10.3390/app6060164>.
- Lee, Lip Kim, and Jianzhong He. 2010. "Reductive Debromination of Polybrominated Diphenyl Ethers by Anaerobic Bacteria from Soils and Sediments." *Applied and Environmental Microbiology* 76 (3): 794–802. <https://doi.org/10.1128/AEM.01872-09>.
- Li, Chao, Pinjing He, Wei Peng, Fan Lü, Rui Du, and Hua Zhang. 2022. "Exploring Available Input Variables for Machine Learning Models to Predict Biogas Production in Industrial-Scale Biogas Plants Treating Food Waste." *Journal of Cleaner Production* 380 (December):135074. <https://doi.org/10.1016/j.jclepro.2022.135074>.
- Li, Jinhui, Nana Zhao, Xue Liu, and Xiaoyang Wu. 2014. "Promoting Environmentally Sound Management of Polybrominated Diphenyl Ethers in Asia." *Waste Management & Research: The Journal for a Sustainable Circular Economy* 32 (6): 527–35. <https://doi.org/10.1177/0734242X14534517>.
- Linares, Victoria, Montserrat Bellés, and José L. Domingo. 2015. "Human Exposure to PBDE and Critical Evaluation of Health Hazards." *Archives of Toxicology*. Springer Verlag. <https://doi.org/10.1007/s00204-015-1457-1>.
- Liu, Zongtang, Haini Yang, Mian Wang, Yufeng Sun, Zhenghao Fei, Shujuan Chen, Rui Luo, Lin Hu, and Chenggang Gu. 2022. "Enhanced Reductive Debromination of Decabromodiphenyl Ether by Organic-Attapulgitic Supported Fe/Pd Nanoparticles: Synergetic Effect and Mechanism." *Journal of Colloid and Interface Science* 613 (May):337–48. <https://doi.org/10.1016/j.jcis.2022.01.064>.
- Lombard, Nathalie J., Upal Ghosh, Birthe V. Kjellerup, and Kevin R. Sowers. 2014. "Kinetics and Threshold Level of 2,3,4,5-Tetrachlorobiphenyl Dechlorination by an Organohalide Respiring Bacterium." *Environmental Science & Technology* 48 (8): 4353–60. <https://doi.org/10.1021/es404265d>.
- MathWorks, The. 2024a. "Plot Error Histogram." Accessed September 27, 2024. <https://www.mathworks.com/help/thingspeak/plot-error-histogram.html>.
- MathWorks, The. 2024b. "Plot Perform." Accessed November 4, 2024. <https://www.mathworks.com/help/deeplearning/ref/plotperform.html>.
- MathWorks, The. 2024c. "Plot Train State." Accessed July 24, 2024. <https://www.mathworks.com/help/deeplearning/ref/plottrainstate.html>.

- MathWorks, The. 2024d. "Regression Neural Network." Accessed September 12, 2024. <https://www.mathworks.com/help/stats/regressionneuralnetwork.html>.
- MathWorks, The. 2024e. "Neural Network." Accessed September 20, 2024. [https://www.mathworks.com/discovery/neural-network.html?s\\_tid=srchtitle\\_support\\_results\\_2\\_neural](https://www.mathworks.com/discovery/neural-network.html?s_tid=srchtitle_support_results_2_neural).
- McGrath, Thomas J., Paul D. Morrison, Christopher J. Sandiford, Andrew S. Ball, and Bradley O. Clarke. 2016. "Widespread Polybrominated Diphenyl Ether (PBDE) Contamination of Urban Soils in Melbourne, Australia." *Chemosphere* 164 (December):225–32. <https://doi.org/10.1016/j.chemosphere.2016.08.017>.
- Mishra, Dharendra, P. Goyal, and Abhishek Upadhyay. 2015. "Artificial Intelligence Based Approach to Forecast PM 2.5 during Haze Episodes: A Case Study of Delhi, India." *Atmospheric Environment* 102 (February):239–48. <https://doi.org/10.1016/j.atmosenv.2014.11.050>.
- Motamedi, Mahsa, Laleh Yerushalmi, Fariborz Haghghat, Zhi Chen, and Yanbin Zhuang. 2023. "Comparison of Photocatalysis and Photolysis of 2,2,4,4-Tetrabromodiphenyl Ether (BDE-47): Operational Parameters, Kinetic Studies, and Data Validation Using Three Modern Machine Learning Models." *Chemosphere* 326 (June):138363. <https://doi.org/10.1016/j.chemosphere.2023.138363>.
- Nyholm, Jenny Rattfelt, Charlott Lundberg, and Patrik L. Andersson. 2010. "Biodegradation Kinetics of Selected Brominated Flame Retardants in Aerobic and Anaerobic Soil." *Environmental Pollution* 158 (6): 2235–40. <https://doi.org/10.1016/j.envpol.2010.02.010>.
- Ochs, Cory, Kaitlyn Garrison, Priyam Saxena, Kristen Romme, and Atanu Sarkar. 2024. "Contamination of Aquatic Ecosystems by Persistent Organic Pollutants (POPs) Originating from Landfills in Canada and the United States: A Rapid Scoping Review." *Science of the Total Environment*. Elsevier B.V. <https://doi.org/10.1016/j.scitotenv.2024.171490>.
- Oloruntoba, Kike, Omotayo Sindiku, Oladele Osibanjo, Christine Herold, and Roland Weber. 2021. "Polybrominated Diphenyl Ethers (PBDEs) Concentrations in Soil and Plants around Municipal Dumpsites in Abuja, Nigeria." *Environmental Pollution* 277 (May):116794. <https://doi.org/10.1016/j.envpol.2021.116794>.
- Omokhagbor Adams, Godleads, Prekeyi Tawari Fufeyin, Samson Eruke Okoro, and Igelenyah Ehinomen. 2020. "Bioremediation, Biostimulation and Bioaugmentation: A Review." *International Journal of Environmental Bioremediation & Biodegradation* 3 (1): 28–39. <https://doi.org/10.12691/ijebb-3-1-5>.
- Peter, Swathik Clarancia, Jaspreet Kaur Dhanjal, Vidhi Malik, Navaneethan Radhakrishnan, Mannu Jayakanthan, and Durai Sundar. 2019. "Quantitative Structure-Activity Relationship (QSAR): Modeling Approaches to Biological Applications." *In Encyclopedia of Bioinformatics and Computational Biology*, 661–76. Elsevier. <https://doi.org/10.1016/B978-0-12-809633-8.20197-0>.

- Raghavendra. N, Sujay, and Paresh Chandra Deka. 2014. "Support Vector Machine Applications in the Field of Hydrology: A Review." *Applied Soft Computing* 19 (June):372–86. <https://doi.org/10.1016/j.asoc.2014.02.002>.
- Ragosta, M., M. D'Emilio, and G. A. Giorgio. 2015. "Input Strategy Analysis for an Air Quality Data Modelling Procedure at a Local Scale Based on Neural Network." *Environmental Monitoring and Assessment* 187 (5): 307. <https://doi.org/10.1007/s10661-015-4556-9>.
- Reible, Danny D., ed. 2014. *Processes, Assessment and Remediation of Contaminated Sediments*. Vol. 6. New York, NY: Springer New York. <https://doi.org/10.1007/978-1-4614-6726-7>.
- Robrock, Kristin R., Peter Korytár, and Lisa Alvarez-Cohen. 2008. "Pathways for the Anaerobic Microbial Debromination of Polybrominated Diphenyl Ethers." *Environmental Science & Technology* 42 (8): 2845–52. <https://doi.org/10.1021/es0720917>.
- Sarigiannis, Dimosthenis A., Antonios K. Stratidakis, and Spyridon P. Karakitsios. 2024. "In Silico Methods and in Silico Toxicology." In *Encyclopedia of Toxicology*, 503–7. Elsevier. <https://doi.org/10.1016/B978-0-12-824315-2.01173-8>.
- Schneider, Astrid, Gerhard Hommel, and Maria Blettner. 2010. "Lineare Regressionsanalyse - Teil 14 Der Serie Zur Bewertung Wissenschaftlicher Publikationen." *Deutsches Arzteblatt*. <https://doi.org/10.3238/arztebl.2010.0776>.
- Schnoor, Jerald L. 2006. *Bioremediation and Natural Attenuation*. Edited by Walter Illman and Pedro Alvarez. Hoboken, NJ: John Wiley & Sons.
- Schwarzenbach, René P., Philip M. Gschwend, and Dieter M. Imboden. 2003. *Environmental Organic Chemistry*. 2nd ed. Hoboken, NJ: Wiley.
- Shih, Yang-hsin, Hsi-Ling Chou, and Yu-Huei Peng. 2012. "Microbial Degradation of 4-Monobrominated Diphenyl Ether with Anaerobic Sludge." *Journal of Hazardous Materials* 213–214 (April):341–46. <https://doi.org/10.1016/j.jhazmat.2012.02.009>.
- Siebielska, Izabela, and Robert Sidelko. 2015. "Polychlorinated Biphenyl Concentration Changes in Sewage Sludge and Organic Municipal Waste Mixtures during Composting and Anaerobic Digestion." *Chemosphere* 126 (May):88–95. <https://doi.org/10.1016/j.chemosphere.2014.12.051>.
- Siddiqi, M. A., R. H. Laessig, and K. D. Reed. 2003. "Polybrominated Diphenyl Ethers (PBDEs): New Pollutants-Old Diseases." *Clinical Medicine & Research* 1 (4): 281–90. <https://doi.org/10.3121/cmr.1.4.281>.
- Smola, Alex J., and Bernhard Schölkopf. 2004. "A Tutorial on Support Vector Regression." *Statistics and Computing* 14 (3): 199–222. <https://doi.org/10.1023/B:STCO.0000035301.49549.88>.
- Song, Mengke, Chunling Luo, Fangbai Li, Longfei Jiang, Yan Wang, Dayi Zhang, and Gan Zhang. 2015. "Anaerobic Degradation of Polychlorinated Biphenyls (PCBs) and Polychlorinated Biphenyls Ethers (PBDEs), and Microbial Community

- Dynamics of Electronic Waste-Contaminated Soil.” *Science of The Total Environment* 502 (January):426–33.  
<https://doi.org/10.1016/j.scitotenv.2014.09.045>.
- Stockholm Convention. 2024. "Stockholm Convention on POPs." Accessed November 4, 2024. <https://www.pops.int/TheConvention/ThePOPs/tabid/673/Default.aspx>.
- Sun, Runxia, Changgui Pan, Qing X. Li, Fengjiao Peng, and Bixian Mai. 2020. “Occurrence and Congener Profiles of Polybrominated Diphenyl Ethers in Green Mussels (*Perna Viridis*) Collected from Northern South China Sea and the Associated Potential Health Risk.” *Science of the Total Environment* 698 (January).  
<https://doi.org/10.1016/j.scitotenv.2019.134276>.
- Suthersan, Suthan S, John Horst, Matthew Schnobrich, Nicklaus Welty, and Jeff McDonough. 2016. *Remediation Engineering*. Boca Raton: CRC Press
- Tokarz, John A., Mi Youn Ahn, June Leng, Timothy R. Filley, and Loring Nies. 2008. “Reductive Debromination of Polybrominated Diphenyl Ethers in Anaerobic Sediment and a Biomimetic System.” *Environmental Science and Technology* 42 (4): 1157–64. <https://doi.org/10.1021/es071989t>.
- Toms, Leisa-Maree L., Fiona A. Harden, Robert K. Symons, Debbie Burniston, Peter Fürst, and Jochen F. Müller. 2006. “Polybrominated Diphenyl Ethers (PBDEs) in Human Milk from Australia.” *Chemosphere* 68 (5): 797–803.  
<https://doi.org/10.1016/j.chemosphere.2007.02.059>.
- U.S. Environmental Protection Agency. 2023. "EPI Suite." Accessed November 01, 2024. <https://www.epa.gov/tsca-screening-tools/epi-suitetm-estimation-program-interface>.
- USEPA. 2022. “National Primary Drinking Water Regulations EPA.” 2022. <https://www.epa.gov/ground-water-and-drinking-water/national-primary-drinking-water-regulations>.
- Valerio, L.G. 2014. “In Silico Methods.” *In Encyclopedia of Toxicology*, 1026–29. Elsevier. <https://doi.org/10.1016/B978-0-12-386454-3.01057-5>.
- Wu, Xiaodan, Siru Yu, Jiahe Zeng, Xiaobo Zheng, Zongling Ren, Yinghua Shu, and Bixian Mai. 2024. “Biomagnification of Persistent Organic Pollutants (POPs) in Detritivorous, Phytophagous, and Predatory Invertebrates: How POPs Enter Terrestrial Food Web?” *Science of the Total Environment* 924 (May).  
<https://doi.org/10.1016/j.scitotenv.2024.171677>.
- Xu, Wen-Long, Ya-Jun Wang, Yi-Tong Wang, Jun-Guo Li, Ya-Nan Zeng, Hua-Wei Guo, Huan Liu, Kai-Li Dong, and Liang-Yi Zhang. 2024. “Application and Innovation of Artificial Intelligence Models in Wastewater Treatment.” *Journal of Contaminant Hydrology* 267 (November):104426.  
<https://doi.org/10.1016/j.jconhyd.2024.104426>.
- Yadav, Vibha, Amit Kumar Yadav, Vedant Singh, and Tej Singh. 2024. “Artificial Neural Network an Innovative Approach in Air Pollutant Prediction for Environmental

- Applications: A Review.” *Results in Engineering*. Elsevier B.V. <https://doi.org/10.1016/j.rineng.2024.102305>.
- Yildirim, Ozgur, and Bestami Ozkaya. 2023. “Prediction of Biogas Production of Industrial Scale Anaerobic Digestion Plant by Machine Learning Algorithms.” *Chemosphere* 335 (September):138976. <https://doi.org/10.1016/j.chemosphere.2023.138976>.
- Zhao, Chenghao, Ming Yan, Hua Zhong, Zhifeng Liu, Liangsheng Shi, Ming Chen, Guangming Zeng, Biao Song, Binbin Shao, and Haopeng Feng. 2018. “Biodegradation of Polybrominated Diphenyl Ethers and Strategies for Acceleration: A Review.” *International Biodeterioration and Biodegradation*. Elsevier Ltd. <https://doi.org/10.1016/j.ibiod.2017.12.010>.
- Zhao, Siyan, Siyan Fan, Yide He, and Yongjun Zhang. 2022. “Microbial Debromination of Polybrominated Diphenyl Ethers by Dehalococoides-Containing Enrichment Culture.” *Frontiers in Microbiology* 12 (February). <https://doi.org/10.3389/fmicb.2021.806795>.
- Zhao, Siyan, Matthew J. Rogers, Chang Ding, and Jianzhong He. 2018. “Reductive Debromination of Polybrominated Diphenyl Ethers - Microbes, Processes and Dehalogenases.” *Frontiers in Microbiology*. Frontiers Media S.A. <https://doi.org/10.3389/fmicb.2018.01292>.
- Zhu, Bingqing, Nelson L.S. Lai, Tak-Cheung Wai, Leo L. Chan, James C.W. Lam, and Paul K.S. Lam. 2014. “Changes of Accumulation Profiles from PBDEs to Brominated and Chlorinated Alternatives in Marine Mammals from the South China Sea.” *Environment International* 66 (May):65–70. <https://doi.org/10.1016/j.envint.2014.01.023>.
- Zhu, Xifen, Yin Zhong, Heli Wang, Dan Li, Yirong Deng, and Ping’an Peng. 2019. “New Insights into the Anaerobic Microbial Degradation of Decabrominated Diphenyl Ether (BDE-209) in Coastal Marine Sediments.” *Environmental Pollution* 255 (December). <https://doi.org/10.1016/j.envpol.2019.113151>.

# APPENDIX A

## PBDE PATHWAYS REVIEW

PBDE congeners have degradation pathways such as ortho, para, and meta positions. These positions determine the specific bromine degradation. For example, BDE-93 has five bromines which are at 2-3-5-6 positions in the first phenyl, and one of bromines at 2 position in the second phenyl structure. That structure looks in the mathematical BDE-93 (2356 – 2). That numerical systems used by IUPAC was used to demonstrate the pathways on degradation positions. BDE-65 (2356) has 4 bromine in the first phenyl structure. For the BDE 93 to BDE-65 degradation, a bromine was removed from BDE-93 second phenyl structure. Due to that breaking, BDE-65 observed because of IUPAC numbering and their structure. In this table, some examples from ortho, meta, and para positions' removal is shown. This data has been generated by ADM as an output.

Table A.1. The list of possible dehalogenation pathways in microcosm data set.

Dehalogenation Pathway				
<b>209</b>	(23456 - 23456)	→	<b>208</b>	(23456 - 2356)
<b>209</b>	(23456 - 23456)	→	<b>206</b>	(23456 - 2345)
<b>209</b>	(23456 - 23456)	→	<b>207</b>	(23456 - 2346)
<b>208</b>	(23456 - 2356)	→	<b>202</b>	(2356 - 2356)
<b>208</b>	(23456 - 2356)	→	<b>199</b>	(2345 - 2356)
<b>208</b>	(23456 - 2356)	→	<b>198</b>	(23456 - 235)
<b>208</b>	(23456 - 2356)	→	<b>201</b>	(2346 - 2356)
<b>208</b>	(23456 - 2356)	→	<b>200</b>	(23456 - 236)
<b>207</b>	(23456 - 2346)	→	<b>201</b>	(2346 - 2356)
<b>207</b>	(23456 - 2346)	→	<b>200</b>	(23456 - 236)
<b>207</b>	(23456 - 2346)	→	<b>203</b>	(23456 - 245)
<b>207</b>	(23456 - 2346)	→	<b>196</b>	(2345 - 2346)
<b>207</b>	(23456 - 2346)	→	<b>195</b>	(23456 - 234)
<b>207</b>	(23456 - 2346)	→	<b>204</b>	(23456 - 246)
<b>207</b>	(23456 - 2346)	→	<b>197</b>	(2346 - 2346)
<b>206</b>	(23456 - 2345)	→	<b>199</b>	(2345 - 2356)
<b>206</b>	(23456 - 2345)	→	<b>198</b>	(23456 - 235)
<b>206</b>	(23456 - 2345)	→	<b>205</b>	(23456 - 345)
<b>206</b>	(23456 - 2345)	→	<b>194</b>	(2345 - 2345)

(cont. on next page)

**Table A (cont.)**

<b>206</b>	(23456 - 2345)	→	<b>203</b>	(23456 - 245)
<b>206</b>	(23456 - 2345)	→	<b>196</b>	(2345 - 2346)
<b>206</b>	(23456 - 2345)	→	<b>195</b>	(23456 - 234)
205	(23456 - 345)	→	193	(2356 - 345)
205	(23456 - 345)	→	192	(23456 - 35)
205	(23456 - 345)	→	189	(2345 - 345)
205	(23456 - 345)	→	191	(2346 - 345)
205	(23456 - 345)	→	190	(23456 - 34)
204	(23456 - 246)	→	188	(2356 - 246)
204	(23456 - 246)	→	186	(23456 - 26)
204	(23456 - 246)	→	182	(2345 - 246)
204	(23456 - 246)	→	181	(23456 - 24)
204	(23456 - 246)	→	184	(2346 - 246)
203	(23456 - 245)	→	187	(2356 - 245)
203	(23456 - 245)	→	185	(23456 - 25)
203	(23456 - 245)	→	180	(2345 - 245)
<b>203</b>	(23456 - 245)	→	<b>183</b>	(2346 - 245)
203	(23456 - 245)	→	181	(23456 - 24)
202	(2356 - 2356)	→	178	(2356 - 235)
202	(2356 - 2356)	→	179	(2356 - 236)
201	(2346 - 2356)	→	179	(2356 - 236)
201	(2346 - 2356)	→	187	(2356 - 245)
201	(2346 - 2356)	→	177	(2356 - 234)
201	(2346 - 2356)	→	175	(2346 - 235)
201	(2346 - 2356)	→	188	(2356 - 246)
201	(2346 - 2356)	→	176	(2346 - 236)
200	(23456 - 236)	→	179	(2356 - 236)
200	(23456 - 236)	→	185	(23456 - 25)
200	(23456 - 236)	→	174	(2345 - 236)
200	(23456 - 236)	→	173	(23456 - 23)
200	(23456 - 236)	→	186	(23456 - 26)
200	(23456 - 236)	→	176	(2346 - 236)
199	(2345 - 2356)	→	178	(2356 - 235)
199	(2345 - 2356)	→	193	(2356 - 345)
199	(2345 - 2356)	→	172	(2345 - 235)
199	(2345 - 2356)	→	187	(2356 - 245)
199	(2345 - 2356)	→	177	(2356 - 234)
199	(2345 - 2356)	→	174	(2345 - 236)
198	(23456 - 235)	→	178	(2356 - 235)
198	(23456 - 235)	→	192	(23456 - 35)
198	(23456 - 235)	→	172	(2345 - 235)
198	(23456 - 235)	→	185	(23456 - 25)
198	(23456 - 235)	→	175	(2346 - 235)
198	(23456 - 235)	→	173	(23456 - 23)
197	(2346 - 2346)	→	176	(2346 - 236)
<b>197</b>	(2346 - 2346)	→	<b>183</b>	(2346 - 245)
197	(2346 - 2346)	→	171	(2346 - 234)
197	(2346 - 2346)	→	184	(2346 - 246)
196	(2345 - 2346)	→	175	(2346 - 235)
196	(2345 - 2346)	→	174	(2345 - 236)
196	(2345 - 2346)	→	191	(2346 - 345)
196	(2345 - 2346)	→	180	(2345 - 245)
196	(2345 - 2346)	→	170	(2345 - 234)
<b>196</b>	(2345 - 2346)	→	<b>183</b>	(2346 - 245)

(cont. on next page)

**Table A (cont.)**

196	(2345 - 2346)	→	171	(2346 - 234)
195	(23456 - 234)	→	177	(2356 - 234)
195	(23456 - 234)	→	173	(23456 - 23)
195	(23456 - 234)	→	190	(23456 - 34)
195	(23456 - 234)	→	170	(2345 - 234)
195	(23456 - 234)	→	181	(23456 - 24)
195	(23456 - 234)	→	171	(2346 - 234)
194	(2345 - 2345)	→	172	(2345 - 235)
194	(2345 - 2345)	→	189	(2345 - 345)
194	(2345 - 2345)	→	180	(2345 - 245)
194	(2345 - 2345)	→	170	(2345 - 234)
184	(2346 - 246)	→	154	(245 - 246)
183	(2346 - 245)	→	149	(236 - 245)
183	(2346 - 245)	→	144	(2346 - 25)
<b>183</b>	(2346 - 245)	→	<b>153</b>	(245 - 245)
183	(2346 - 245)	→	138	(234 - 245)
<b>183</b>	(2346 - 245)	→	<b>154</b>	(245 - 246)
183	(2346 - 245)	→	139	(2346 - 24)
182	(2345 - 246)	→	154	(245 - 246)
180	(2345 - 245)	→	153	(245 - 245)
155	(246 - 246)	→	100	(246 - 24)
154	(245 - 246)	→	103	(246 - 25)
154	(245 - 246)	→	102	(245 - 26)
<b>154</b>	(245 - 246)	→	<b>99</b>	(245 - 24)
<b>154</b>	(245 - 246)	→	<b>100</b>	(246 - 24)
153	(245 - 245)	→	101	(245 - 25)
<b>153</b>	(245 - 245)	→	<b>99</b>	(245 - 24)
140	(234 - 246)	→	100	(246 - 24)
139	(2346 - 24)	→	99	(245 - 24)
139	(2346 - 24)	→	100	(246 - 24)
138	(234 - 245)	→	99	(245 - 24)
137	(2345 - 24)	→	99	(245 - 24)
100	(246 - 24)	→	51	(24 - 26)
100	(246 - 24)	→	50	(246 - 2)
100	(246 - 24)	→	75	(246 - 4)
<b>100</b>	(246 - 24)	→	<b>47</b>	(24 - 24)
99	(245 - 24)	→	49	(24 - 25)
99	(245 - 24)	→	48	(245 - 2)
99	(245 - 24)	→	74	(245 - 4)
<b>99</b>	(245 - 24)	→	<b>47</b>	(24 - 24)
85	(234 - 24)	→	47	(24 - 24)
75	(246 - 4)	→	28	(24 - 4)
74	(245 - 4)	→	28	(24 - 4)
66	(24 - 34)	→	28	(24 - 4)
60	(234 - 4)	→	28	(24 - 4)
47	(24 - 24)	→	17	(24 - 2)
<b>47</b>	(24 - 24)	→	<b>28</b>	(24 - 4)
28	(24 - 4)	→	8	(2 - 4)
28	(24 - 4)	→	7	(24 - 0)
28	(24 - 4)	→	15	(4 - 4)

## APPENDIX B

### NORMALIZED PROFILE DATA SETS

The following tables present the microcosm datasets (mole‰).

Table B.1. Natural attenuation normalized to mole‰ profile.

<b>t (day)</b>	<b>BDE</b>	<b>209</b>	<b>208</b>	<b>207</b>	<b>206</b>	<b>205</b>	<b>204</b>	<b>203</b>	<b>202</b>
<b>0</b>	988.73508	0.00000	4.02937	7.23554	0.00000	0.00000	0.00000	0.00000	0.00000
<b>20</b>	980.37192	2.48886	4.68076	12.45846	0.00000	0.00000	0.00000	0.00000	0.00000
<b>40</b>	959.56353	4.25390	9.14166	22.42453	0.00000	0.23723	0.18594	0.29494	
<b>60</b>	947.45812	9.29089	11.06385	28.54612	0.00000	0.08758	0.11261	0.80077	
<b>90</b>	949.25143	5.47000	10.25892	24.13613	0.00000	0.48441	0.34878	1.78263	
<b>120</b>	897.24725	19.56003	41.03355	33.41828	0.00000	1.26690	0.17156	0.07038	
<b>152</b>	912.80233	13.41390	32.77396	32.89408	0.00000	0.52856	0.22327	0.49211	
<b>180</b>	891.26512	16.48875	27.60688	54.45998	0.00000	0.61759	0.35597	0.89208	
<b>t</b>	<b>BDE</b>	<b>201</b>	<b>200</b>	<b>199</b>	<b>198</b>	<b>197</b>	<b>196</b>	<b>195</b>	<b>194</b>
<b>0</b>	0.00000	0.00000	0.00000	0.00000	0.00000	0.00000	0.00000	0.00000	0.00000
<b>20</b>	0.00000	0.00000	0.00000	0.00000	0.00000	0.00000	0.00000	0.00000	0.00000
<b>40</b>	0.32058	0.18594	0.18594	0.18594	0.23723	0.71810	0.80787	1.25668	
<b>60</b>	0.41290	0.11261	0.11261	0.11261	0.08758	0.93841	0.52551	0.33783	
<b>90</b>	0.85256	0.34878	0.34878	0.34878	0.48441	1.27885	0.89132	2.59644	
<b>120</b>	0.36951	0.17156	0.17156	0.17156	1.26690	3.85348	0.00000	0.00000	
<b>152</b>	0.61970	0.22327	0.22327	0.22327	0.52856	2.78863	0.63792	1.27584	
<b>180</b>	0.96070	0.35597	0.35597	0.35597	0.61759	1.26949	0.00000	0.00000	
<b>t</b>	<b>BDE</b>	<b>183</b>	<b>154</b>	<b>153</b>	<b>100</b>	<b>99</b>	<b>47</b>	<b>28</b>	
<b>0</b>	0.00000	0.00000	0.00000	0.00000	0.00000	0.00000	0.00000	0.00000	
<b>20</b>	0.00000	0.00000	0.00000	0.00000	0.00000	0.00000	0.00000	0.00000	
<b>40</b>	0.00000	0.00000	0.00000	0.00000	0.00000	0.00000	0.00000	0.00000	
<b>60</b>	0.00000	0.00000	0.00000	0.00000	0.00000	0.00000	0.00000	0.00000	
<b>90</b>	0.00000	0.24898	0.40459	0.27307	0.19115	0.00000	0.00000	0.00000	
<b>120</b>	0.00000	0.00000	0.00000	0.59514	0.63234	0.00000	0.00000	0.00000	
<b>152</b>	0.00000	0.35130	0.00000	0.00000	0.00000	0.00000	0.00000	0.00000	
<b>180</b>	0.00000	3.11370	0.22044	0.37474	0.68904	0.00000	0.00000	0.00000	

Table B.2. Biostimulation normalized to mole% profile.

<b>t (day)</b>	<b>BDE</b>	<b>209</b>	<b>208</b>	<b>207</b>	<b>206</b>	<b>205</b>	<b>204</b>	<b>203</b>	<b>202</b>
<b>0</b>	985.12712	0.00000	3.83126	11.04162	0.00000	0.00000	0.00000	0.00000	0.00000
<b>20</b>	929.04731	15.24519	27.98795	23.29988	0.00000	0.06671	0.08139	0.00000	0.00000
<b>40</b>	961.36093	4.00923	8.11391	22.85352	0.00000	0.11587	0.12539	0.37702	0.00000
<b>60</b>	958.29929	4.18782	9.01676	26.26985	0.00000	0.22259	0.07291	0.00000	0.00000
<b>90</b>	961.66094	4.62665	8.12297	22.76467	0.00000	0.00000	0.11914	0.00000	0.00000
<b>120</b>	880.15208	25.75103	47.27514	39.35639	0.00000	0.11268	0.13748	0.00000	0.00000
<b>152</b>	922.23218	9.18250	20.74372	24.33864	0.00000	0.13157	0.14716	0.00000	0.00000
<b>180</b>	891.17559	15.18742	27.87357	61.62517	0.00000	0.18344	0.32940	0.00000	0.00000
<b>t</b>	<b>BDE</b>	<b>201</b>	<b>200</b>	<b>199</b>	<b>198</b>	<b>197</b>	<b>196</b>	<b>195</b>	<b>194</b>
<b>0</b>	0.00000	0.00000	0.00000	0.00000	0.00000	0.00000	0.00000	0.00000	0.00000
<b>20</b>	0.05803	0.08139	0.08139	0.08139	0.06671	3.14315	0.00000	0.00000	0.00000
<b>40</b>	0.23248	0.12539	0.12539	0.12539	0.11587	0.50592	0.00000	0.91485	0.00000
<b>60</b>	0.68405	0.07291	0.07291	0.07291	0.22259	0.22924	0.18013	0.25081	0.00000
<b>90</b>	0.46261	0.11914	0.11914	0.11914	0.00000	0.37193	0.00000	0.50756	0.00000
<b>120</b>	0.09802	0.13748	0.13748	0.13748	0.11268	5.30918	0.00000	0.00000	0.00000
<b>152</b>	0.00000	0.14716	0.14716	0.14716	0.13157	0.85987	0.00000	0.00000	0.00000
<b>180</b>	0.12427	0.32940	0.32940	0.32940	0.18344	1.01143	0.00000	0.19041	0.00000
<b>t</b>	<b>BDE</b>	<b>183</b>	<b>154</b>	<b>153</b>	<b>100</b>	<b>99</b>	<b>47</b>	<b>28</b>	
<b>0</b>	0.00000	0.00000	0.00000	0.00000	0.00000	0.00000	0.00000	0.00000	
<b>20</b>	0.00000	0.00000	0.00000	0.33548	0.42401	0.00000	0.00000	0.00000	
<b>40</b>	0.29627	0.23530	0.08135	0.12345	0.00000	0.16246	0.00000	0.00000	
<b>60</b>	0.00000	0.00000	0.00000	0.14524	0.00000	0.00000	0.00000	0.00000	
<b>90</b>	0.18173	0.12695	0.11474	0.30539	0.14720	0.13009	0.00000	0.00000	
<b>120</b>	0.00000	0.00000	0.00000	0.56666	0.71621	0.00000	0.00000	0.00000	
<b>152</b>	0.00000	0.38095	0.94307	11.76834	0.58517	8.11379	0.00000	0.00000	
<b>180</b>	0.00000	0.04150	0.17301	0.42873	0.48444	0.00000	0.00000	0.00000	

Table B.3. Bioaugmentation normalized to mole% profile.

<b>t (day)</b>	<b>BDE</b>	<b>209</b>	<b>208</b>	<b>207</b>	<b>206</b>	<b>205</b>	<b>204</b>	<b>203</b>	<b>202</b>
<b>0</b>	981.18942	0.00000	7.02577	11.78481	0.00000	0.00000	0.00000	0.00000	0.00000
<b>20</b>	982.43512	0.00000	4.79134	12.77354	0.00000	0.00000	0.00000	0.00000	0.00000
<b>40</b>	954.54108	5.29039	11.15833	27.40608	0.00000	0.03225	0.07884	0.15329	
<b>60</b>	954.34635	4.25521	8.79235	25.60651	0.00000	0.24003	0.20191	0.50770	
<b>90</b>	962.11716	4.14419	7.89752	21.20104	0.00000	0.29281	0.20358	0.53530	
<b>120</b>	888.08488	21.37605	40.23220	42.84990	0.00000	0.82180	0.31369	0.74058	
<b>152</b>	944.47300	6.53720	14.40506	16.02969	0.00000	0.28906	0.14977	0.08107	
<b>180</b>	903.20903	12.76809	24.41136	52.38089	0.00000	0.84025	0.38074	0.15245	
<b>t</b>	<b>BDE</b>	<b>201</b>	<b>200</b>	<b>199</b>	<b>198</b>	<b>197</b>	<b>196</b>	<b>195</b>	<b>194</b>
<b>0</b>	0.00000	0.00000	0.00000	0.00000	0.00000	0.00000	0.00000	0.00000	0.00000
<b>20</b>	0.00000	0.00000	0.00000	0.00000	0.00000	0.00000	0.00000	0.00000	0.00000
<b>40</b>	0.16281	0.07884	0.07884	0.07884	0.03225	0.24772	0.00000	0.20278	
<b>60</b>	1.57077	0.20191	0.20191	0.20191	0.24003	1.28520	0.00000	1.88671	
<b>90</b>	0.45567	0.20358	0.20358	0.20358	0.29281	0.62625	0.00000	1.26284	
<b>120</b>	0.56815	0.31369	0.31369	0.31369	0.82180	2.17501	0.00000	0.00000	
<b>152</b>	0.18993	0.14977	0.14977	0.14977	0.28906	0.97231	2.21443	0.80050	
<b>180</b>	0.85942	0.38074	0.38074	0.38074	0.84025	1.38969	0.00000	1.24735	
<b>t</b>	<b>BDE</b>	<b>183</b>	<b>154</b>	<b>153</b>	<b>100</b>	<b>99</b>	<b>47</b>	<b>28</b>	
<b>0</b>	0.00000	0.00000	0.00000	0.00000	0.00000	0.00000	0.00000	0.00000	
<b>20</b>	0.00000	0.00000	0.00000	0.00000	0.00000	0.00000	0.00000	0.00000	
<b>40</b>	0.00000	0.00000	0.12552	0.19975	0.00000	0.13238	0.00000	0.00000	
<b>60</b>	0.00000	0.00000	0.00000	0.23403	0.00000	0.08458	0.14290		
<b>90</b>	0.00000	0.00000	0.00000	0.20445	0.15566	0.00000	0.00000	0.00000	
<b>120</b>	0.00000	0.00000	0.00000	0.44075	0.63413	0.00000	0.00000	0.00000	
<b>152</b>	0.00000	1.93110	1.05872	5.44967	2.61266	2.06742	0.00000	0.00000	
<b>180</b>	0.00000	0.06127	0.00000	0.17346	0.00000	0.00000	0.14349		

Table B.4. Negative control normalized to mole% profile.

<b>t (days)</b>	<b>BDE</b>	<b>209</b>	<b>208</b>	<b>207</b>	<b>206</b>	<b>205</b>	<b>204</b>	<b>203</b>	<b>202</b>
<b>0</b>		988.42190	0.00000	1.77406	9.80404	0.00000	0.00000	0.00000	0.00000
<b>20</b>		977.20928	1.80648	7.25819	13.72605	0.00000	0.00000	0.00000	0.00000
<b>40</b>		960.84866	4.27544	9.23687	25.01452	0.00000	0.15249	0.00000	0.00000
<b>60</b>		968.90845	3.64530	6.95037	18.85834	0.00000	0.00000	0.11799	0.00000
<b>90</b>		970.31664	3.45546	6.82745	17.21053	0.00000	0.19756	0.09878	0.00000
<b>120</b>		880.11420	25.15827	46.37979	40.22863	0.00000	1.25297	0.37099	0.00000
<b>152</b>		948.57080	8.27823	19.20348	16.43845	0.00000	0.34535	0.18419	0.00000
<b>180</b>		924.87522	10.91108	20.19093	39.47563	0.00000	0.61051	0.27638	0.00000
<b>t</b>	<b>BDE</b>	<b>201</b>	<b>200</b>	<b>199</b>	<b>198</b>	<b>197</b>	<b>196</b>	<b>195</b>	<b>194</b>
<b>0</b>		0.00000	0.00000	0.00000	0.00000	0.00000	0.00000	0.00000	0.00000
<b>20</b>		0.00000	0.00000	0.00000	0.00000	0.00000	0.00000	0.00000	0.00000
<b>40</b>		0.00000	0.00000	0.00000	0.00000	0.15249	0.31951	0.00000	0.00000
<b>60</b>		0.42773	0.11799	0.11799	0.11799	0.00000	0.45723	0.00000	0.00000
<b>90</b>		0.37992	0.09878	0.09878	0.09878	0.19756	0.33433	0.00000	0.00000
<b>120</b>		0.85398	0.37099	0.37099	0.37099	1.25297	1.97395	0.00000	0.00000
<b>152</b>		0.00000	0.18419	0.18419	0.18419	0.34535	0.62930	0.00000	0.00000
<b>180</b>		0.82501	0.27638	0.27638	0.27638	0.61051	0.59401	0.00000	0.00000
<b>t</b>	<b>BDE</b>	<b>183</b>	<b>154</b>	<b>153</b>	<b>100</b>	<b>99</b>	<b>47</b>	<b>28</b>	
<b>0</b>		0.00000	0.00000	0.00000	0.00000	0.00000	0.00000	0.00000	
<b>20</b>		0.00000	0.00000	0.00000	0.00000	0.00000	0.00000	0.00000	
<b>40</b>		0.00000	0.00000	0.00000	0.00000	0.00000	0.00000	0.00000	
<b>60</b>		0.00000	0.00000	0.00000	0.28061	0.00000	0.00000	0.00000	
<b>90</b>		0.15071	0.00000	0.25630	0.16063	0.11779	0.00000	0.00000	
<b>120</b>		0.00000	0.31481	0.00000	0.45378	0.53270	0.00000	0.00000	
<b>152</b>		0.00000	0.40678	0.00000	3.15814	0.38936	1.49801	0.00000	
<b>180</b>		0.26776	0.37104	0.00000	0.00000	0.16278	0.00000	0.00000	

Table B.5. Sterile control normalized to mole% profile.

<b>t (day)</b>	<b>BDE 209</b>	<b>208</b>	<b>207</b>	<b>206</b>	<b>205</b>	<b>204</b>	<b>203</b>	<b>202</b>
<b>0</b>	989.4071	0.0000	0.0000	10.5929	0.0000	0.0000	0.0000	0.0000
<b>20</b>	988.9207	0.0000	0.0000	11.0793	0.0000	0.0000	0.0000	0.0000
<b>40</b>	985.2366	0.0000	0.0000	14.7634	0.0000	0.0000	0.0000	0.0000
<b>60</b>	985.4456	0.0000	0.0000	14.5544	0.0000	0.0000	0.0000	0.0000
<b>90</b>	984.9959	0.0000	0.0000	15.0041	0.0000	0.0000	0.0000	0.0000
<b>120</b>	998.6952	0.0000	0.0000	1.3048	0.0000	0.0000	0.0000	0.0000
<b>152</b>	986.1121	0.0000	0.0000	13.8879	0.0000	0.0000	0.0000	0.0000
<b>180</b>	989.6332	0.0000	0.0000	10.3668	0.0000	0.0000	0.0000	0.0000
<b>t</b>	<b>BDE 201</b>	<b>200</b>	<b>199</b>	<b>198</b>	<b>197</b>	<b>196</b>	<b>195</b>	<b>194</b>
<b>0</b>	0.0000	0.0000	0.0000	0.0000	0.0000	0.0000	0.0000	0.00
<b>20</b>	0.0000	0.0000	0.0000	0.0000	0.0000	0.0000	0.0000	0.00
<b>40</b>	0.0000	0.0000	0.0000	0.0000	0.0000	0.0000	0.0000	0.00
<b>60</b>	0.0000	0.0000	0.0000	0.0000	0.0000	0.0000	0.0000	0.00
<b>90</b>	0.0000	0.0000	0.0000	0.0000	0.0000	0.0000	0.0000	0.00
<b>120</b>	0.0000	0.0000	0.0000	0.0000	0.0000	0.0000	0.0000	0.00
<b>152</b>	0.0000	0.0000	0.0000	0.0000	0.0000	0.0000	0.0000	0.00
<b>180</b>	0.0000	0.0000	0.0000	0.0000	0.0000	0.0000	0.0000	0.00
<b>t</b>	<b>BDE 183</b>	<b>154</b>	<b>153</b>	<b>100</b>	<b>99</b>	<b>47</b>	<b>28</b>	
<b>0</b>	0.00	0.00	0.00	0.00	0.00	0.00	0.00	0.00
<b>20</b>	0.00	0.00	0.00	0.00	0.00	0.00	0.00	0.00
<b>40</b>	0.00	0.00	0.00	0.00	0.00	0.00	0.00	0.00
<b>60</b>	0.00	0.00	0.00	0.00	0.00	0.00	0.00	0.00
<b>90</b>	0.00	0.00	0.00	0.00	0.00	0.00	0.00	0.00
<b>120</b>	0.00	0.00	0.00	0.00	0.00	0.00	0.00	0.00
<b>152</b>	0.00	0.00	0.00	0.00	0.00	0.00	0.00	0.00
<b>180</b>	0.00	0.00	0.00	0.00	0.00	0.00	0.00	0.00

## APPENDIX C

### ANALYSIS OF ML PERFORMANCE

The coefficient of regression values obtained from machine learning results have been evaluated, and it has been decided to proceed with the FNN model. The coefficient of regression values obtained are listed in the table.

Table C.1. Coefficient of regression test microcosms.

<b>Microcosm</b>	<b>Day 0-180</b>	<b>Coefficient of Regression R<sup>2</sup></b>
Natural attenuation	FNN:	0.571
	SVM:	0.096
	LR:	0.062
Biostimulation	FNN:	0.966
	SVM:	0.060
	LR:	0.032
Bioaugmentation	FNN:	0.906
	SVM:	0.105
	LR:	0.045

LR: linear regression

## APPENDIX D

### MODEL MANUAL

```
18 %%  
19 % Model user manual:Review the following details before starting the model  
20 % Use the ctrl+f command to quickly locate each section listed below  
21  
22 %modelmanual1 modelmanual6  
23 %modelmanual2 modelmanual7  
24 %modelmanual3 modelmanual8  
25 %modelmanual4 modelmanual9  
26 %modelmanual5 modelmanual10  
27  
28 % A total of 10 details need to be checked
```

Figure D.1. Model manual.

A user manual was created to assist users in properly configuring the ADM-IE model before execution. This manual provides a structured checklist, with key sections numbered from modelmanual1 to modelmanual10. Users are advised to review each section thoroughly to ensure that all necessary parameters are set correctly. The Ctrl+F command can be used to quickly locate these sections within the code, facilitating an efficient setup process. Following this manual is essential to achieve accurate and reliable results from the model.